

# $dS$ extremal surfaces, replicas, boundary Renyi entropies in $dS/CFT$ and time entanglement

Kanhu Kishore Nanda, K. Narayan, Somnath Porey, Gopal Yadav

*Chennai Mathematical Institute,  
H1 SIPCOT IT Park, Siruseri 603103, India.*

Email: kanhukishore, narayan, sporey, gopalyadav at cmi.ac.in

We develop further previous work on de Sitter extremal surfaces and time entanglement structures in quantum mechanics. In the first part, we first discuss explicit quotient geometries. Then we construct smooth bulk geometries with replica boundary conditions at the future boundary and evaluate boundary Renyi entropies in  $dS/CFT$ . The bulk calculation pertains to the semiclassical de Sitter Wavefunction and thus evaluates pseudo-Renyi entropies. In 3-dimensions, the geometry in quotient variables is Schwarzschild de Sitter. The 4-dim  $dS$  geometry involves hyperbolic foliations and is a complex geometry satisfying a regularity criterion that amounts to requiring a smooth Euclidean continuation. Overall this puts on a firmer footing previous Lewkowycz-Maldacena replica arguments based on analytic continuation for the extremal surface areas via appropriate cosmic branes.

In the second part (independent of de Sitter), we study various aspects of time entanglement in quantum mechanics, in particular the reduced time evolution operator, weak values of operators localized to subregions, a transition matrix operator with two copies of the time evolution operator, autocorrelation functions for operators localized to subregions, and finally future-past entangled states and factorization. Based on these, we then give some comments on a cosmological transition matrix using the de Sitter Wavefunction.

# Contents

<b>1</b>	<b>Introduction</b>	<b>1</b>
<b>2</b>	<b>Review: no-boundary <math>dS</math> extremal surfaces</b>	<b>4</b>
<b>3</b>	<b>de Sitter quotient geometries</b>	<b>7</b>
3.1	$dS_3$ quotient and boundary EE . . . . .	8
3.2	$dS_4/CFT_3$ boundary EE via replica quotient . . . . .	10
<b>4</b>	<b>de Sitter replicas: boundary Renyi via <math>dS/CFT</math></b>	<b>12</b>
4.1	$dS_3$ replica geometry: boundary Renyi . . . . .	13
4.2	$dS_4$ replica geometry: boundary Renyi . . . . .	17
4.2.1	Real $dS_4$ -like hyperbolic cosmologies . . . . .	22
4.3	Higher dimensional $dS$ and boundary Renyi . . . . .	23
<b>5</b>	<b>Time entanglement in quantum mechanics: review</b>	<b>24</b>
<b>6</b>	<b>Time evolution operator, partial traces: weak values, autocorrelation functions, future-past entanglement</b>	<b>26</b>
6.1	Weak values and the reduced time evolution operator . . . . .	26
6.2	Autocorrelation functions: the $T$ operator . . . . .	29
6.3	Future-past entangled states, time evolution . . . . .	31
6.3.1	Autocorrelation functions, factorization . . . . .	34
<b>7</b>	<b>Attempting a synthesis: <math>\Psi_{dS}</math> and time entanglement</b>	<b>35</b>
<b>8</b>	<b><math>dS</math> extremal surfaces: other aspects and speculations</b>	<b>37</b>
8.1	$dS$ extremal surfaces, timelike components, maximal areas . . . . .	37
8.2	The imaginary part in no-boundary $dS$ areas . . . . .	39
<b>9</b>	<b>Discussion</b>	<b>41</b>
<b>A</b>	<b>More on <math>dS</math>-like quotient geometries</b>	<b>45</b>
A.1	Future-past extremal surface area via quotient . . . . .	45
A.2	$dS \rightarrow$ Euclidean sphere: $dS$ entropy . . . . .	47
A.3	No-boundary slow-roll inflation, extremal surfaces, quotient . . . . .	48
<b>B</b>	<b><math>dS_{d+1} \rightarrow -AdS</math> and boundary Renyi</b>	<b>50</b>
<b>C</b>	<b>The on-shell action for <math>dS_{d+1}</math></b>	<b>52</b>
<b>D</b>	<b>Autocorrelation functions, <math>T</math> operator: examples</b>	<b>54</b>

## 1 Introduction

Various fascinating generalizations of quantum information structures arise in the context of holography [1–3] towards de Sitter space [4–7]. Certain generalizations of the Ryu-Takayanagi formulation [8–11] of  $AdS$  holographic entanglement to de Sitter space were studied in [12–17] with more recent reinventions in [18, 19] (also [20–23]). These pertain to RT/HRT extremal surfaces anchored at the  $dS$  future boundary  $I^+$  and amount to considering the bulk analog of setting up boundary entanglement entropy in the dual CFT at  $I^+$ , in part towards understanding de Sitter entropy [24] (reviewed in [25]) as some sort of holographic entanglement entropy. There are no  $I^+ \rightarrow I^+$  turning points [12] so the surfaces necessarily have timelike components and the bulk areas are complex-valued. Conjectured  $dS/CFT$  dualities [4–7] suggest Euclidean non-unitary ghost-like CFTs dual to de Sitter space (note that on general grounds we expect that the gravity dual to an ordinary Euclidean CFT is Euclidean  $AdS$ ). Studies in various toy models of “entanglement entropy” in ghost-like theories explicitly reveal complex-valued entropies arising naturally [26, 27],

the negative norm contributions here leading to imaginary components. Thus the time-like components in the bulk areas are necessary to mirror this complex-valued boundary entanglement entropy.

Recent investigations suggest that the areas of these extremal surfaces are best interpreted as encoding pseudo-entropy or time-entanglement [18], [19], entanglement-like structures involving timelike separations. Pseudo-entropy [28] is the entropy based on the transition matrix  $|f\rangle\langle i|$  regarded as a generalized density operator. In some sense this is perhaps the natural object here since the absence of  $I^+ \rightarrow I^+$  returns for extremal surfaces suggests that extra data is required in the interior, somewhat reminiscent of scattering amplitudes (equivalently the time evolution operator), and of [5] viewing de Sitter space as a collection of past-future amplitudes. This is also suggested by the  $dS/CFT$  dictionary  $Z_{CFT} = \Psi_{dS}$  [6]: boundary entanglement entropy formulated via  $Z_{CFT}$  translates to a bulk object formulated via the Wavefunction  $\Psi_{dS}$  (a single ket, rather than a density matrix), leading (not surprisingly) to non-hermitian structures. In [22], the  $dS$  extremal surfaces were recast via analytic continuation from  $AdS$ , amounting to a space-time rotation: so they are analogous to  $AdS$  RT ones on constant time slices turned sideways. This then suggested a heuristic version of the Lewkowycz-Maldacena argument for the no-boundary  $dS$  extremal surfaces for maximal (IR) subregions. Roughly the boundary replica argument on  $Z_{CFT}$  translates now to a bulk replica argument on the Wavefunction  $\Psi_{dS}$  which is essentially pseudo-entropy. The area now is interpreted as the amplitude for creation of a cosmic brane that localizes on the part Euclidean, part timelike no-boundary extremal surface.

These have fuelled parallel developments in quantum mechanics and CFT, independent of  $dS$ , pertaining to entanglement-like structures involving timelike separations. Two aspects of this “time-entanglement” in simple toy models were described in [19], based on (1) the time evolution operator and reduced transition amplitudes, dovetailing with pseudo-entropy [28] (and some discussions in [18]), and (2) two copies of future-past entangled states and entirely positive structures. In [21], this was developed further, with the time evolution operator regarded as a generalized density operator. Partial traces lead to a reduced time evolution operator for subregions and the corresponding complex-valued von Neumann entropy, with sharp parallels with finite temperature entanglement structures at imaginary temperature. Entanglement structures for the time evolution operator along with a projection operator onto some initial state towards isolating components thereof ends up amounting to pseudo-entropy for this state and its time-evolved final state. (Other partially related work that we found useful here include [29–58].)

This paper contains explorations divided into two parts broadly.

In the first part, we put on a firmer footing the heuristic analytic-continuation-based ar-

gements in [22] of the Lewkowycz-Maldacena replica formulation (reviewed in sec. 2). We first discuss  $n$ -quotient geometries as a tool to evaluate the extremal surface areas (sec. 3, with more detail in  $dS_3, dS_4$ , sections 3.1, 3.2, as well as future-past extremal surfaces in entirely Lorentzian  $dS$  (sec. A.1), real Euclidean extremal surfaces in the Euclidean sphere giving  $dS$  entropy (sec. A.2), and no-boundary surfaces in slow-roll inflation (sec. A.3)). Then we construct smooth bulk geometries (sec. 4) with replica boundary conditions at the future boundary (reflecting  $I^+$ -anchored extremal surfaces), and evaluate boundary Renyi entropies in  $dS/CFT$ . The bulk calculation pertains to the semiclassical  $dS$  Wavefunction and thus evaluates pseudo-Renyi entropies. Technically this uses the bulk action alongwith the Gibbons-Hawking boundary term as well as appropriate counterterms. The  $dS_3$  case (sec. 4.1) is most easily expressed in the static coordinatization which enable a simple visualization of the way the replica copies are glued together for these maximal subregions. This finally results in the boundary Renyi entropies being pure imaginary, consistent with the imaginary central charge in  $dS_3/CFT_2$  [6]: the  $n = 1$  limit recovers the boundary entanglement entropy matching the extremal surface area. In terms of boundary quotiented variables, the cosmic brane can be identified with the bulk conical singularity in corresponding Schwarzschild  $dS_3$  geometries with mass related to  $n$ . This  $dS_3$  analysis has close parallels with the  $AdS_3$  replica discussion in [59]. The 4-dim  $dS$  geometry (sec. 4.2) involves hyperbolic foliations, with close parallels with the  $AdS$  hyperbolic black holes in [60]. Here this is a complex geometry which satisfies a regularity criterion that amounts to requiring a smooth Euclidean continuation. The embedding of the hyperbolic foliations into global  $dS_4$  is non-trivial and illustrates how the  $n = 1$  limit recovers the known complex-valued no-boundary extremal surface area. This analysis can be also understood via analytic continuation from a  $-AdS$  framework, and is valid for de Sitter in any dimension (sec. 4.3). Overall this firms up the arguments in [22] for the extremal surface areas via appropriate cosmic branes.

In the second part, we develop further various aspects of time-entanglement structures in quantum mechanics, building on [19], [21], [22] (reviewed in sec. 5). We relate the reduced time evolution operator to weak values of operators localized to subregions (sec. 6.1): this also relates singularities in the corresponding pseudo-entropies to those in these weak values. These quantities involve one copy of the time evolution operator: we then introduce (sec. 6.2) a related transition matrix operator  $T$  containing time-evolved versions of two distinct states, which thus contains two copies of the time evolution operator. We then show how autocorrelation functions (especially for operators localized to subregions) can be naturally recast via  $T$  and partial traces thereof: this connects with some of the discussion in [58]. In sec. 6.3, we consider future-past entangled states and recast correlation functions for operators localized to subregions in terms of these, and comment on factorization aspects of

these future-past states in relation to that of correlation functions for long time separations.

This suggests a synthesis of these quantum mechanical time entanglement aspects with de Sitter space. In sec. 7, we consider a “cosmological transition matrix” involving two copies of the de Sitter Wavefunction, at the past and the future. We discuss how de Sitter entropy and the future-past surface area arise from special cases here. We also comment on some future work on related aspects in two copies of the dual ghost-like CFT.

Lastly, we comment on certain maximal area aspects of these no-boundary extremal surfaces containing timelike components in sec. 8.1, and make some speculations on the sign of the imaginary parts in these areas and their interpretations via cosmic branes in sec. 8.2. Sec. 9 contains a Discussion of various aspects. The appendices provide various calculational details (in particular App. A on quotient geometries, App. B on  $-AdS$ , App. C on the  $dS$  action and App. D on examples with the  $T$  operator).

## 2 Review: no-boundary $dS$ extremal surfaces

We briefly review [19, 22] and previous work here on generalizations of RT/HRT extremal surfaces to de Sitter space (see also [18]). These involve considering the bulk analog of setting up entanglement entropy in the dual Euclidean *CFT* on the future boundary, restricting to some boundary Euclidean time slice, defining subregions on these, and looking for extremal surfaces anchored at  $I^+$  dipping into the time (holographic) direction: analysing this shows that there are no spacelike surfaces connecting points on  $I^+$  [12]. In entirely Lorentzian  $dS$ , there are future-past timelike surfaces stretching between  $I^\pm$  [15, 17], akin to rotated analogs of the Hartman-Maldacena surfaces [61] in the eternal  $AdS$  black hole [62]: these have pure imaginary area, relative to  $AdS$  spacelike RT/HRT surfaces. With a no-boundary type Hartle-Hawking boundary condition, the top half of these timelike surfaces joins with a spacelike part on the hemisphere giving a complex-valued area [18], [19] (and [31, 32] for  $dS_3/CFT_2$ ). The real part of the area arises from the hemisphere and is precisely half de Sitter entropy. Due to the presence of timelike components in these extremal surfaces, these areas are best interpreted as pseudo-entropy, as we see below. From the dual side, in various toy models of “entanglement entropy” in ghost-like theories and “ghost-spin” lattice models, complex-valued entropies arise naturally [26, 27]: generic states, their reduced density matrices via partial traces and the corresponding von Neumann entropies show that the negative norm states here lead to imaginary components of the boundary entanglement entropies (which are also strictly speaking pseudo-entropies since the adjoints of states are nontrivial). Thus the timelike components in the bulk areas are necessary to mirror this complex-valued boundary entanglement entropy.

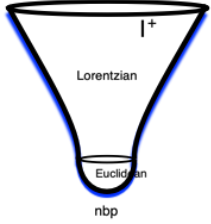


Figure 1: No-boundary de Sitter space, with the top Lorentzian region continuing smoothly into the Euclidean hemisphere region ending at the no-boundary point. Also shown are IR no-boundary extremal surfaces (blue) anchored at the future boundary  $I^+$  dipping into the time direction, timelike in the Lorentzian region and going around the hemisphere.

Overall, directly analysing the bulk extremization and calculating the no-boundary extremal surface areas for the IR (maximal) subregions at the future boundary gives

$$(dS_4) \quad S_{nb} = -i \frac{\pi l^2}{2G_4} \frac{R_c}{l} + \frac{\pi l^2}{2G_4}; \quad (dS_3) \quad S_{nb} = -i \frac{l}{2G_3} \log \frac{2R_c}{l} + \frac{\pi l}{4G_3}, \quad (2.1)$$

with the pure imaginary piece from the top Lorentzian part of  $dS$  and the real piece (precisely half de Sitter entropy) from the Euclidean hemisphere.  $R_c$  is the cutoff near  $I^+$ .

These can also be realized via analytic continuations from the  $AdS$  RT surfaces which all lie on a constant time slice. Under the  $dS \leftrightarrow AdS$  analytic continuation, this  $AdS$  constant time slice continues to  $dS$  in the Lorentzian region  $r > l$  as

$$ds_{(r>L)}^2 = \frac{dr^2}{1 + \frac{r^2}{L^2}} + r^2 d\Omega_{d-1}^2 \xrightarrow{L^2 \rightarrow -l^2} ds_{(r>l)}^2 = -\frac{dr^2}{\frac{r^2}{l^2} - 1} + r^2 d\Omega_{d-1}^2. \quad (2.2)$$

The  $AdS$  boundary at  $r \rightarrow \infty$  maps to the  $dS$  future boundary  $I^+$  at  $r \rightarrow \infty$ , and the  $AdS$  region  $r \in [L, \infty]$  maps to the  $dS$  future universe  $F$  parametrized by  $r \in [l, \infty]$  (and  $r$  is time here). The  $dS$  hemisphere  $r < l$  is  $\tau_E = -it = [0, \frac{\pi}{2}]$  where  $-\frac{dr^2}{\frac{r^2}{l^2} - 1} > 0$  is Euclidean.

The IR  $dS$  surface starts at the boundary of the maximal subregion of the  $S^{d-1}$  (i.e. hemisphere) so it is anchored on the equator of the  $S^{d-1}$  (blue shadow in Figure 1) and wraps the equatorial  $S^{d-2}$ . From (2.2), it is clear that the IR  $dS$  extremal surface becomes a space-time rotation of that in  $AdS$ . Its area continues as

$$\begin{aligned} \frac{V_{S^{d-2}}}{4G_{d+1}} \int_0^{R_c} \frac{r^{d-2} dr}{\sqrt{1 + \frac{r^2}{L^2}}} &\xrightarrow{L \rightarrow -il} \frac{V_{S^{d-2}}}{4G_{d+1}} \int_0^l \frac{r^{d-2} dr}{\sqrt{1 - \frac{r^2}{l^2}}} + \frac{V_{S^{d-2}}}{4G_{d+1}} \int_l^{R_c} r^{d-2} \sqrt{\frac{dr^2}{-(\frac{r^2}{l^2} - 1)}} , \\ &= \frac{1}{2} \frac{l^{d-1} V_{S^{d-1}}}{4G_{d+1}} - i \# \frac{l^{d-1}}{4G_{d+1}} \frac{R_c^{d-2}}{l^{d-2}} + \dots \end{aligned} \quad (2.3)$$

where the  $\dots$  are subleading imaginary terms. For  $AdS_4 \rightarrow dS_4$  and  $AdS_3 \rightarrow dS_3$ , we obtain

$$\frac{V_{S^1}}{4G_4} \int_0^{R_c} \frac{r dr}{\sqrt{1 + \frac{r^2}{L^2}}} = \frac{\pi L^2}{2G_4} \left( \frac{R_c}{L} - 1 \right) \xrightarrow{L \rightarrow -il} -i \frac{\pi l^2}{2G_4} \frac{R_c}{l} + \frac{\pi l^2}{2G_4} = S_{dS_4}^{IR}, \quad (2.4)$$

$$\frac{V_{S^0}}{4G_3} \int_0^{R_c} \frac{dr}{\sqrt{1 + \frac{r^2}{L^2}}} = \frac{2L}{4G_3} \log \frac{2R_c}{L} \xrightarrow{L \rightarrow -il} -i \frac{l}{2G_3} \log \frac{2R_c}{l} + \frac{\pi l}{4G_3} = S_{dS_3}^{IR}. \quad (2.5)$$

We continue to focus on these IR extremal surfaces pertaining to maximal subregions here.

The fact that the  $dS$  areas arise from analytic continuations from  $AdS$  suggests a natural way to obtain the no-boundary de Sitter extremal surface areas through a heuristic replica argument [22] involving an analytic continuation of the Lewkowycz-Maldacena formulation [59] in  $AdS$  to derive RT entanglement entropy (generalized in [63], [64], [65]; see also [66] and the review [11]). In  $AdS$ , the boundary replica space  $M_n$  extends into a smooth  $n$ -sheeted bulk replica space  $\tilde{\mathcal{B}}_n$  which is a smooth covering space with replica boundary conditions. The quotient  $\tilde{\mathcal{B}}_n$  of the bulk space by the  $\mathbb{Z}_n$  replica symmetry (so its boundary is  $\partial\tilde{\mathcal{B}}_n = M_n/\mathbb{Z}_n = M_1$ , the original boundary space) contains conical (orbifold) singularities corresponding to  $\mathbb{Z}_n$  fixed points in the bulk for  $n \neq 1$ . These reflect the fact that the bulk quotient space is a solution to the bulk Einstein equations only in the presence of a source with nontrivial backreaction. The fixed points extend out from the subregion boundary so the required source is a codim-2 (cosmic) brane with tension  $\frac{n-1}{n} \frac{1}{4G}$  (giving deficit angle  $2\pi - \frac{2\pi}{n}$ ) and area  $A$  (wrapping all the transverse directions). The smooth action is  $I_n = nI_1 + I_{brane}$  with  $I_{brane} = \frac{n-1}{n} \frac{A}{4G}$ . Defining the bulk partition function  $Z_n \equiv Z[\tilde{\mathcal{B}}_n]$  on the replica quotient space  $\tilde{\mathcal{B}}_n$ , the entropy via replica is  $S = -\lim_{n \rightarrow 1} n\partial_n(\log Z_n - n \log Z_1) = -\lim_{n \rightarrow 1} (1 - n\partial_n)I_n$  in the semiclassical approximation where  $Z_n \sim e^{-I_n}$ , with  $I_n$  the action. Thus as  $n \rightarrow 1$ , we obtain  $S = \frac{A}{4G}$  which is the area of the extremal RT/HRT entangling surface. The analytic continuation from  $AdS$  and the  $dS/CFT$  dictionary  $Z_{CFT} = \Psi_{dS}$  gives

$$Z_{bulk} \sim e^{-I_{bulk}} \longrightarrow \Psi_{dS} \sim e^{iS_{cl}} \sim e^{iS^{(r>l)}} e^{S_E^{(r<l)}} \quad (2.6)$$

enabling a heuristic understanding of boundary entanglement entropy [22] in the Euclidean CFT dual to  $dS$  via replica. Semiclassically, the Wavefunction is given by the action, the top Lorentzian part (with real  $S^{(r>l)}$ ) being a pure phase while the bottom Euclidean hemisphere has real action. We pick boundary Euclidean time slices as  $S^d$  equatorial planes at  $I^+$  (*i.e.* some  $S^{d-1}$ ) and consider the IR extremal surface obtained from the maximal subregion (half the  $S^{d-1}$ ). We construct  $n$  copies and appropriately glue them cyclically, with replica boundary conditions. The  $n$ -copy replica Wavefunction  $\Psi_n$  on the quotient bulk replica space satisfies, semiclassically,  $Z_n \sim e^{-I_n} \rightarrow \Psi_n \sim e^{iS_n}$  with  $-I_n \rightarrow iS_n = iS_n^{(r>l)} + S_E^{(r<l)}$ . The codim-2 brane source generating the conical singularities for  $n \neq 1$  has nontrivial (part Euclidean, part Lorentzian) time evolution: in the  $n \rightarrow 1$  limit it satisfies the no-boundary condition and wraps the will-be no-boundary  $dS$  extremal surface. Now continuing from above gives  $-I_{brane} \rightarrow -\frac{n-1}{n} \frac{A_{brane}}{4G}$  and  $S_t = \lim_{n \rightarrow 1} (1 - n\partial_n) \log \Psi_n = \frac{A_{brane}}{4G}$  as the area/entropy in  $dS$ , giving boundary entanglement entropy in the dual ghost-like Euclidean CFT. A crucial point here is that since the analytic continuation maps  $Z_{bulk}^{AdS}$  to the de Sitter Wavefunction  $\Psi_{dS}$ , this is now a replica formulation on  $\Psi_{dS}$ , considering the  $dS/CFT$

dictionary  $Z_{CFT} = \Psi_{dS}$  [6]. With the Wavefunction  $\Psi_{dS}$  regarded as an amplitude (or transition matrix from “nothing”), this gives pseudo-entropy. In particular the codim-2 brane that smooths out bulk (orbifold) singularities is now a time-evolving, part Euclidean, part timelike, brane: this gives a complex area semiclassically. In this Lewkowycz-Maldacena formulation, the area of these no-boundary  $dS$  extremal surfaces arises as the amplitude for cosmic brane creation. So it is important that the divergent pieces of the area arising from near the future boundary are pure imaginary, since otherwise this amplitude would diverge. As it is, there is a finite probability: the real part arises from the maximal hemisphere, with size set by  $dS$  entropy. In [23], no-boundary extremal surfaces in slow-roll inflation models were studied (see App. A.3): there are new features in the area integrals which must be defined carefully as complex-time-plane integrals with appropriate time contours (Figure 10). In the end the cosmic brane probability matches the corresponding parts in the Wavefunction, vindicating the above picture.

The above Lewkowycz-Maldacena replica is fuelled by the analytic continuation. In what follows, we will flesh this out more elaborately, without recourse to analytic continuation.

### 3 de Sitter quotient geometries

In this section we will study explicit quotient metrics near  $n = 1$  for various de Sitter like spaces (which are similar to Fursaev’s constructions [67]) and recover boundary entanglement entropy by evaluating the areas of no-boundary  $dS$  extremal surfaces in [19, 22] (reviewed in sec. 2). In subsequent sections, we will construct smooth bulk replica geometries for various  $dS$  spaces, which we will then use to construct boundary Renyi entropies via  $dS/CFT$ .

Denoting the bulk quotient space as  $B_n/Z_n = O_n$ , near  $n = 1$  we have  $O_{1+\epsilon} = O_1 = B_1$  which is the original space (*e.g.*  $dS_{d+1}$ ). Including the cosmic brane as explicit source gives a smooth description of the bulk+brane space: the cosmic brane action is  $I_{brane} = \frac{n-1}{n} \frac{A_{brane}}{4G}$  with  $A_{brane}$  the area given by the action over the singular locus. Near  $n = 1$  we expand as  $n = 1 + \epsilon$  and obtain  $I[B_{1+\epsilon}] = (1 + \epsilon)I[B_1] + \epsilon \frac{A_{brane}}{4G}$ , which gives the extremal surface area as the entropy

$$S = \lim_{n \rightarrow 1} n \partial_n (I[B_n] - nI[B_1]) = \partial_\epsilon (I[B_{1+\epsilon}] - (1 + \epsilon)I[B_1]) = \frac{A_{brane}}{4G}. \quad (3.1)$$

We thus recover the entropy or extremal surface area through the  $n \rightarrow 1$  limit of a family of quotient spaces. Thus the boundary entanglement entropy in these no-boundary  $dS$ -like spaces is obtained using the above arguments and the  $dS/CFT$  dictionary  $Z_{CFT} = \Psi_{dS}$  with

$$\log Z_n^{CFT} = \log \Psi_n \equiv -I[B_n]; \quad \log \Psi_n = n \log \Psi_1 - nI_{brane}, \quad (3.2)$$

with  $I[B_n]$  comprising the Euclidean part (from the hemisphere) and the Lorentzian part (and  $\Psi_1$  indicates a single copy). We obtain

$$\mathcal{S} = -n\partial_n(\log Z_n^{CFT} - n\log Z_1^{CFT})|_{n=1} = -n\partial_n(\log \Psi_n - n\log \Psi_1)|_{n=1} = \frac{A_{brane}}{4G}. \quad (3.3)$$

We will now display quotient metrics, valid near  $n = 1$ , in various  $dS$ -like spaces and use the above.

### 3.1 $dS_3$ quotient and boundary EE

We first consider the calculation of no-boundary extremal surfaces and the associated boundary entanglement entropy (or bulk pseudo-entropy) in  $dS_3$ . We will compute the pseudo-entropy in two different but equivalent ways. First, we will consider  $dS_3$  and an appropriate quotient geometry, and thereby obtain the pseudo-entropy via cosmic branes. Second, we will follow [68] to obtain the pseudo-entropy directly from the on-shell action (App. C).

As reviewed in sec. 2, recall that we had defined boundary Euclidean time slices as equatorial ( $S^1$ ) planes of the  $S^2$  at  $I^+$  and then defined the IR boundary subregion as the half circle on that  $S^1$ . The extremal surface then stretches out into the bulk  $r$ -direction from the semicircle endpoints giving the areas (2.1), (2.5). In the present context, we consider the boundary Euclidean time slice as some  $\theta_2 = \text{const}$  slice: the IR subregion is then the interval defined by  $\theta_1 = [0, \pi]$  on that slice, and the endpoints are the North/South Poles (Figure 2).

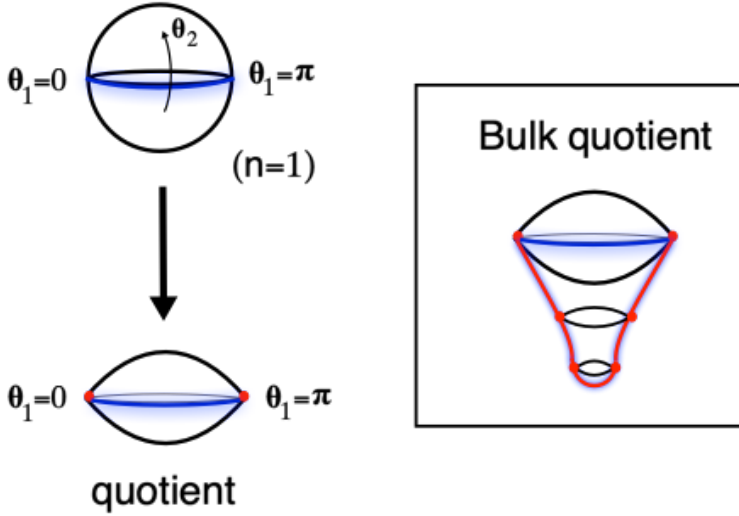


Figure 2: The boundary  $S^2$  with the IR subregion  $\theta_1 = [0, \pi]$  on the boundary Euclidean time slice given by the equatorial plane  $\theta_2 = 0$ . The quotient space arises from the replica-like space with  $n$  copies, and contains conical singularities at the North/South Pole endpoints. The box shows the bulk quotient space and the cosmic brane (red).

Thus consider the quotient metric

$$ds^2 = -\frac{dr^2}{\frac{r^2}{l^2} - 1} + r^2(d\theta_1^2 + \frac{1}{n^2} \sin^2 \theta_1 d\theta_2^2). \quad (3.4)$$

For  $n = 1$ , this is global no-boundary  $dS_3$ . It is Lorentzian for  $r > l$  where  $r$  is a timelike direction and describes the Euclidean hemisphere for  $r < l$ . The sphere smoothly shrinks to zero size at  $r = 0$  which is the no-boundary point, implementing Hartle-Hawking boundary conditions. For  $n \gtrsim 1$ , this is akin to the singular spaces in [67], adequate near the  $n = 1$  limit to calculate boundary entanglement entropy (but not for Renyi entropies).

The  $S^2$  at  $n = 1$  is defined by the latitude angle  $\theta_1$  and the azimuthal angle  $\theta_2$ , with ranges  $\theta_1 = [0, \pi]$  and  $\theta_2 = [0, 2\pi]$ . In (3.4), roughly speaking, the azimuthal  $\theta_2$ -direction is squashed so the equator of original size  $2\pi$  now has size  $\frac{2\pi}{n}$ : thus we have the (approximate) shape of a rugby ball (or American football), with conical singularities at the North and South poles (Figure 2),  $\theta_1 = 0$  and  $\theta_1 = \pi$ . These singularities apart, the metric is locally  $dS_3$  with  $R = 6/l^2$ ; at  $n = 1$  the space is  $dS_3$ . The bulk metric in the vicinity of the singular locus is  $ds^2 = -\frac{dr^2}{\frac{r^2}{l^2}-1} + r^2(d\theta_1^2 + \frac{\theta_1^2}{n^2}d\theta_2^2)$ . The singular locus runs along the  $r$ -direction, starting at the future boundary  $I^+$  at the North Pole ( $\theta_1 = 0$ ), down the Lorentzian  $r$ -direction to the complexification point  $r = 1$  and then along the Euclidean hemisphere to the no-boundary point  $r = 0$  and back to  $r = 1$ , up the Lorentzian  $r$ -direction at the South Pole ( $\theta_1 = \pi$ ) to  $I^+$ . At  $n = 1$ , this traces out the no-boundary extremal surface. With  $n \gtrsim 1$  this family of metrics represent the conical spacetime geometry (with deficit angle  $2\pi\frac{n-1}{n}$  from the  $\theta_2$ -periodicity  $\frac{2\pi}{n}$ ) sourced by cosmic branes of tension  $\frac{n-1}{n} \frac{1}{4G}$  at the singular loci above.

We will focus on this quotient space (3.4) analytically continuing  $n$  to non-integer values near  $n = 1$ . Then the space is almost smooth with mild conical singularities. Taking  $n = 1 + \epsilon$  the deficit angle is  $2\pi\epsilon$  upto  $O(\epsilon)$ . Following [69], we can calculate curvature invariants due to the conical singularity: for (3.4) we have

$$\int d^3x \sqrt{g} \mathbf{R} = 4\pi \left(1 - \frac{1}{n}\right) \int dr \sqrt{g_{rr}} + \frac{1}{n} \int d^3x \sqrt{g} \mathbf{R}_{dS}, \quad (3.5)$$

where  $\mathbf{R}_{dS}$  is the Ricci scalar  $\frac{6}{l^2}$  of the smooth  $dS_3$  space. Note that this is no-boundary  $dS_3$ , with  $\sqrt{g_{rr}} = \frac{1}{\sqrt{1-r^2/l^2}}$  defined in the Euclidean hemisphere region  $r < l$  and then continued to the Lorentzian region  $r > l$ . The above equation is schematically of the form  $I[B_n/\mathbb{Z}_n] = I_{brane} + \frac{1}{n}I[B_1]$  (and  $O_1 = B_1$ ), so multiplying by  $n$  essentially gives the analog of (3.1). Then employing the arguments there, we recover the associated entropy which gives the extremal surface area (one could have instead equivalently used a version of the replica formula for the quotient space object  $I[O_n] \equiv I[B_n/\mathbb{Z}_n]$  without the extra  $n$ -factor). The area of this 1-dimensional surface in the entropy (3.3) is then as given in (2.1), (2.5). The factor of 2 in (2.3) is  $V_{S^0}$  which can be interpreted as the two halves of the cosmic brane curve in the  $r$ -direction, along  $R_c \rightarrow l \rightarrow 0 \rightarrow l \rightarrow R_c$ .

We have thus obtained boundary entanglement entropy in  $dS_3/CFT_2$  from the quotient  $dS_3$  via  $Z_{CFT} = \Psi_{dS}$ . We now derive this result in an alternative way, generalizing the

arguments in [68]. The semiclassical Wavefunction  $\Psi_1 \sim e^{iI}$  of no-boundary  $dS_3$  is (App. C)

$$\log \Psi_1 = \frac{1}{16\pi G_3} \left( 4\pi^2 l - 8i\pi l \log\left(\frac{2R_c}{l}\right) + 8i\pi \frac{R_c^2}{l} - 4i\pi l \right). \quad (3.6)$$

$\Psi_1$  indicates a single copy here. The spherical symmetry of the boundary  $S^2$  implies that the boundary stress tensor is symmetric: this can then be used to trade the  $\partial_n$  derivative of  $\log Z_{CFT}$  in the Weyl anomaly of the  $CFT$  on  $S^2$  for  $\partial_{R_c}$ , following the arguments in [68] (which do not depend on unitarity of the CFT). Thus, using the  $dS/CFT$  dictionary  $Z_1^{CFT} = \Psi_1^{dS}$ , we obtain the boundary entanglement entropy

$$\mathcal{S} = \left( 1 - \frac{R_c}{2} \partial_{R_c} \right) \log \Psi_1 = \frac{\pi l}{4G_3} - i \frac{l}{2G_3} \log\left(\frac{2R_c}{l}\right). \quad (3.7)$$

It is important to note that in this calculation, the  $AdS$  analytic continuation (C.11) employed renders the sign of the leading divergence to be the opposite of that in (C.7), (C.4). This in turn ensures that the first subleading term in (3.6) then has the same sign as the extremal surface area (3.7). Relatedly, the first subleading term in (3.6) differs by a factor of  $l^2$  from the leading term, which thus contributes one relative minus sign under the  $AdS \rightarrow dS$  analytic continuation: thus  $L \rightarrow \pm il$  lead to  $\pm i$  in the imaginary part in the extremal surface area (3.7) above. Further comments appear in sec. 8.2.

### 3.2 $dS_4/CFT_3$ boundary EE via replica quotient

In this subsection we discuss a  $dS_4$  quotient geometry along the same lines as for  $dS_3$  above. The metric of the  $n$ -quotient  $dS_4$  space is

$$ds^2 = -\frac{dr^2}{\frac{r^2}{l^2} - 1} + r^2 \left( d\theta_1^2 + \frac{1}{n^2} \sin^2 \theta_1 d\theta_2^2 + \cos^2 \theta_1 d\theta_3^2 \right). \quad (3.8)$$

The  $n$  factor here is similar to that in (3.4) for the  $dS_3$  quotient. The geometry near  $\theta_1 = 0$  is  $ds^2 = -\frac{dr^2}{\frac{r^2}{l^2} - 1} + r^2 (d\theta_1^2 + \frac{\theta_1^2}{n^2} d\theta_2^2 + d\theta_3^2)$ . Thus the angles  $\theta_1, \theta_2$  define the 2-dim cone at the tip of which the cosmic brane is localized, generating the conical singularity. The  $S^3$  geometry in (3.8) for  $n = 1$  is the Hopf fibration: this description dovetails with the boundary subregion as reviewed in sec. 2 as follows. We define the boundary Euclidean time slice as some  $\theta_2 = \text{const}$  slice, giving  $d\theta_1^2 + \cos^2 \theta_1 d\theta_3^2$  defining an  $S^2$ . The equator here is  $\theta_1 = 0$  while the North/South Poles are  $\theta_1 = \frac{\pi}{2}$ . The boundary of the maximal (hemispherical) subregion on this  $S^2$  is the equator at  $\theta_1 = 0$ . The cosmic brane thus extends out from  $I^+$  from this subregion boundary, wrapping the equatorial  $S^1$  parametrized by  $\theta_3$  and going along the bulk  $r$ -direction over  $0 \rightarrow l \rightarrow R_c$ : its action/area is

$$\mathcal{S} \equiv \frac{A_{brane}}{4G_4} = \frac{V_{S^1}}{4G_4} \int_0^l \frac{r dr}{\sqrt{1 - \frac{r^2}{l^2}}} + \frac{V_{S^1}}{4G_4} \int_l^{R_c} \frac{r dr}{\sqrt{-\left(\frac{r^2}{l^2} - 1\right)}} = -i \frac{\pi l^2}{2G_4} \frac{R_c}{l} + \frac{\pi l^2}{2G_4}, \quad (3.9)$$

which gives the  $dS_4/CFT_3$  boundary entanglement entropy as the no-boundary  $dS_4$  IR extremal surface area, using (3.3), (C.1), (C.5), (C.6): this matches (2.4). The analog of (3.5) useful for the action calculation here is  $\int \mathbf{R} = 4\pi(1 - \frac{1}{n})A_{brane} + \frac{1}{n}\int \mathbf{R}_{dS}$  with the conical singularity giving a  $\delta$ -function which when integrated over the  $S^3$  reduces to  $A_{brane}$ .

We can also recover this from the semiclassical Wavefunction for a single copy

$$\log \Psi_1 = \frac{\pi l^2}{2G_4} - i \frac{\pi R_c^3}{8G_4} \left( -\frac{4}{l} + \frac{6l}{R_c^2} \right). \quad (3.10)$$

Then following [68] and using the boundary  $S^3$  spherical symmetry, we can obtain the boundary entanglement entropy in  $dS_4/CFT_3$  as

$$\mathcal{S} = \left( 1 - \frac{R_c}{3} \partial_{R_c} \right) \log \Psi_1 = \frac{\pi l^2}{2G_4} - i \frac{\pi l^2}{2G_4} \frac{R_c}{l}, \quad (3.11)$$

along the lines of (3.7). The above answer matches (3.9) obtained from the explicit quotient metric and cosmic brane.

The expression for  $\log \Psi_1$  above can also be obtained from the Euclidean  $AdS_4$  partition function with the analytic continuation (C.11). Thus, as in the comments after (3.7), we note that relative to (C.5), the signs of the imaginary terms in  $\log \Psi_1$  here have been reversed by the analytic continuation  $L \rightarrow -il$ , which then ensures that the divergent term in the entropy above (which differs by one  $l^2$ -factor from the leading divergence in  $\log \Psi$ ) matches that in the extremal surface area.

**$dS_{d+1}$  quotient:** Considering a general  $dS_{d+1}$  space ( $d > 2$ ), the  $n$ -quotient metric near  $n = 1$  is

$$ds^2 = -\frac{dr^2}{\frac{r^2}{l^2} - 1} + r^2 \left( d\theta_1^2 + \frac{1}{n^2} \sin^2 \theta_1 d\theta_2^2 + \cos^2 \theta_1 d\Omega_{d-2}^2 \right), \quad (3.12)$$

where  $d\Omega_{d-2}^2$  is the metric of  $S^{d-2}$ . As in the earlier analysis,  $\theta_1, \theta_2$  form a cone. This gives

$$I = \frac{n-1}{n} \frac{V_{S^{d-2}}}{4G_{d+1}} \int_0^{R_c} dr r^{d-2} \frac{1}{\sqrt{1 - \frac{r^2}{l^2}}}, \quad (3.13)$$

as the cosmic brane action and thereby the entropy via (3.3) (matching (2.3)). We can also obtain the entanglement entropy by continuing the  $AdS$  action to  $dS$  with  $L \rightarrow -il$  and then using the formula,

$$\mathcal{S} = \left( 1 - \frac{R_c}{d-1} \partial_{R_c} \right) \log \Psi_1, \quad (3.14)$$

with  $R_c$  the UV cutoff near the future boundary.

Various generalizations of these quotient constructions can be analysed: see App. A.1 for future-past extremal surface areas (see also [70] for related discussions in a slightly different context), App. A.2 for real extremal surfaces in the Euclidean sphere giving  $dS$  entropy, and App. A.3 for slow-roll no-boundary extremal surfaces.

## 4 de Sitter replicas: boundary Renyi via $dS/CFT$

In general we imagine constructing a bulk replica (covering) space  $B_n$  comprising  $n$  copies of the original space  $B_1$  glued together with replica boundary conditions: this is a branched cover branched over the subregion boundary, and we go from the  $k$ th copy to the next cyclically. If we now quotient this space by the  $\mathbb{Z}_n$  replica symmetry which permutes the  $n$  copies, then we obtain an orbifold-like space with conical singularities localized at the  $\mathbb{Z}_n$  fixed points. The quotient space can be interpreted as the backreacted geometry of codim-2 cosmic branes which are localized at the locus that becomes the extremal surface. As  $n \rightarrow 1$ , there is no backreaction: the tensionless cosmic brane becomes the extremal surface.

At finite  $n$  however, this requires new bulk geometries that satisfy replica boundary conditions at the holographic boundary and are smooth in the bulk with no singularities. This requirement of a smooth bulk replica space is in accord with  $AdS/CFT$  intuition as pointed out in [71], where we require bulk perturbations to satisfy regularity conditions in the interior. This logic, implemented by Lewkowycz-Maldacena [59], and implicit in [66] for entanglement entropy and developed in detail in [60] for Renyi entropies (see also [72, 73]), is conceptually and technically distinct from the quotient spaces (akin to [67]) discussed in the previous section.

In this section we will describe smooth bulk  $dS$ -like replica spaces which we will then use to calculate boundary Renyi entropies using the  $dS/CFT$  dictionary  $Z_1^{CFT} = \Psi_1^{dS}$  [6] where the subscript 1 denotes a single copy ( $n = 1$ ). The boundary Renyi entropy for the replica- $n$  geometry with  $Z_n^{CFT} = \Psi_n^{dS}$  is defined by

$$S_n = \frac{1}{1-n} \log \left( \frac{Z_n}{Z_1^n} \right) = \frac{1}{1-n} \log \left( \frac{\Psi_n}{\Psi_1^n} \right) \sim i \frac{I_n - nI_1}{1-n}, \quad (4.1)$$

where the Wavefunction in the semiclassical regime is  $\Psi_n \sim e^{iI_n}$ , with  $I_n$  the action for the replica- $n$  space. Our  $dS$  analysis has close parallels with the  $AdS$  studies in [59] and [60]. We describe  $dS_3$  first, and then  $dS_4$  and higher dimensional  $dS$ .

It is worth noting that the broad logic of our replica construction in these cosmological cases is along the lines of the generalization of [59] in [63] to the general time-dependent  $AdS$  context. However several central aspects here are really features in de Sitter with the spacelike future boundary and  $dS/CFT$  in mind, and so have no analog in  $AdS$  (which pertain to spacelike surfaces anchored on the timelike boundary, even when there is nontrivial time dependence). For instance, bulk time is not boundary (Euclidean) time here: the maximal subregions at  $I^+$  considered throughout this work lie on boundary Euclidean time slices (well-defined given the existence of boundary spatial isometries), which are essentially “vertical” slices in the bulk. The extremal surfaces lie on these slices of the bulk geometry

and dip into the bulk time direction (Figure 1), with timelike components necessarily arising (due to the absence of  $I^+ \rightarrow I^+$  turning points [12]). Overall the picture here is a space-time rotation of the  $AdS$  story, and so is more analogous to the  $AdS$  RT formulation on constant time slices turned sideways (akin to [15, 17]), than HRT with time dependence. Thus in an essential sense, we expect the full richness of [63] to only enter for generic subregions (and their correspondingly more complicated extremal surfaces). Likewise, the replica space also exhibits new geometric features as we will see: for instance, the cosmic brane locus is not spacelike and relatedly, a boundary replica on  $Z_{CFT}$  translates to a bulk replica on  $\Psi_{dS}$  as we already saw in sec. 2, reviewing [22]. Here this results in (4.1), a complex-valued pseudo-Renyi-entropy in general. In the end, it will turn out that our formulations here amount to analytic continuation from  $AdS$  (which executes the space-time rotation), so in some essential sense there are of course close interrelations between our analysis here and that in [59], [60], [63]. At various places in the text, we will try to highlight specific novel features, from an intrinsically  $dS$  perspective.

## 4.1 $dS_3$ replica geometry: boundary Renyi

Consider the 3-dim geometry described by

$$ds^2 = -\frac{dr^2}{\frac{r^2}{l^2} - \frac{1}{n^2}} + \left( \frac{r^2}{l^2} - \frac{1}{n^2} \right) dt^2 + r^2 d\phi^2, \quad \phi \equiv \phi + 2\pi n. \quad (4.2)$$

This has  $R = \frac{6}{l^2}$ . For  $n = 1$ , this is  $dS_3$  in the static coordinatization. The  $r > \frac{l}{n}$  region describes the future and past universes with  $g_{rr} < 0$  and  $r$  is bulk time. The  $r < \frac{l}{n}$  region is the static patch where  $g_{tt} < 0$  and  $t$  is the time coordinate.

For large  $r \rightarrow \infty$ , the metric approaches  $ds^2 \sim -l^2 \frac{dr^2}{r^2} + r^2 (\frac{dt^2}{l^2} + d\phi^2)$  so the boundary space has replica boundary conditions with  $t$  noncompact but  $\phi \equiv \phi + 2\pi n$ . One way to understand this as a replica space is as follows: start with the boundary space as a 2-sphere  $S^2$  and then make a boundary conformal transformation to the cylinder, with the boundary metrics

$$ds^2 = \sin^2 \theta \left( \frac{d\theta^2}{\sin^2 \theta} + d\phi^2 \right) \quad \rightarrow \quad ds'^2 = dt^2 + d\phi^2, \quad (4.3)$$

where  $t = \int \frac{d\theta}{\sin \theta}$  is now the noncompact cylinder length direction. This is essentially the sphere-to-cylinder map familiar from radial quantization around the North pole of the  $S^2$ , the latitudes  $\theta = \text{const}$  now becoming  $t = \text{const}$  slices. Now consider a  $\phi = 0$  slice regarded as a boundary Euclidean time slice of the  $S^2$  and the (maximal) subregion defined by a semicircle  $\theta = [0, \pi]$ : in terms of the cylinder picture, this is a “longitudinal” slice  $\phi = 0$  with the subregion defined by the entire line  $t = [-\infty, \infty]$  on this slice. A replica space corresponding to  $n$  copies of this subregion can be constructed by introducing a cut along

this  $t$ -line in each cylinder copy and joining the cylinder copies  $k$  to  $k + 1$  along the cuts cyclically. Since the cylinder copies are being glued along their entire length directions, the effective cross-section enlarges thus making a “fatter” replica-cylinder with cross-section angle  $\phi$ -periodicity  $2\pi n$ . For  $n = 2$  this is depicted in Figure 3.

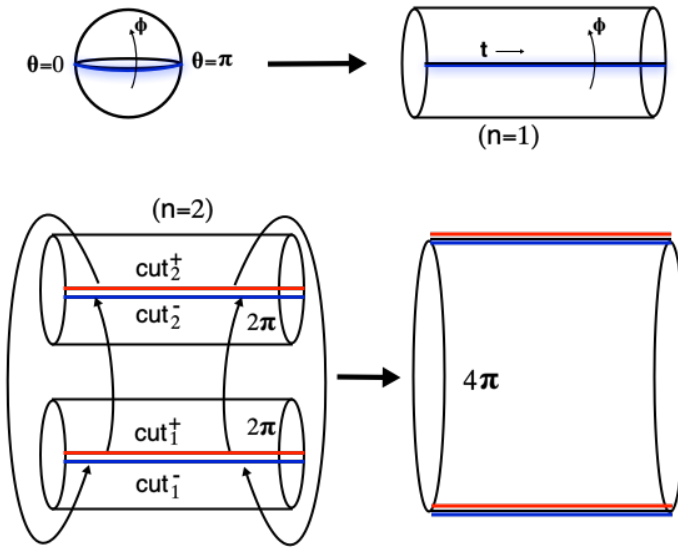


Figure 3: Depicted (top) is the boundary  $S^2$  with a conformal transformation to the cylinder. Also shown is the maximal (IR) subregion as the semicircle  $\theta = [0, \pi]$  on the boundary Euclidean time slice given by the equatorial plane  $\phi = 0$ , which maps to a line along the entire cylinder length. The bottom shows the  $n = 2$  replica space obtained by gluing two copies of the cylinder cyclically along the cuts as  $1^+ \rightarrow 2^- \rightarrow 2^+ \rightarrow 1^-$  and back to  $1^+$ . Since the gluing is along the entire cylinder length, this gives a fatter cylinder with  $\phi$ -periodicity  $4\pi$ .

The bulk geometry above is then constructed as a smooth geometry whose future boundary satisfies these replica boundary conditions. Thus the  $n$ -factors in (4.2) have been fixed by demanding regularity of the full geometry. For instance starting with

$$ds^2 = -\frac{dr^2}{f(r)} + f(r)dt^2 + r^2d\phi^2, \quad f(r) = \frac{r^2}{l^2} - r_h^2, \quad (4.4)$$

satisfying replica boundary conditions at the future boundary  $r \rightarrow \infty$ , and requiring that the metric near  $r = 0$  is smooth with no conical singularities gives

$$ds^2 \sim -r_h^2dt^2 + \frac{dr^2}{r_h^2} + n^2r^2d\tilde{\phi}^2 \quad \Rightarrow \quad r_h = \frac{1}{n}, \quad (4.5)$$

where we have redefined  $\tilde{\phi} \equiv \frac{\phi}{n}$  which has periodicity  $2\pi$ . Near  $r \gtrsim r_h$  this metric becomes  $ds^2 \sim -\frac{dr^2}{2r_h(\frac{r}{l} - r_h)} + 2r_h(\frac{r}{l} - r_h)dt^2 + r_h^2l^2d\phi^2 \equiv -d\rho^2 + \frac{\rho^2}{n^2l^2}dt^2 + l^2d\tilde{\phi}^2$  which is ordinary regular Milne in the  $(\rho, t)$ -subplane (since  $t$  is noncompact) and in the  $(\rho, \tilde{\phi})$ -subplane. Further since  $t$  is a noncompact direction, there are no issues with closed timelike curve pathologies (unlike if the blackening  $f(r)$  factor appeared in  $g_{\tilde{\phi}\tilde{\phi}}$ ). Thus we recover the smooth  $dS_3$ -like replica space (4.2). As an interesting aside, it is worth noting that this geometry can be realized as an analytic continuation  $l^2 \rightarrow -L^2$  from the corresponding  $AdS_3$ -like geometry with replica boundary conditions studied by Lewkowycz-Maldacena [59].

**Boundary Renyi entropies:** We will now evaluate the boundary Renyi entropies in  $dS/CFT$  using (4.1). Towards this, we use the (bare) action (which is (C.1))

$$16\pi G_3 \tilde{I} = \int d^3x \sqrt{-g} \left( R - \frac{2}{l^2} \right) - 2 \int d^2x \sqrt{\gamma} K, \quad (4.6)$$

with the extrinsic curvature at the future boundary  $r = R_c$  given by

$$K = \frac{1}{\sqrt{-g}} \partial_r (\sqrt{-g} n^r) = \frac{1}{lr} \partial_r \left( lr \sqrt{\frac{r^2}{l^2} - n^{-2}} \right) \xrightarrow{r \rightarrow R_c} \frac{2R_c^2 - l^2 n^{-2}}{l^2 R_c \sqrt{\frac{R_c^2}{l^2} - n^{-2}}}. \quad (4.7)$$

Then the action for the replica geometry (4.2), using  $R = \frac{6}{l^2}$ , is

$$\tilde{I}_n = \frac{1}{16\pi G_3} \int r d\phi dt dr \frac{4}{l^2} - \frac{2}{16\pi G_3} \int d\phi dt R_c \sqrt{\frac{R_c^2}{l^2} - \frac{1}{n^2}} K = \frac{4\pi n}{16\pi G_3 l^2} L_t (n^{-2} l^2 - R_c^2), \quad (4.8)$$

where  $L_t = \int dt$  which we will evaluate below. We now add a counterterm to remove divergences and render the action finite:

$$I_{ct} = \frac{\Lambda}{16\pi G_3} \int d^2x \sqrt{\gamma} = \frac{\Lambda}{16\pi G_3} \int d\phi dt R_c \sqrt{\frac{R_c^2}{l^2} - n^{-2}} \sim \frac{\Lambda 2\pi n}{16\pi G_3} \frac{L_t}{l} \left( R_c^2 - \frac{l^2}{2n^2} \right). \quad (4.9)$$

Choosing  $\Lambda = \frac{2}{l}$  gives the regulated action

$$I_n = \tilde{I}_n + I_{ct} = \frac{2\pi n}{16\pi G_3 l^2} L_t n^{-2} l^2. \quad (4.10)$$

Now we note that  $L_t = \int dt = \int_0^\pi \frac{d\theta}{\sin \theta}$  is the length of the subregion given by the semicircle interval stated above. This however diverges over  $\theta \in [0, \pi]$ , so we regulate as  $\theta = [\delta, \pi - \delta]$ .

This gives

$$L_t = 2 \log \left( \frac{2}{\delta} \right) \equiv 2 \log \left( \frac{2R_c}{l} \right), \quad (4.11)$$

where we have identified  $\delta = \frac{l}{R_c}$  to match the known boundary entanglement entropy at  $n = 1$  with the extremal surface area. Thus using the regulated actions, we finally obtain the boundary Renyi entropy (4.1) as

$$S_n = \frac{i}{1-n} \frac{2\pi n}{16\pi G_3 l} L_t l (n^{-2} - 1) = \left( 1 + \frac{1}{n} \right) i \frac{l}{4G_3} \log \frac{2R_c}{l} \equiv \left( 1 + \frac{1}{n} \right) \frac{c}{6} \log \frac{2R_c}{l}, \quad (4.12)$$

where  $c = i \frac{3l}{2G_3}$  is the  $dS_3/CFT_2$  central charge [6]. The  $n \rightarrow 1$  limit gives the boundary entanglement entropy  $\frac{c}{3} \log \frac{2R_c}{l}$ , which is half the future-past extremal surface area [15, 19].

The Euclidean part of the  $dS_3$  replica space can be obtained from the  $r < \frac{l}{n}$  part of (4.2) with Euclidean time  $t \rightarrow i\tau_E$  and  $\tau_E = [0, \frac{\pi}{2}]$ . The Renyi entropy calculation with the Euclidean gravity action then gives

$$S_n^E = \left( 1 + \frac{1}{n} \right) \frac{l}{4G_3} \frac{L_{\tau_E}}{2} = \left( 1 + \frac{1}{n} \right) \frac{l}{4G_3} \frac{\pi}{2}, \quad (4.13)$$

with  $L_{\tau_E} = 2 \int_0^{\pi/2} d\tau_E = \pi$  arising from the great circle path in the hemisphere. Thus the boundary Renyi entropy for no-boundary  $dS_3$  is given by appending the Lorentzian and Euclidean contributions as

$$S_n^{nb} = \frac{1+n}{2n} \left( \frac{\pi l}{4G_3} + \frac{il}{2G_3} \log \frac{2R_c}{l} \right), \quad (4.14)$$

and the  $n \rightarrow 1$  limit gives the boundary entanglement entropy which matches the no-boundary extremal surface area (2.5), but with the imaginary part being  $+i$ , obtained via the analytic continuation  $L \rightarrow il$  in (2.5). In the present calculation we have used the expanding branch Wavefunction (C.7), (C.4), in contrast with (3.6) used in (3.7): see also the comments there.

**Cosmic brane:** While we have used the smooth replicated geometry (4.2) to evaluate the Renyi entropies, it is interesting to understand how this geometry is recast in terms of the boundary variables quotiented by the  $\mathbb{Z}_n$  replica symmetry. This is most easily seen by considering the same geometry (4.2) but featuring the quotient angle variable  $\tilde{\phi} = \frac{\phi}{n}$ , *i.e.*

$$ds^2 = -\frac{dr^2}{\frac{r^2}{l^2} - \frac{1}{n^2}} + \left( \frac{r^2}{l^2} - \frac{1}{n^2} \right) dt^2 + r^2 d\tilde{\phi}^2, \quad \tilde{\phi} \equiv \tilde{\phi} + 2\pi. \quad (4.15)$$

Now we see that there is a singularity at  $r = 0$ , with

$$ds^2 \sim -\frac{dt^2}{n^2} + n^2 dr^2 + r^2 d\tilde{\phi}^2 \quad (4.16)$$

revealing a conical deficit angle. The location  $r = 0$  in fact corresponds to the North and South poles of the  $S^2$  that we began with (before conformal transforming to the cylinder). In fact this quotient metric (4.15) can be recognized as Schwarzschild  $dS_3$  with metric in conventional form written as

$$ds^2 = -\left(1 - 8G_3 E - \frac{r^2}{l^2}\right) dt^2 + \frac{dr^2}{1 - 8G_3 E - \frac{r^2}{l^2}} + r^2 d\tilde{\phi}^2, \quad 8G_3 E = 1 - \frac{1}{n^2}, \quad (4.17)$$

with the black hole mass  $E$  encoding  $n$ . In this quotiented space, the singular locus at  $r = 0$  which is timelike in the Lorentzian region (and Euclidean in the hemisphere after Euclideanizing  $t \rightarrow i\tau_E$ ) can be recognized as the location of the cosmic brane for  $n \neq 1$ . In terms of the global structure of the geometry, the cosmic brane is localized as a timelike curve at the North and South poles in the Lorentzian part and wraps the great semicircle in the Euclidean hemisphere. In the  $n \rightarrow 1$  limit, this is the no-boundary extremal surface in  $dS_3$  extending out from the boundary of the subregion along the  $t$ -direction at the future boundary.

We have thus recovered the boundary Renyi entropies (4.1), (4.14), from a bulk replica calculation via  $dS/CFT$ . As can be seen the answer is structurally similar to those in ordinary unitary 2-dim CFTs with  $AdS_3$ -like gravity duals: as such, our analysis can also be realized as an analytic continuation from  $AdS_3$  which is not surprising since these are boundary quantities (analogous to dual operator correlation functions being analytic continuations [6]). In particular the  $n$ -dependence appears as a simple multiplicative factor. This might appear surprising since the dual CFT here is exotic with pure imaginary central charge  $c = i \frac{3l}{2G_3}$ , so in this sense our result here is a prediction for the dual CFT per se. However since we are considering fairly simple subregions, the boundary replica space is relatively simple (simply a fatter cylinder as we have seen, Figure 3) and in effect the Renyi entropies are only sensitive to the CFT central charge and not more intricate CFT data. It would be interesting to understand this better intrinsically in the CFT.

A more basic question is whether the  $dS_3$  replica geometry we have employed is the dominant one. In the current 3-dim case, it is very likely that this is in fact the unique geometry with these boundary conditions pertaining to the maximal subregion. In 3-dimensions, the only maximally symmetric geometries are de Sitter or Schwarzschild de Sitter. We have seen that the replica geometry (4.2) is mappable to ordinary  $dS_3$  after appropriately re-absorbing the  $n$ -factors into the coordinates so the replica space is just the smooth bulk completion of the boundary replica space. Likewise the boundary quotiented geometry is precisely Schwarzschild  $dS_3$  with the mass encoding the replica- $n$ . For generic non-maximal subregions or multiple subregions, the replica geometry is likely to be rather nontrivial, and would be interesting to understand. In this regard, it would appear that generalizations of the  $AdS_3/CFT_2$  studies in [74], [75], might be of relevance here: naively these suggest that the Renyi entropies would depend on detailed properties of the 2-dim CFT, nonunitary in the current  $dS_3$  case.

## 4.2 $dS_4$ replica geometry: boundary Renyi

Now we will consider replica geometries for  $dS_4$ -like spaces. The boundary here is the 3-sphere  $S^3$ : we consider some equatorial plane as the boundary Euclidean time slice (which gives an  $S^2$ ) and consider the maximal subregion comprising say the Northern hemisphere so its boundary is the  $S^1$  interface between the Northern/Southern hemispheres. Towards constructing the replicated geometries, we will find it convenient to instead consider hyperbolic boundary foliations of de Sitter since the corresponding  $AdS$  versions are known [60] and serve as a useful crutch. Pulling out a conformal factor in the  $S^3$  Hopf fibration gives  $\sin^2 \theta \left( d\phi^2 + \frac{d\theta^2 + \cos^2 \theta d\psi^2}{\sin^2 \theta} \right) \equiv \sin^2 \theta (d\phi^2 + dH_2^2)$ : this is analogous to the sphere-to-cylinder conformal transformation (4.3) in the  $dS_3$  case. However we will find it more convenient to

consider the boundary space in the form below (instead of the  $\theta$ -coordinate)

$$ds_3^2 = d\phi^2 + dH_2^2 = d\phi^2 + d\chi^2 + \sinh^2 \chi d\psi^2 \quad (4.18)$$

i.e. as  $S^1 \times H_2$ , with  $H_2$  the above 2-dim hyperbolic metric. Pure  $dS_4$  in this hyperbolic boundary conformal frame is

$$ds^2 = -\frac{dr^2}{f(r)} + l^2 f(r) d\phi^2 + r^2 dH_2^2, \quad f(r) = \frac{r^2}{l^2} + 1, \quad r = [il, 0] \cup [0, R_c]. \quad (4.19)$$

Here  $r$  is bulk time which is defined along a complex time-contour comprising a Lorentzian part over  $[0, R_c]$  (with  $R_c$  the future boundary cutoff) and a Euclidean part over  $[il, 0]$ . In the Euclidean part, the geometry can be mapped to  $S^4$  by also Wick rotating  $\chi = i\varphi$  as

$$r = i\rho, \quad \chi = i\varphi : \quad ds^2 = \frac{d\rho^2}{1 - \frac{\rho^2}{l^2}} + l^2 \left(1 - \frac{\rho^2}{l^2}\right) d\phi^2 + \rho^2 (d\varphi^2 + \sin^2 \varphi d\psi^2), \quad (4.20)$$

which is the Hopf fibration, the  $\phi$ -circle shrinking smoothly at  $\rho = l$  which is a complex zero of  $f(r)$  with  $r = il$ .

The analytic continuation  $l^2 \rightarrow -L^2$  applied to (4.19) gives

$$ds^2 = \frac{dr^2}{\frac{r^2}{L^2} - 1} + L^2 \left(\frac{r^2}{L^2} - 1\right) d\phi^2 + r^2 dH_2^2 \quad (4.21)$$

which is Euclidean  $AdS_4$  (with  $\phi \equiv it$  Wick-rotated from Lorentzian time  $t$ ) in hyperbolic foliations studied fruitfully in [60]: our analysis below of the Renyi story has close parallels with the  $AdS$  discussions there.

Consider now the  $\phi = 0$  slice and the maximal subregion defined by half the  $H_2$ , its boundary being the  $S^1$  parametrized by  $\psi$ . We now consider the replica space obtained by gluing  $n$  copies of the 3-dim space along the cuts at the subregions in the  $H_2$ : since the subregions run along the entire  $H_2$   $\chi$ -direction (wrapping the  $\psi$ -circle) on the  $\phi = 0$  slice, the effective geometry enlarges in the  $\phi$ -direction which puffs up to have periodicity  $2\pi n$ . This is similar to the fatter replica-cylinder described in the paragraph after (4.3). Visualizing the present 3-dim  $S^1 \times H_2$  replica geometry in detail appears difficult unfortunately!

We want to construct a bulk replica space with these replica boundary conditions where  $\phi \equiv \phi + 2\pi n$ : so consider (with  $c_1$  a parameter)

$$ds^2 = -\frac{dr^2}{f(r)} + l^2 f(r) d\phi^2 + r^2 dH_2^2, \quad f(r) = \frac{r^2}{l^2} + 1 + \frac{c_1}{r}, \quad \phi \equiv \phi + 2\pi n. \quad (4.22)$$

We want to require that this be a smooth geometry: towards this, we define an auxiliary Euclidean metric by Wick-rotating  $r \rightarrow i\rho$  and demand that this Euclidean metric satisfy

regularity conditions in the interior. This criterion for regularity of a de Sitter like geometry was used effectively in [76] for a  $dS$ -brane, which ended up giving a complex geometry in the  $dS_4$  case and we will see some parallels here: similar arguments appear in [77]. Wick-rotating gives a  $-AdS$  type space with metric

$$ds^2 = - \left( \frac{d\rho^2}{-f(\rho)} + l^2(-f(\rho))d\phi^2 + \rho^2 dH_2^2 \right), \quad -f(\rho) = \frac{\rho^2}{l^2} - 1 + \frac{ic_1}{\rho}. \quad (4.23)$$

Now note that  $f(r)$  develops a complex zero at  $r_h = i\rho_h$  so

$$f(\rho_h) = 0 \quad \rightarrow \quad c_1 = -i\rho_h \frac{l^2 - \rho_h^2}{l^2}. \quad (4.24)$$

Now we demand that the  $-AdS$  geometry at the complex zero of  $f(r)$  is regular with no conical deficit: with  $f(\rho) \sim f'(\rho_h)(\rho - \rho_h)$  near  $\rho_h$ , regularity with  $\phi$ -periodicity  $2\pi n$  requires

$$\frac{l}{2} f'(\rho_h) 2\pi n = 2\pi \quad \Rightarrow \quad \rho_h = \frac{l}{3n}(\sqrt{1 + 3n^2} + 1). \quad (4.25)$$

For  $n = 1$ , this gives  $\rho_h = l$  and  $c_1 = 0$ , which is pure  $dS_4$  in (4.19) above. In terms of the original  $r$ -variable in (4.22), we have pure imaginary  $r_h$  and  $c_1$

$$c_1 = r_h \frac{l^2 + r_h^2}{l^2}, \quad r_h = i \frac{l}{3n}(\sqrt{1 + 3n^2} + 1), \quad f(r_h) = 0, \quad (4.26)$$

and for  $n = 1$  we have  $r_h = il$  and  $c_1 = 0$ .

We would like to evaluate the boundary Renyi entropies (4.1) for these  $dS_4$ -like geometries using the semiclassical  $dS/CFT$  dictionary as in the  $dS_3$  case. The action is given by

$$\tilde{I}_n = \frac{1}{16\pi G_4} \int d^4x \sqrt{-g} (R - 2\Lambda) - \frac{1}{8\pi G_4} \int d^3x \sqrt{\gamma} K, \quad (4.27)$$

with

$$R = \frac{12}{l^2}, \quad \sqrt{-g} d^4x = l dH_2 d\phi r^2 dr, \quad \sqrt{\gamma} K d^3x = \left( \frac{3R_c^3}{l} + 2lR_c + \frac{3l}{2}c_1 \right) dH_2 d\phi, \quad (4.28)$$

where we have used the unit normal  $n^\mu = (n^r, 0, 0, 0)$  to the  $r = R_c$  boundary and the extrinsic curvature  $K = \nabla_\mu n^\mu$  as

$$n^r = \sqrt{\frac{r^2}{l^2} + 1 + \frac{c_1}{r}}, \quad K = \frac{1}{\sqrt{-g}} \partial_r (\sqrt{-g} n^r) = \frac{3\frac{r^3}{l^2} + 2r + \frac{3c_1}{2}}{r^2 (f(r))^{\frac{1}{2}}}, \quad \sqrt{\gamma} = l R_c^2 \sqrt{f(R_c)} \sinh \chi. \quad (4.29)$$

In evaluating the bulk term, we take the bulk (complex) time range as  $r = [R_c, r_h]$ , *i.e.* from the future boundary cutoff to the complex zero at  $r_h$ . This gives

$$\tilde{I}_n = -\frac{4\pi A n}{16\pi G_4 l} \left( 2R_c^3 + 2l^2 R_c + \frac{3l^2}{2} c_1 + r_h^3 \right). \quad (4.30)$$

To remove the cutoff-dependent divergent terms, we add the counterterm (following well-known holographic renormalization procedures [78–81])

$$16\pi G_4 I_{ct} = \int \sqrt{\gamma} (\alpha R_b + \beta), \quad R_b = -\frac{2}{R_c^2}, \quad \beta = \frac{4}{l}, \quad \alpha = -l. \quad (4.31)$$

Adding these, the full regulated action finally becomes (using (4.26))

$$I_n = \tilde{I}_n + I_{ct} = -\frac{2\pi An}{16\pi G_4 l} r_h (r_h^2 - l^2) \quad (4.32)$$

where  $A = \int dH_2$  is the area of the hyperboloid (which has interesting features as we will see in detail below). The semiclassical Wavefunction of the replica space then becomes

$$\log \Psi_n = iI_n = i \frac{2\pi An}{16\pi G_4 l} r_h (-r_h^2 + l^2), \quad (4.33)$$

giving the boundary Renyi entropy (4.1) as (with  $r_h$  in (4.26))

$$S_n = \frac{i}{1-n} \frac{2\pi An}{16\pi G_4 l} \left( r_h (-r_h^2 + l^2) - 2il^3 \right). \quad (4.34)$$

In the  $n \rightarrow 1$  limit, it can be seen that  $I_n \sim I_1 + \frac{I_1}{2}(n-1)^2$  so we obtain the boundary entanglement entropy as

$$S_1 = -\frac{l^2}{4G_4} A \equiv \frac{\pi l^2}{2G_4} \left( \frac{iR_c}{l} + 1 \right), \quad (4.35)$$

where the expression on the right is the no-boundary  $dS_4$  extremal surface area (2.4), but with the imaginary part being  $+i$ , obtained via the analytic continuation  $L \rightarrow il$  (analogous to the comments after (4.14)).

Thus we see that the area  $A$  of the hyperboloid is complex-valued! Of course this is the analytic continuation of the entanglement entropy from the  $AdS$  hyperbolic black hole [60]. To see how this arises directly in the present de Sitter context, it is instructive to look at the way  $dS_4$  in the hyperbolic foliation (4.19) arises via a nontrivial cutoff surface embedded in global  $dS_4$  for the simplest  $n = 1$  case. Towards this, we recall that  $dS_4$  is defined [25] as the hyperboloid surface

$$X_1^2 + X_2^2 + X_3^2 + X_4^2 - T^2 = l^2 \quad (4.36)$$

in 5-dim Minkowski space. Then global  $dS_4$  is given by the parametrization

$$\begin{aligned} X_1 &= l \cosh(\eta) \sin(\alpha) \cos(\beta), & T &= l \sinh(\eta), & X_2 &= l \cosh(\eta) \cos(\alpha) \cos(\gamma), \\ X_3 &= l \cosh(\eta) \cos(\alpha) \sin(\gamma), & X_4 &= l \cosh(\eta) \sin(\alpha) \sin(\beta), \end{aligned} \quad (4.37)$$

where we have the Hopf fibration form of the  $S^3$  metric. Thus the metric becomes

$$ds^2 = -l^2 d\eta^2 + l^2 \cosh^2(\eta) d\Omega_3^2 = -\frac{d\hat{r}^2}{\frac{\hat{r}^2}{l^2} - 1} + \hat{r}^2 d\Omega_3^2, \quad \hat{r} = l \cosh(\eta), \quad (4.38)$$

where the second form is the no-boundary  $dS_4$  metric and the coordinate relation above is in the Lorentzian region.

On the other hand, the hyperbolic  $dS_4$  (4.19) arises from the parametrization

$$\begin{aligned} X_1 &= \sqrt{r^2 + l^2} \cos(\phi), & X_4 &= \sqrt{r^2 + l^2} \sin(\phi), & X_2 &= r \sinh(\chi) \cos(\psi), \\ X_3 &= r \sinh(\chi) \sin(\psi), & T &= r \cosh(\chi). \end{aligned} \quad (4.39)$$

In the overlapping charts, we match the coordinates obtaining relations. For instance, matching  $T$  in (4.37) and (4.39) using (4.38), and likewise matching  $X_1/X_4$  and  $X_2/X_3$ , and using those and matching  $X_1$  and  $X_2$  gives

$$\begin{aligned} \sqrt{\hat{r}^2 - l^2} &= r \cosh \chi, & \beta &= \phi, & \gamma &= \psi, \\ \hat{r} \sin \alpha &= \sqrt{r^2 + l^2}, & \hat{r} \cos \alpha &= r \sinh \chi. \end{aligned} \quad (4.40)$$

These then give

$$\cot(\alpha) = \frac{r}{\sqrt{r^2 + l^2}} \sinh \chi. \quad (4.41)$$

Using (4.40) and (4.41) we obtain

$$\frac{1}{\cosh \chi} = \sqrt{\frac{\hat{r}^2 \sin^2 \alpha - l^2}{\hat{r}^2 - l^2}}, \quad r = \sqrt{\hat{r}^2 \sin^2 \alpha - l^2}. \quad (4.42)$$

These are nontrivial relations for the embedding of the hyperbolic angle  $\chi(\hat{r}, \alpha)$  and the radial coordinate  $r(\hat{r}, \alpha)$  as functions of the global coordinates  $\hat{r}, \alpha$ . The full range of  $\alpha$  (which is real-valued) is  $\alpha \in [0, \frac{\pi}{2}]$ : this however translates to complex values for  $\chi$  via the embedding relation above in the Lorentzian part  $\hat{r} > l$  of no-boundary  $dS_4$ . In particular on a fixed cutoff slice  $\hat{r} = R_c$  of no-boundary  $dS_4$  (4.38), we find

$$\sin \alpha < \frac{l}{R_c} \quad \rightarrow \quad \frac{1}{\cosh \chi} = i \sqrt{\frac{l^2 - R_c^2 \sin^2 \alpha}{R_c^2 - l^2}}, \quad (4.43)$$

so that  $\chi$  acquires imaginary values. In particular, as  $\alpha \rightarrow 0$ , we have

$$\frac{1}{\cosh \chi_{max}} \sim \frac{il}{R_c}, \quad (4.44)$$

with  $\chi_{max}$  the limiting (imaginary) value of  $\chi$ . On the other hand, as  $\alpha \rightarrow \frac{\pi}{2}$  we see that  $\chi \rightarrow 0$ . Thus the area of the hyperboloid  $H_2$  in the inherited  $\chi$ -range here becomes

$$A = 2\pi \int_0^{\chi_{max}} \sinh \chi d\chi = 2\pi(\cosh \chi_{max} - 1) = 2\pi \left( \frac{-iR_c}{l} - 1 \right). \quad (4.45)$$

It is worth noting that (4.42) gives real values on the strict future boundary  $R_c \rightarrow \infty$  (at fixed  $\alpha$ ) since  $\frac{1}{\cosh \chi} \rightarrow \sin \alpha$ : the feature (4.44) arises for a fixed boundary screen  $R_c$  as we vary  $\alpha$ . It is also interesting to note from (4.40) that for fixed  $\hat{r} = R_c \gg l$  we have  $r \cosh \chi \sim R_c$  so that the region (4.43) with imaginary  $\cosh \chi$  requires  $r$  to also be pure imaginary, *i.e.* we are in the Euclidean region (4.20). This is also directly seen from the second relation in (4.42), when  $\sin \alpha < \frac{l}{R_c}$ . In other words, the hyperbolic future boundary screen  $r = r_c$  is a nontrivial embedding (4.42) into global  $dS_4$ . This is expected: in the global foliation, we have finite size  $S^3$  slices at  $\hat{r} = \text{const}$ , so hyperbolic cross-sections can only be obtained with the  $S^1 \times H_2$  foliations embedded as nontrivially curved slices.

Using the area  $A$  in (4.45) then corroborates the  $n = 1$  limit as matching the extremal surface areas (4.35): thus finally the boundary Renyi entropies we have evaluated are (4.34) with the area  $A$  above. The real part of the Renyi entropies (4.34) using  $A$  above is

$$\text{Re } S_n = \frac{n}{1-n} \frac{\pi}{4G_4 l} (\rho_h (\rho_h^2 + l^2) - 2l^3), \quad (4.46)$$

with  $\rho_h$  in (4.25). In the  $n \rightarrow 1$  limit it can be seen that this becomes half  $dS_4$  entropy.

#### 4.2.1 Real $dS_4$ -like hyperbolic cosmologies

The asymptotically  $dS_4$  spacetimes (4.22) regarded as real geometries with  $c_1$  real (and  $l\phi \rightarrow t$  taken noncompact) are interesting in their own right, independent of  $dS/CFT$ : we have

$$ds^2 = -\frac{dr^2}{f(r)} + f(r)dt^2 + r^2 dH_2^2, \quad f(r) = \frac{r^2}{l^2} + 1 + \frac{c_1}{r}. \quad (4.47)$$

These are analogous to the real  $dS_4$  bluewall geometry in [76] (distinct from the complex  $dS_4$  brane there), and are in a different class from the complex geometry (4.22) relevant for the  $dS/CFT$  Renyi analysis.

At large  $r$ , the spacetime (4.47) approaches  $dS_4$ . However the interior structure differs depending on  $c_1$ . For  $c_1 < 0$ , we find a single real zero

$$f(r_h) = \frac{r_h^2}{l^2} + 1 - \frac{|c_1|}{r_h} = 0. \quad (4.48)$$

This is identical structurally to the blackening factor in the  $AdS_4$  Schwarzschild black hole. However now the singularity at  $r = 0$  inside the horizon is timelike, since

$$r \rightarrow 0 : \quad ds^2 \sim +\frac{r dr^2}{|c_1|} - \frac{|c_1|}{r} dt^2 + r^2 dH_2^2. \quad (4.49)$$

The extended Penrose diagram is similar to that in the  $dS_4$  bluewall, with asymptotic  $dS_4$  universes flanked by horizons that cloak the timelike singularity. As in that case, this resembles the interior region (within the inner horizons) of the Reissner-Nordstrom black hole.

On the other hand,  $c_1 > 0$  implies there is no real zero to the function  $f(r)$  so

$$c_1 > 0, \quad r \rightarrow 0 : \quad ds^2 \sim -\frac{rdr^2}{c_1} + \frac{c_1}{r} dt^2 + r^2 dH_2^2, \quad (4.50)$$

and the  $r = 0$  locus is now a spacelike, naked singularity.

### 4.3 Higher dimensional $dS$ and boundary Renyi

Various features of our analysis for  $dS_3, dS_4$  carry over to higher dimensional  $dS$  as well: in an essential way, this amounts to analytic continuation from an auxiliary  $-AdS$  calculation as we describe in App. B. There are several parallels with the Renyi analyses in [60] via  $AdS$  hyperbolic black holes. We describe some aspects directly in  $dS$  here.

The embedding formalism that we employed to find the range of  $\chi$  in  $dS_4$  can be extended to higher dimensional  $dS$ . Consider a replicated  $dS_{d+1}$  with a boundary sphere  $S^d$  with the following metric

$$d\Omega_d^2 = d\alpha^2 + \sin^2(\alpha)d\phi^2 + \cos^2(\alpha)d\Omega_{d-2}^2 \quad (4.51)$$

with  $\phi \equiv \phi + 2\pi n$ . Using the standard arguments as before the above metric is conformally equivalent to  $S^1 \times H_{d-1}$  where

$$dH_{d-1}^2 = d\chi^2 + \sinh^2(\chi)d\Omega_{d-2}^2 \quad (4.52)$$

So the  $dS$  metric here is

$$ds^2 = -\frac{dr^2}{f(r)} + l^2 f(r) d\phi^2 + r^2 dH_{d-1}^2, \quad f(r) = \frac{r^2}{l^2} + 1 + \frac{c_1}{r^{d-2}}. \quad (4.53)$$

When we embed this metric (4.53) into the global  $dS$  metric

$$ds^2 = -\frac{d\hat{r}^2}{\frac{\hat{r}^2}{l^2} - 1} + \hat{r}^2 d\Omega_d^2 \quad (4.54)$$

we can use the  $U(1) \times SO(d-1)$  symmetry of (4.53) to fix  $d-1$  parameters out of a possible  $d+1$ . That then leaves us with 2 parameters in each metric and as a result (4.40) will always be valid for any  $d$ . Consequently the maximum value  $\chi_{max}$  will always be given by (4.44).

The on-shell action can then be evaluated as before (see also App. B), yielding the boundary Renyi entropy (4.1)

$$S_n = -\frac{i}{1-n} \frac{2\pi n}{l} V_{d-1} \frac{1}{16\pi G_{d+1}} (r_h^{d-2} (r_h^2 - l^2) - i^d 2l^d), \quad (4.55)$$

generalizing (4.34) for  $dS_4$ . The boundary entanglement entropy in the limit  $n \rightarrow 1$  is given by

$$S_{EE} = -\frac{2\pi}{l} V_{d-1} 2i i^d l^d \frac{1}{16\pi G_{d+1}} = \frac{1}{4G_{d+1}} i^{d-1} l^{d-1} V_{d-1}, \quad (4.56)$$

where

$$V_{d-1} = \Omega_{d-2} \int \sinh^{d-2}(\chi) d\chi \quad (4.57)$$

is the hyperboloid volume. As a check of the above, we can verify that this recovers the earlier  $dS_3, dS_4$  results. Now for  $d = 4$ , (4.56) gives

$$V_3 = -2\pi \left( \frac{R_c^2}{l^2} + \log\left(\frac{2R_c}{l}\right) + \frac{1}{2} - \frac{i\pi}{2} \right). \quad (4.58)$$

So, analogous to (4.35), we get

$$S_{EE} = \frac{\pi^2 l^3}{4G} + i \frac{\pi l^3}{2G} \left( \frac{R_c^2}{l^2} + \log\left(\frac{2R_c}{l}\right) \right), \quad (4.59)$$

(with  $+i$  in the imaginary parts) and the real part is exactly half  $dS_5$  entropy, matching that in the extremal surface area (2.3).

## 5 Time entanglement in quantum mechanics: review

We first briefly review various entanglement-like structures in quantum mechanics discussed in [19, 21, 22]. The fact that extremal surfaces anchored at the  $dS$  future boundary do not return suggests that extra data is required in the far past, somewhat reminiscent of scattering amplitudes or equivalently time evolution (*i.e.* final states from initial states). With this analogy, we consider the normalized time evolution operator as a generalized density operator, normalized at any time  $t$ , in quantum mechanics per se, independent of  $dS$ : these lead to various interesting entanglement-like structures with timelike separations in their own right. Then based on these studies of toy models without gravity, we will return to de Sitter space in sec. 7. Then partial traces lead to a reduced time evolution operator and the corresponding von Neumann entropy:

$$\mathcal{U}(t) = e^{-iHt} \rightarrow \rho_t(t) \equiv \frac{\mathcal{U}(t)}{\text{Tr } \mathcal{U}(t)} \rightarrow \rho_t^A = \text{tr}_B \rho_t \rightarrow S_A = -\text{tr}(\rho_t^A \log \rho_t^A). \quad (5.1)$$

There are sharp parallels with ordinary finite temperature entanglement structures, except with imaginary temperature  $\beta = it$ .

A closely related quantity is pseudo-entropy, the entropy of the reduced transition matrix [28]. Starting with the time evolution operator and including projection operators onto initial states  $|I\rangle$  leads to transition matrices between these initial states and their time-evolved final states  $|F\rangle$ : then taking partial traces leads to reduced transition amplitudes and the associated pseudo-entropies: we have

$$\rho_{t,|I\rangle} = \left( \frac{\mathcal{U}(t) |I\rangle \langle I|}{\text{Tr}(\mathcal{U}(t) |I\rangle \langle I|)} \right) \xrightarrow{\text{Tr}_B} \rho_{t,|I\rangle}^A \equiv \mathcal{T}_{F|I}^A = \text{Tr}_B \left( \frac{|F\rangle \langle I|}{\text{Tr}(|F\rangle \langle I|)} \right), \quad |F\rangle = \mathcal{U}(t) |I\rangle. \quad (5.2)$$

Thus the reduced time evolution operator with projection  $\rho_{t,|I\rangle}^A$  is equivalent to the pseudo-entropy reduced transition matrix  $\mathcal{T}_{F|I}^A$  when the final state is the time-evolved initial state, *i.e.*  $|F\rangle = \mathcal{U}(t)|I\rangle$ .

These can be evaluated explicitly for bipartite systems with the Hilbert space being characterized by Hamiltonian eigenstates  $|i, i'\rangle$  with energies  $E_{i,i'}$ . For instance, consider a 2-qubit system with Hamiltonian  $H = E_{ij}|ij\rangle$  where  $i, j = 1, 2$ , label the energy eigenstate basis (with  $E_{21} = E_{12}$ ). Then, with  $\theta_1 \equiv -(E_{22} - E_{11})t$  and  $\theta_2 \equiv -(E_{12} - E_{11})t$ , the normalized time evolution operator and the reduced time evolution operator obtained by a partial trace over the second qubit are

$$\rho_t = \sum_{i,j} \frac{e^{-iE_{ij}t}}{\sum_{kl} e^{-iE_{kl}t}} |ij\rangle\langle ij| \quad \rightarrow \quad \rho_t^A = \frac{(1 + e^{i\theta_2})|1\rangle\langle 1| + (e^{i\theta_1} + e^{i\theta_2})|2\rangle\langle 2|}{1 + e^{i\theta_1} + 2e^{i\theta_2}}. \quad (5.3)$$

This generically has complex-valued von Neumann entropy.

Including projections onto states  $|I\rangle$ , using the normalization  $|c_{11}|^2 + |c_{22}|^2 = 1$  and redefining  $|c_{11}|^2 = x$ , we have from (5.2),

$$\begin{aligned} |I\rangle &= c_{11}|11\rangle + c_{22}|22\rangle, \quad |F\rangle = \mathcal{U}(t)|I\rangle = c_{11}e^{-iE_{11}t}|11\rangle + c_{22}e^{-iE_{22}t}|22\rangle, \\ \rho_{t,|I\rangle}^1 &= \frac{1}{x + (1-x)e^{i\theta}} \left( x|1\rangle\langle 1| + (1-x)e^{i\theta}|2\rangle\langle 2| \right), \quad \theta = -(E_{22} - E_{11})t = -\Delta E t, \\ S_{t,|I\rangle}^1 &= -\frac{x}{x + (1-x)e^{i\theta}} \log \frac{x}{x + (1-x)e^{i\theta}} - \frac{(1-x)e^{i\theta}}{x + (1-x)e^{i\theta}} \log \frac{(1-x)e^{i\theta}}{x + (1-x)e^{i\theta}}. \end{aligned} \quad (5.4)$$

Here  $S_{t,|I\rangle}^1$  is the pseudo-entropy of the reduced transition matrix corresponding to states  $|I\rangle, |F\rangle$ . This is a real-valued entropy, periodic in  $t$ , exhibiting a divergent value at  $e^{i\theta} = -\frac{x}{1-x}$ . The maximally entangled thermofield-double (Bell-pair) type state with  $x = \frac{1}{2}$  has a singularity at  $e^{i\theta} = -1$ , *i.e.*  $t = \frac{(2n+1)\pi}{E_{22}-E_{11}}$ .

Now consider the entirely timelike future-past surfaces [15, 17]: these suggest some sort of generalized entanglement between  $I^\pm$ . By analogy, consider future-past states, entangling states between a past time slice  $P$  and a future time slice  $F$ ,

$$|\psi\rangle_{fp} = \sum \psi^{i_n^F, i_n^P} |i_n\rangle_F |i_n\rangle_P. \quad (5.5)$$

The corresponding future-past density matrix  $\rho_{fp} = |\psi\rangle_{fp}\langle\psi|_{fp}$  after a partial trace over the second ( $P$ ) copy then gives a reduced density matrix with nontrivial entanglement entropy. To see how this works, let us consider a very simple toy example of a 2-state system in ordinary quantum mechanics. The action of the Hamiltonian  $H$  on these (orthogonal basis) eigenstates and the resulting (simple) time evolution are  $H|k\rangle = E_k|k\rangle$  with  $k = 1, 2$  and  $|k\rangle_F \equiv |k(t)\rangle = e^{-iE_k t}|k\rangle_P$ . We consider the  $F$  and  $P$  slices to be separated by time  $t$  and

obtain the  $F$  state from the  $P$  state by time evolution through  $t$ . The future-past TFD state (5.5) in this toy case and the corresponding future-past density matrix are

$$\begin{aligned} |\psi\rangle_{fp} &= \frac{1}{\sqrt{2}}|1\rangle_F|1\rangle_P + \frac{1}{\sqrt{2}}|2\rangle_F|2\rangle_P = \frac{1}{\sqrt{2}}e^{-iE_1 t}|1\rangle_P|1\rangle_P + \frac{1}{\sqrt{2}}e^{-iE_2 t}|2\rangle_P|2\rangle_P, \\ \rho_f &= \text{Tr}_P|\psi\rangle_{fp}\langle\psi|_{fp} = \frac{1}{2}|1\rangle_F\langle 1|_F + \frac{1}{2}|2\rangle_F\langle 2|_F. \end{aligned} \quad (5.6)$$

We have normalized the coefficients for maximal entanglement at  $t = 0$ . For nonzero  $t$ , there are extra phases due to the time evolution but they cancel in the reduced density matrix obtained by tracing  $|\psi\rangle_{fp}\langle\psi|_{fp}$  over the entire second copy as  $\delta_{ij}\psi_{fp}^{ki}(\psi_{fp}^*)^{lj}$ , so we have obtained an entirely positive structure. This is true for general future-past states, via the doubling and partial trace. We will explore this further later.

## 6 Time evolution operator, partial traces: weak values, autocorrelation functions, future-past entanglement

In what follows, we will find various relations between the time evolution operator and partial traces thereof with weak values of operators localized to subregions, as well as autocorrelation functions thereof. We have in mind a bipartite decomposition of the full system: we will use notation specific to a 2-qubit system for illustration but the indices will also suffice more generally.

### 6.1 Weak values and the reduced time evolution operator

Consider two generic states  $|\psi\rangle$ ,  $|\phi\rangle$ , and an operator  $A$  localized to subregion-1 (first index):

$$|\psi\rangle = c_{ij}|ij\rangle, \quad |\phi\rangle = c'_{ij}|ij\rangle, \quad A = A_{\alpha\beta}|\alpha\rangle\langle\beta|. \quad (6.1)$$

The weak value of  $A$  in the states  $|\psi\rangle$ ,  $|\phi\rangle$  is the (normalized) amplitude

$$\frac{\langle\phi|A|\psi\rangle}{\langle\phi|\psi\rangle} = \frac{\sum_{kl, ij} \langle kl|c'^*_{kl} A_{\alpha\beta}|\alpha\rangle\langle\beta| c_{ij}|ij\rangle}{\sum_{kl, ij} \langle kl|c'^*_{kl} c_{ij}|ij\rangle} = \frac{\sum_{\alpha, \beta, j} A_{\alpha\beta} c'^*_{\alpha j} c_{\beta j}}{\sum_{ij} c'^*_{ij} c_{ij}} = \text{Tr}(A \mathcal{T}_{\psi|\phi}^1), \quad (6.2)$$

where the index contractions  $k = \alpha$ ,  $l = j$ ,  $\beta = i$ , arise from the fact that  $A$  is localized to subregion-1 (first index). In the last expression, we have recast the weak value in terms of

$$\mathcal{T}_{\psi|\phi}^1 = \text{Tr}_2 \left( \frac{|\psi\rangle\langle\phi|}{\text{Tr}(|\psi\rangle\langle\phi|)} \right), \quad (\mathcal{T}_{\psi|\phi}^1)_{\alpha\beta} = \frac{\sum_j c'^*_{\alpha j} c_{\beta j}}{\sum_{ij} c'^*_{ij} c_{ij}}, \quad (6.3)$$

where  $\mathcal{T}_{f|i}^1$  is the reduced transition matrix for two arbitrary states  $|i\rangle$ ,  $|f\rangle$  obtained after a partial trace over subregion-2. Diagrammatically, the reduced transition matrix and the weak value are represented in Figure 4 and Figure 5.

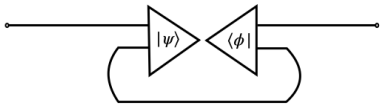


Figure 4: The reduced transition matrix for states  $|\psi\rangle$  and  $|\phi\rangle$ .

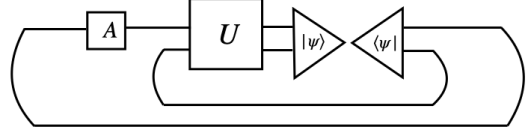


Figure 5: The weak value of  $A$  localized to subregion-1 with state  $|\psi\rangle$  and its time-evolution.

The expectation value of  $A$  in  $|\psi\rangle$  is then obtainable by thinking of  $|\phi\rangle$  as a post-selected state and summing over all post-selected states weighted by the amplitude for post-selection:

$$\frac{\langle\psi|A|\psi\rangle}{\langle\psi|\psi\rangle} = \sum_{\phi} \frac{\langle\psi|\phi\rangle \langle\phi|A|\psi\rangle}{\text{Tr}(|\phi\rangle\langle\phi|) \langle\psi|\psi\rangle} = \sum_{\phi} \frac{\langle\psi|\phi\rangle \langle\phi|A|\psi\rangle}{\langle\phi|\phi\rangle \langle\psi|\psi\rangle}. \quad (6.4)$$

We see that the weak value can be interpreted as the amplitude for an initial state  $|\psi\rangle$  “kicked” by an operator  $A$  to land in a final state  $|\phi\rangle$ . It is then interesting to evaluate this weak value or kick amplitude when the final state is the time evolution of the initial state, *i.e.*  $|\phi\rangle = \mathcal{U}(t)|\psi\rangle = \sum c_{ij} e^{-iE_{ij}t} |ij\rangle$ . A closely related object, the conjugate of the above, is

$$\frac{\langle\psi|A|\psi(t)\rangle}{\langle\psi|\psi(t)\rangle} = \frac{\sum_{kl,ij} \langle kl| c_{kl}^* A_{\alpha\beta} |\alpha\rangle \langle\beta| c_{ij} |ij\rangle e^{-iE_{ij}t}}{\sum_{kl,ij} \langle kl| c_{kl}^* c_{ij} |ij\rangle e^{-iE_{ij}t}} = \frac{\sum A_{\alpha\beta} c_{\alpha j}^* c_{\beta j} e^{-iE_{\beta j}t}}{\sum c_{ij}^* c_{ij} e^{-iE_{ij}t}} = \text{Tr}(A \rho_{t,|\psi\rangle}^1), \quad (6.5)$$

where  $\rho_{t,|\psi\rangle}^1$  is the reduced time evolution operator with projection onto the state  $|\psi\rangle$  (5.2), obtained by a partial trace over subregion-2 (second index),

$$\rho_{t,|\psi\rangle}^1 = \text{Tr}_2(\rho_{t,|\psi\rangle}) = \frac{\sum_j c_{\alpha j}^* c_{\beta j} e^{-iE_{\beta j}t}}{\sum c_{ij}^* c_{ij} e^{-iE_{ij}t}} |\alpha\rangle\langle\beta| \equiv \text{Tr}_2\left(\frac{|\psi(t)\rangle\langle\psi|}{\text{Tr}(|\psi(t)\rangle\langle\psi|)}\right). \quad (6.6)$$

The last expression is written to make manifest the fact that the time evolution operator with projection onto  $|\psi\rangle$  amounts to the transition matrix between the initial state  $|\psi\rangle$  and its time evolved final state  $|\psi(t)\rangle = \mathcal{U}(t)|\psi\rangle$ .

Let us now recall that the time-entanglement (or pseudo) entropy of this reduced time evolution operator with projection exhibits singularities at certain specific time locations (5.4). These singularities can be traced to the zeroes of the normalization factor in the denominator: for instance the generic initial state  $|I\rangle = c_{11}|11\rangle + c_{22}|22\rangle$  gives the inner product in the normalization

$$\text{Tr}(|F\rangle\langle I|) = \langle I|F\rangle = \frac{1}{2}(x e^{-iE_{11}t} + (1-x)e^{-iE_{22}t}) = 0 \quad \rightarrow \quad e^{-i(E_{22}-E_{11})t} = -\frac{x}{1-x}. \quad (6.7)$$

Thus the singularity in (5.4) essentially stems from the fact that a generic initial state becomes orthogonal to its time-evolved final state at specific time locations. Note that it

is necessary that the initial state is not an energy eigenstate: otherwise the normalization gives a single time evolution phase which cannot vanish.

We now see that at precisely these time locations, the weak value (6.5) also diverges:

$$\langle A \rangle_t \equiv \frac{\langle \psi | A | \psi(t) \rangle}{\langle \psi | \psi(t) \rangle} = \text{Tr}(A \rho_{t,|\psi\rangle}^1) = \frac{1}{x + (1-x)e^{i\theta}} (xA_{11} + (1-x)e^{i\theta}A_{22}). \quad (6.8)$$

The overall factor leading to the divergence (matching with (5.4)) traces back to the inner product  $\langle \psi | \psi(t) \rangle$  vanishing, as in (6.7). At  $t = 0$  this becomes  $\langle A \rangle = xA_{11} + (1-x)A_{22}$ , the expectation value, while at  $e^{-i(E_{22}-E_{11})t} = -\frac{x}{1-x}$  the weak value acquires a singularity, reflecting the singularity in the entropy at these time locations. Since this holds for generic hermitian operators  $A$  (distinct from the identity operator), this singularity is an intrinsic property of the state and its time evolution defined by the quantum system.

Along the same lines, it is interesting to note a more general weak value, involving the time-evolved state  $|\psi(t)\rangle$  and a distinct state  $|\phi\rangle$ : consider

$$\begin{aligned} \frac{\langle \phi | A | \psi(t) \rangle}{\langle \phi | \psi(t) \rangle} &= \text{Tr}(A \rho_{t,|\psi\rangle,|\phi\rangle}^1), \\ \rho_{t,|\psi\rangle,|\phi\rangle}^1 &= \text{Tr}_2\left(\frac{\mathcal{U}(t) |\psi\rangle\langle\phi|}{\text{Tr}(\mathcal{U}(t) |\psi\rangle\langle\phi|)}\right) = \text{Tr}_2\left(\frac{|\psi(t)\rangle\langle\phi|}{\text{Tr}(|\psi(t)\rangle\langle\phi|)}\right) = \frac{\sum_j c_{\alpha j}^{*} c_{\beta j} e^{-iE_{\beta j}t}}{\sum_i c_{ij}^{*} c_{ij} e^{-iE_{ij}t}} |\beta\rangle\langle\alpha|, \end{aligned} \quad (6.9)$$

Here we have the time evolution operator along with the transition matrix  $|\psi\rangle\langle\phi|$  from the state  $|\phi\rangle$  to the state  $|\psi\rangle$ . The last expression is expressed in component form, using the basis decomposition (6.1), similar to the expressions in (6.2), (6.5).

It is of course straightforward to see that at the initial time slice  $t = 0$ , the weak value (6.5) collapses down to the expectation value in the initial state  $|\psi\rangle$ ,

$$\frac{\langle \psi | A | \psi(t) \rangle}{\langle \psi | \psi(t) \rangle} \Big|_{t=0} = \langle A \rangle, \quad \rho_{t,|\psi\rangle}^1 = \rho_{|\psi\rangle}^1 = \text{Tr}_2\left(\frac{|\psi\rangle\langle\psi|}{\text{Tr}(|\psi\rangle\langle\psi|)}\right), \quad (6.10)$$

and the reduced time evolution operator collapses to the reduced density matrix for  $|\psi\rangle$ .

**Evolution of subregions and the reduced time evolution operator:** It is natural to ask if time evolution for a subregion is governed by the reduced time evolution operator (5.1) pertaining to that subregion. To address this, we note that subregion-1 states can be constructed by starting with states of the full system but deleting access to information about the subregion-2 components of the states. So amplitudes or inner products of states with information localized to subregion-1 are obtained by partial traces over subregion-2, *i.e.* with states in (6.1), we have

$$\text{Tr}_2(\langle \phi | \psi(t) \rangle) = \text{Tr}_2(\langle kj | c_{kj}^{*} c_{ij} e^{-iE_{ij}t} | ij \rangle) \quad (6.11)$$

Including the normalization, we see that this is in fact closely related to the matrix elements of the reduced time evolution operator appended with the transition matrix projector  $\rho_{t,|\psi\rangle,|\phi\rangle}^1$  in (6.9), *i.e.*

$$\frac{\sum_j c_{kj}^* c_{ij} e^{-iE_{ij}t}}{\sum_{ij} c_{ij}^* c_{ij} e^{-iE_{ij}t}} = (\rho_{t,|\psi\rangle,|\phi\rangle}^1)_{ik}. \quad (6.12)$$

Likewise the matrix elements of the reduced time evolution operator with projection onto state  $|\psi\rangle$  are related to the inner products

$$\text{Tr}_2(\langle\psi|\psi(t)\rangle) \longleftrightarrow \frac{\sum_j c_{kj}^* c_{ij} e^{-iE_{ij}t}}{\sum_{ij} c_{ij}^* c_{ij} e^{-iE_{ij}t}} = (\rho_{t,|\psi\rangle}^1)_{ik}. \quad (6.13)$$

In this sense, the reduced time evolution operator controls the evolution of the subregion, through its matrix elements after partial traces over subregion-2: we have

$$\text{Tr}_2(\langle ij| \left( \frac{\mathcal{U}(t)}{\text{Tr } \mathcal{U}(t)} \right) |kl\rangle) = (\rho_t^1)_{ik}. \quad (6.14)$$

## 6.2 Autocorrelation functions: the $\mathbb{T}$ operator

Noting  $|\psi(t)\rangle = \mathcal{U}(t)|\psi\rangle$  above, we have  $\langle\psi(t)|\psi(t)\rangle = \langle\psi|\psi\rangle$ . Now consider the expectation value of the time-dependent Heisenberg picture operator  $A(t) = \mathcal{U}(t)^\dagger A \mathcal{U}(t)$  (with  $A \equiv A(0)$ )

$$\frac{\langle\psi|A(t)|\psi\rangle}{\langle\psi|\psi\rangle} = \frac{\langle\psi(t)|A|\psi(t)\rangle}{\langle\psi|\psi\rangle} = \text{Tr}(A \mathbb{T}^\rho), \quad \mathbb{T}^\rho \equiv \frac{|\psi(t)\rangle\langle\psi(t)|}{\text{Tr}(|\psi\rangle\langle\psi|)}. \quad (6.15)$$

This  $\mathbb{T}^\rho$  operator is of course just the density operator at general time  $t$ : writing it in this manner with open legs on both sides is just convenient to see how expectation values work for operators localized on subregions.

It is worth noting that the operator  $\mathbb{T}^\rho$  coincides with the operator  $\rho_{t,|\psi\rangle,|\phi\rangle}$  before the partial trace in (6.9) when  $|\phi\rangle = \mathcal{U}|\psi\rangle$ , *i.e.* when  $|\phi\rangle$  is time-evolved from the state  $|\psi\rangle$ . This is evident directly from (6.15) and the transition matrix operator inside the  $\text{Tr}_2$ -bracket in (6.9), *i.e.*

$$\mathbb{T}^\rho = \frac{|\psi(t)\rangle\langle\psi(t)|}{\text{Tr}(|\psi\rangle\langle\psi|)} \longleftrightarrow \frac{\mathcal{U}(t)|\psi\rangle\langle\phi|}{\text{Tr}(\mathcal{U}(t)|\psi\rangle\langle\phi|)} \equiv \rho_{t,|\psi\rangle,|\phi\rangle}, \quad |\phi\rangle = \mathcal{U}(t)|\psi\rangle. \quad (6.16)$$

Along the lines of the more general weak values in (6.2), (6.9), we can construct a more general version of this  $\mathbb{T}^\rho$  operator as

$$\mathbb{T} \equiv \frac{|\psi(t)\rangle\langle\phi(t)|}{\text{Tr}(|\psi\rangle\langle\phi|)} = \frac{\mathcal{U}(t)|\psi\rangle\langle\phi|\mathcal{U}(t)^\dagger}{\text{Tr}(|\psi\rangle\langle\phi|)}. \quad (6.17)$$

This is a transition matrix involving time-evolved copies of two distinct states  $|\psi\rangle$  and  $|\phi\rangle$ . When the states are the same,  $\mathbb{T} = \mathbb{T}^\rho$ , *i.e.* we obtain the density matrix at time  $t$ , but

more generally this is a new object, useful in constructing 2-point autocorrelation functions and connects with related structures studied in [58]. This  $\mathbb{T}$ -operator is essentially similar to the transition matrices for pseudo-entropy [28], except with two copies of the time evolution operator explicitly stuck in.

Diagrammatically, the time evolution operator and the time-dependent transition matrix operator  $\mathbb{T}$  are represented in Figure 6 and Figure 7.

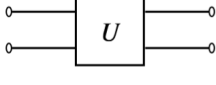


Figure 6: The time evolution operator  $\mathcal{U}(t)$ .

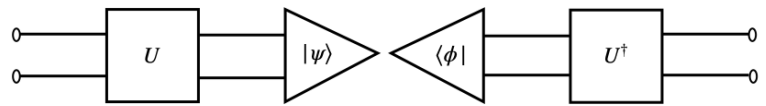


Figure 7: The transition matrix operator  $\mathbb{T}$  for states  $|\psi\rangle$  and  $|\phi\rangle$ .

**Expectation values:** Picking an eigenstate basis, we can write this explicitly as

$$\mathbb{T}^\rho \equiv \frac{\mathcal{U}(t)|\psi\rangle\langle\psi|\mathcal{U}(t)^\dagger}{\text{Tr}(|\psi\rangle\langle\psi|)} = \frac{e^{-iE_{ij}t}c_{ij}c_{kl}^*e^{iE_{kl}t}}{\sum c_{ij}^*c_{ij}} |ij\rangle\langle kl| \equiv T_{ij,kl}^\rho |ij\rangle\langle kl|. \quad (6.18)$$

Unlike the previous cases of weak values that involve a single copy of the time evolution operator, the operator  $\mathbb{T}$  here involves two copies of the time evolution operator, acting from the left and from the right.

With a bipartite decomposition, consider as before an operator  $A$  localized to subregion-1. Then its time-dependent expectation value (6.15) simplifies since subregion-2 does not enter and we obtain, using an explicit basis decomposition:

$$\langle\psi(t)|A|\psi(t)\rangle = \frac{\sum_{\alpha=k, j=l, \beta=i} \langle kl|c_{kl}^*e^{iE_{kl}t} A_{\alpha\beta}|\alpha\rangle\langle\beta| c_{ij}e^{-iE_{ij}t}|ij\rangle}{\sum c_{ij}^*c_{ij}} \equiv \text{Tr}(A \mathbb{T}^{\rho,1}), \quad (6.19)$$

where

$$\mathbb{T}^{\rho,1} = \text{Tr}_2 \mathbb{T}^\rho = \frac{\sum_j c_{kj}^* e^{iE_{kj}t} c_{ij} e^{-iE_{ij}t}}{\sum c_{ij}^* c_{ij}} |i\rangle\langle k| \quad (6.20)$$

is the partial trace over subregion-2 of the  $\mathbb{T}_\rho$  operator in (6.18). It is worth noting that this operator  $\mathbb{T}^{\rho,1}$  coincides with the operator  $\rho_{t,|\psi\rangle,|\phi\rangle}^1$  in (6.9) when  $|\phi\rangle = \mathcal{U}|\psi\rangle$ , *i.e.* when  $|\phi\rangle$  is time-evolved from the state  $|\psi\rangle$ .

**2-point autocorrelation functions:** To explore these, we first pick an eigenstate basis and write the  $\mathbb{T}$ -operator (6.17) as

$$\mathbb{T} = \frac{\mathcal{U}(t)|\psi\rangle\langle\phi|\mathcal{U}(t)^\dagger}{\text{Tr}(|\psi\rangle\langle\phi|)} = \frac{e^{-iE_{ij}t}c_{ij}c_{kl}^*e^{iE_{kl}t}}{\sum c_{ij}^*c_{ij}} |ij\rangle\langle kl| \equiv \mathbb{T}_{ij,kl} |ij\rangle\langle kl|. \quad (6.21)$$

Now consider first the 2-point autocorrelation function in state  $|\psi\rangle$  of operator  $A$  localized to subregion-1 at time  $t = 0$  and operator  $B(t)$  localized to subregion-2 at time  $t$ : with the understanding that  $\alpha, \beta \in$  subregion-1 and  $\mu, \nu \in$  subregion-2, we have

$$\begin{aligned} A^1 &= A_{\alpha\beta} |\alpha\rangle\langle\beta|, \quad B^2 = B_{\mu\nu} |\mu\rangle\langle\nu|, \\ \langle\psi| A(0) B(t) |\psi\rangle &= \langle kl | c_{kl}^* A_{\alpha\beta} |\alpha\rangle\langle\beta| \mathcal{U}^\dagger B_{\mu\nu} |\mu\rangle\langle\nu| \mathcal{U} c_{ij} |ij\rangle \\ &= \sum \langle\beta l | c_{\alpha l}^* A_{\alpha\beta} e^{iE_{\beta l} t} B_{\mu j} c_{ij} e^{-iE_{ij} t} |i\mu\rangle = \sum A_{\alpha\beta} c_{\alpha\mu}^* e^{iE_{\beta\mu} t} B_{\mu\nu} e^{-iE_{\beta\nu} t} c_{\beta\nu}. \end{aligned} \quad (6.22)$$

We have implemented the index contractions  $\alpha = k$ ,  $\nu = j$ ,  $\mu = l$ ,  $\beta = i$  to arrive at the final expression. This is thus recast now as

$$\langle\psi| A(0) B(t) |\psi\rangle = \text{Tr}((T A) B), \quad T_{\alpha\beta\mu\nu} = e^{iE_{\beta\mu} t} c_{\alpha\mu}^* c_{\beta\nu} e^{-iE_{\beta\nu} t}. \quad (6.23)$$

Then we see that

$$\text{Tr}(T A)_{\mu\nu} = \sum_{\alpha\beta} (T_{\alpha\beta\mu\nu} A_{\alpha\beta}) = \sum c_{\alpha\mu}^* c_{\beta\nu} A_{\alpha\beta} e^{iE_{\beta\mu} t} e^{-iE_{\beta\nu} t}. \quad (6.24)$$

We now see that this object can be recovered from a particular  $\mathbb{T}$  in the basis (6.21) as:

$$(T A) = \text{Tr}_1(\mathbb{T}), \quad c_{\beta\mu}^* = c_{\alpha\mu}^* A_{\alpha\beta}, \quad (6.25)$$

where we have taken a partial trace over subregion-1, *i.e.* the first index. In other words,  $\mathbb{T}$  here comprises the specific states  $|\psi\rangle$  and  $\langle\phi| = \langle\psi|A$ . With this, we then evaluate the 2-point autocorrelation function as an effective 1-point function of  $B$ . As we see, this is closely related to the  $T_{AB}$  operator discussed for autocorrelation functions in [58].

Diagrammatically, the manipulations above involving the time-dependent transition matrix operator  $\mathbb{T}$  and the operators  $A$  and  $B$  localized on different subregions are represented in Figure 8 and Figure 9. Various examples are discussed in Appendix D.

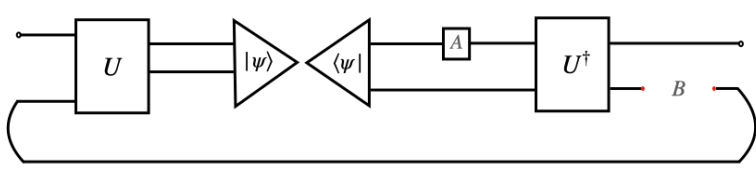


Figure 8: The transition matrix operator  $\mathbb{T}$  for states  $|\psi\rangle$  and  $|\phi\rangle$  contracted partially (*i.e.* with open legs) with operators  $A$  and  $B$  localized to different subregions.

### 6.3 Future-past entangled states, time evolution

The fact that entirely Lorentzian de Sitter necessitates entirely timelike future-past extremal surfaces connecting the future boundary to the past one suggests some sort of future-past

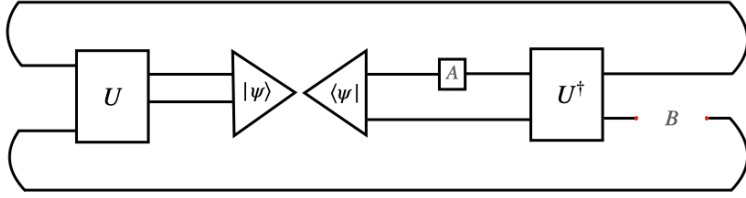


Figure 9: The transition matrix operator  $\mathbb{T}$  for states  $|\psi\rangle$  and  $|\phi\rangle$  contracted with operators  $A$  and  $B$  localized to different subregions. With the operator  $B$  contracted, this is the autocorrelation function.

entanglement between two copies of the ghost CFT dual to  $dS$  [15]. Future-past thermofield double type states were written down based on the expectation that these are entirely positive objects in the ghost-like  $CFT_3$  with various negative norm signs cancelling, an observation borne out in detail in toy ghost-spin models [26, 27] regarded as microscopic lattice variables for such ghost CFTs.

From the bulk point of view, this sort of future-past connectedness is a timelike version of entanglement. Some heuristic observations on these on this bulk point of view were made in toy models in quantum mechanics in [19, 21, 22]. We will develop this further here.

Consider the future-past entangled state written in terms of basis energy eigenstates  $|I_P\rangle$  at the past time slice and an isomorphic copy  $|I_F\rangle$  at the future time slice. Here  $I$  is a label denoting all the qubit degrees of freedom in the system. We have

$$|\Psi_{fp}\rangle = \sum c_{IJ} |I_F\rangle |J_P\rangle = c_{IJ} e^{-iE_I t} |I_P^1\rangle |J_P^2\rangle, \quad (6.26)$$

where we have written the explicit simple time evolution phase arising since these are basis energy eigenstates. In the second expression we have written explicit labels 1, 2, to distinguish the two past copies in this doubling: from this point of view, we have doubled the Hilbert space and then separated one copy thereof in time to the future time slice.

The corresponding future-past density matrix now is

$$\rho_{fp} = |\Psi_{fp}\rangle \langle \Psi_{fp}| = c_{IJ} c_{KL}^* |I_F\rangle \langle K_F| |I_P^1\rangle \langle J_P^2| = c_{IJ} c_{KL}^* e^{-iE_I t} e^{iE_K t} |I_P^1\rangle |J_P^2\rangle \langle K_P^1| \langle L_P^2|. \quad (6.27)$$

The partial trace over the past copy (as written in the form with explicit  $F, P$ -labels) is a partial trace over the copy-2 in the second form with only  $P$ -labels. This is the index contraction  $J = L$  and we have

$$\begin{aligned} \text{Tr}_P(\rho_{fp}) &= \sum c_{IJ} c_{KJ}^* |I_F\rangle \langle K_F| \\ &= \text{Tr}_2(c_{IJ} c_{KL}^* e^{-iE_I t} e^{iE_K t} |I_P^1\rangle |J_P^2\rangle \langle K_P^1| \langle L_P^2|) = c_{IJ} c_{KJ}^* e^{-iE_I t} e^{iE_K t} |I_P^1\rangle \langle K_P^1|. \end{aligned} \quad (6.28)$$

The second line expression is of course identical to the first one noting the basis eigenstate time evolution  $|I_F\rangle = e^{-iE_I t} |I_P\rangle$ . In the first line form, we see a manifestly positive object

recognizable as the reduced density matrix at the future time slice with von Neumann entropy equal to the entanglement entropy at the future time slice.

Consider now a bipartite system, with 2-qubits for simplicity: the label is  $I \equiv \{i, j\}$ . Then (assuming the states are normalized to avoid cumbersome notation)

$$\begin{aligned} \rho_{fp} &= \sum c_{ij}{}_{ab} c_{kl}^*{}_{cd} e^{-iE_{ij}t} e^{iE_{kl}t} |ij\rangle^1 |ab\rangle^2 \langle kl|^1 \langle cd|^2 \\ \xrightarrow{\text{Tr}_2} \quad \rho_f &= \sum c_{ij}{}_{ab} c_{kl}^*{}_{ab} e^{-iE_{ij}t} e^{iE_{kl}t} |ij\rangle \langle kl|. \end{aligned} \quad (6.29)$$

In [22], some observations were made in analogy with the discussions in [82], [83], of space emerging from entanglement. In the current context, an analogy was made relating the connectedness of time evolution from the past time slice to the future time slice to the entangled nature of the future-past states above. In particular a factorized future-past state with just a single nonzero coefficient  $c_{IJ}$  gives

$$|\psi_{fp}\rangle^{fac} = |\psi_F\rangle |\psi_P\rangle \quad \rightarrow \quad \text{Tr}_P(\rho_{fp}) = |\psi_F\rangle \langle \psi_F| \quad (6.30)$$

which is pure at the future time slice, with zero entropy. Note also that the time evolution operator  $\mathcal{U}(t)$  has disappeared in the future-past density matrix. This calculation thus does not care whether  $|\psi_F\rangle$  and  $|\psi_P\rangle$  belong in the same Hilbert space: the state effectively is  $|\psi_F\rangle^{(1)} |\psi_P\rangle^{(2)}$  with two disconnected spaces 1, 2, unrelated in particular by time evolution.

Note that  $\mathcal{H}_F \times \mathcal{H}_P$  (motivated by future-past  $dS$  surfaces) is somewhat different qualitatively from factorizing a Hilbert space as  $\mathcal{H} = \mathcal{H}_L \times \mathcal{H}_R$  (as in the  $CFT_L \times CFT_R$  dual to the eternal  $AdS$  black hole [62]). In the latter case there is no causal connection between the components  $\mathcal{H}_L$  and  $\mathcal{H}_R$ , which are independent. In the current case  $\mathcal{H}_F$  is the time evolution of  $\mathcal{H}_P$ , *i.e.* the time evolution operator acts as the isomorphism. So a state  $|\Psi\rangle_{FP}$  is isomorphic to a corresponding state  $|\Psi\rangle_{FF}$ . Since the time evolution phases cancel, the state  $|\Psi\rangle_{FP}$  is future-past entangled if the corresponding state  $|\Psi\rangle_{FF}$  is entangled in the ordinary sense on the (constant) late time slice  $F$ . This suggests that nonzero entanglement entropy at the future time slice arises from non-factorizable future-past states.

The time evolution operator itself can be obtained as a reduced transition matrix

$$\mathcal{U}(t) = \sum_{i=1}^N |i\rangle_F \langle i|_P = \text{Tr}_2 (|\psi_{FP}\rangle \langle \psi_I|) = \sum_{i,j} \delta_{ij}^{(2)} (|i\rangle_F^{(1)} |i\rangle_P^{(2)} \langle j|_P^{(1)} \langle j|_P^{(2)}). \quad (6.31)$$

with thermofield double type states  $|\psi_{FP}\rangle = \sum_i |i\rangle_F^{(1)} |i\rangle_P^{(2)}$  and  $|\psi_I\rangle = \sum_i |i\rangle_P^{(1)} |i\rangle_P^{(2)}$ , using  $|I_F\rangle = e^{-iE_F t} |I_P\rangle$ . The time evolution operator acts as the map from the past space to the future one (which is not independent from the past one). Thus the existence of the time evolution operator appears to be tantamount to the existence of future-past entangled states of the form  $|\psi_{FP}\rangle$ . The existence of future-past entangled states is thus equivalent to this time-connectedness of the future and past slices.

### 6.3.1 Autocorrelation functions, factorization

It is now natural to ask if a factorized future-past state implies factorization of the 2-point auto-correlation function between two operators, in other words no correlations in time. Naively it would appear that time-connectedness is required to encode a nontrivial correlation with time separations. Towards exploring this, consider an operator  $A$  localized to subregion-1 (*i.e.* qubit-1) and another operator  $B$  localized to subregion-2 (*i.e.* qubit-2) defined as  $A = A_{\alpha\beta} |\alpha\rangle_P \langle\beta|_P$  and  $B(t) = U^\dagger B_{\gamma\sigma} |\gamma\rangle_P \langle\sigma|_P U$ .

To explore the above, let us start by computing the one-point functions of the operators  $A$  and  $B$ , and then proceed to evaluate the two-point function. We use the notation  $|i_F j_P\rangle = \sum_{i,j} C_{ij} |i\rangle_F |j\rangle_P$  to represent future-past states.

The expectation value of an operator  $A$ , localized in subregion-1 (at  $t = 0$ ), is given by

$$\begin{aligned} \langle A(0) \rangle &= \langle \psi_{FP} | A(0) | \psi_{FP} \rangle = \sum C_{lm}^* \langle l |_F \langle m |_P A_{\alpha\beta} |\alpha\rangle_P \langle\beta|_P C_{ij} |i\rangle_F |j\rangle_P \\ &= \sum_{\substack{i, j, l \\ m, \alpha, \beta}} C_{ij} C_{lm}^* e^{i(E_l - E_i)t} A_{\alpha\beta} \delta_{li} \delta_{m\alpha} \delta_{\beta j} = \sum_{\alpha, \beta, l} C_{l\beta} C_{l\alpha}^* A_{\alpha\beta}, \end{aligned} \quad (6.32)$$

where in the third line we used  $|i_F\rangle = e^{-iE_i t} |i_P\rangle$ , although we could also proceed by using  $\langle l_F | i_F \rangle = \delta_{li}$ . Similarly, the one-point function of the operator  $B$ , localized in subregion-2 (at  $t \neq 0$ ), is computed as follows:

$$\begin{aligned} \langle B(t) \rangle &= \langle \psi_{FP} | B(t) | \psi_{FP} \rangle \\ &= \sum_{\substack{i, j, l \\ m, \gamma, \sigma}} C_{ij} C_{lm}^* e^{i(E_l - E_i)t} e^{i(E_m - E_j)t} B_{\gamma\sigma} \delta_{li} \delta_{m\gamma} \delta_{\sigma j} = \sum_{l, \gamma, \sigma} C_{l\sigma} C_{l\gamma}^* B_{\gamma\sigma} e^{i(E_\gamma - E_\sigma)t}. \end{aligned} \quad (6.33)$$

Now, we compute the two-point function of the operators  $A$  and  $B$ :

$$\begin{aligned} \langle A(0) B(t) \rangle &= \langle \psi_{FP} | A(0) B(t) | \psi_{FP} \rangle \\ &= \sum_{\substack{i, j, l, m \\ \alpha, \beta, \gamma, \sigma}} C_{ij} C_{lm}^* \langle l |_F m |_P (A_{\alpha\beta} |\alpha\rangle_P \langle\beta|_P) (U^\dagger B_{\gamma\sigma} U |\gamma\rangle_P \langle\sigma|_P) |i_F j_P\rangle \\ &= \sum_{\substack{i, j, l, m \\ \alpha, \beta, \gamma, \sigma}} C_{ij} C_{lm}^* A_{\alpha\beta} B_{\gamma\sigma} e^{i(E_l - E_i)t} e^{i(E_\beta - E_j)t} \delta_{m\alpha} \delta_{li} \delta_{\beta\gamma} \delta_{\sigma j} \\ &= \sum_{l, \alpha, \sigma, \gamma} C_{l\sigma} C_{l\alpha}^* A_{\alpha\gamma} B_{\gamma\sigma} e^{i(E_\gamma - E_\sigma)t}. \end{aligned} \quad (6.34)$$

From equations (6.32), (6.33), and (6.34), we see that  $\langle A(0) B(t) \rangle \neq \langle A(0) \rangle \langle B(t) \rangle$  for a non-factorized future-past state  $|\psi_{FP}\rangle = \sum C_{ij} |i\rangle_F |j\rangle_P$ .

Let us now consider the case where the future-past state is factorized, *i.e.*,  $|\psi_{FP}\rangle = |i\rangle_F |i\rangle_P$ . In this case, the one-point and two-point functions simplify to:

$$\begin{aligned}\langle A(0) \rangle &= A_{ll}, & \langle B(t) \rangle &= B_{ll}, \\ \langle A(0)B(t) \rangle &= \sum A_{l\gamma} B_{\gamma l} e^{i(E_\gamma - E_l)t} = A_{ll}B_{ll} + \sum_{l \neq \gamma} A_{l\gamma} B_{\gamma l} e^{i(E_\gamma - E_l)t}.\end{aligned}\quad (6.35)$$

Even in this factorized case, we observe that in general  $\langle A(0)B(t) \rangle \neq \langle A(0) \rangle \langle B(t) \rangle$ , from (6.35). Hence, a factorized future-past state does not necessarily imply the factorization of the auto-correlation function between the two operators. However, upon taking a long-time average, the second term in (6.35) vanishes, giving factorization.

We have seen that factorized future-past states continue to lead to non-factorized 2-point autocorrelation functions unless we perform a long time average. The long time average reflects the fact that cross-correlations die for large timelike separations between the future and past time slices where the two operators are localized. This is a bit reminiscent of ER=EPR [84] and the picture of long wormholes, but now in the timelike direction. To elaborate: the past time slice has a domain of dependence given by its future lightcone (causal) wedge: the tip of this cone lies some time to the future of the past time slice. Likewise the future time slice has a domain of dependence given by its past lightcone (causal) wedge. Thus the correlation function between operator  $A$  localized on the past time slice and operator  $B$  on the future time slice is expected to factorize only if the operators cannot influence each other in time. In other words, we require that their domains of dependence do not overlap, *i.e.* the two time slices are adequately well-separated in time. It appears that this feature reflects in the above factorization of autocorrelation functions under long time averaging despite the state being a factorized future-past state. It would be interesting to explore aspects of timelike ER=EPR further.

## 7 Attempting a synthesis: $\Psi_{dS}$ and time entanglement

The previous two sections, sec. 5-6, discussed aspects of entanglement-like structures with timelike separations in a nongravitational quantum mechanics context. While this is independent of de Sitter issues per se, it was motivated by those, in [19]. It is interesting to ask if we can import some of the lessons and technology here returning to de Sitter space. Let us recall the transition matrix operator T-operator (6.17) (motivated by [58]) and apply it to the de Sitter Wavefunction: thus consider

$$\mathbb{T}_{dS} \equiv \Psi[I^+] \Psi^*[I^-], \quad (7.1)$$

which is a “cosmological transition matrix” from an initial  $dS$  Wavefunction  $\Psi[I^-]$  at the past boundary  $I^-$  to the late time  $dS$  Wavefunction  $\Psi[I^+]$  at the future boundary  $I^+$  (this is reminiscent of [5] and de Sitter space as a collection of past-future amplitudes). This is a complicated object as such since the Wavefunction contains all information about the history of the Universe. In the context of de Sitter, we imagine it must have some “boundedness” property, since de Sitter entropy is finite (albeit large). Let us examine this in the semi-classical context, focussing on the simple case when both  $\Psi[I^\pm]$  correspond to the (ground state) Hartle-Hawking Wavefunction, *i.e.*  $\Psi[I^-] = \Psi[I^+] = \Psi_{dS}^{HH}$ . Then using (C.5), App. C, we have

$$dS_4 : \quad \log \Psi[I^+, R_c] = \frac{\pi l^2}{2G_4} + i \frac{\pi R_c^3}{8G_4} \left( -\frac{4}{l} + \frac{6l}{R_c^2} \right). \quad (7.2)$$

Using (3.11), we can associate to  $\mathbb{T}_{dS}$  an entropy (via replica) as

$$\Psi[I^-] = \Psi[I^+] = \Psi_{dS}^{HH} : \quad S_{\mathbb{T}_{dS}} = \left( 1 - \frac{R_c}{3} \partial_{R_c} \right) \log \mathbb{T}_{dS} = S_{nb} + S_{nb}^* = \frac{\pi l^2}{G_4}, \quad (7.3)$$

with  $S_{nb} = (1 - \frac{R_c}{3} \partial_{R_c}) \log \Psi[I^+] = \frac{\pi l^2}{2G_4} + i \frac{\pi l^2}{2G_4} \frac{R_c}{l}$  the no-boundary extremal surface area (4.35), with  $+i$  as from the expanding branch Wavefunction. Not surprisingly,  $S_{\mathbb{T}_{dS}}$  is  $dS_4$  entropy arising from the Euclidean sphere. In effect this is the calculation in App. A.2, but recast in terms of two copies of the Wavefunction (see App. A.1 for a similar discussion for future-past surface areas). Likewise we can obtain  $dS_{d+1}$  entropy from  $S_{\mathbb{T}_{dS_{d+1}}}$  for  $dS_{d+1}$ . Not surprisingly, the transition matrix in this special case is simply a density matrix  $\mathbb{T}_{dS} \equiv \Psi_{dS}^{HH} (\Psi_{dS}^{HH})^*$ . More generally,  $\mathbb{T}_{dS}$  is a cosmological transition matrix for general future/past  $dS$  Wavefunctions, with the corresponding pseudo-entropy being complex-valued. For instance, considering an entirely Lorentzian de Sitter suggests taking the past boundary Wavefunction to be the conjugate of the future one: this gives

$$\Psi[I^-] = \Psi[I^+]^* : \quad S_{\mathbb{T}_{dS}} = \left( 1 - \frac{R_c}{3} \partial_{R_c} \right) \log \mathbb{T}_{dS} = 2S_{nb} = \frac{\pi l^2}{G_4} + i \frac{\pi l^2}{G_4} \frac{R_c}{l}. \quad (7.4)$$

The real part here is  $dS_4$  entropy as for the sphere: the imaginary part is the future-past surface area, App. A.1. In some sense, normalizing  $\Psi[I^\pm]$  to be the pure phase from the Lorentzian part alone (*i.e.* removing the real hemisphere part) gives the pure imaginary future-past area above. Related quantities suggest analogs of relative entropy where *e.g.* we fix  $\Psi[I^-]$  but consider different  $\Psi[I^+]$ .

In this regard, it is worth noting that issues related to the Wheeler de Witt equation for the Wavefunction and the Hamiltonian constraint will play important roles in a deeper understanding of how this transition matrix  $\mathbb{T}_{dS}$  encodes bulk time evolution (since in the gravity case the Hamiltonian simply gives the constraint). It would be interesting to explore these further.

The above discussion pertains to constructing a bulk transition matrix operator from bulk de Sitter Wavefunctions. Via  $dS/CFT$ , this is a transition matrix of the schematic form  $\mathbf{T}_{dS} \equiv Z_{CFT}[I^+] Z_{CFT}^*[I^-]$ , with  $Z_{CFT} = \Psi_{dS}$  the dual partition function of the Euclidean CFT. Taking  $Z_{CFT}[I^+] = Z_{CFT}[I^-]$  makes this a positive object, with real-valued entropy. In a sense, this appears to have close interrelations with the future-past density matrix obtained from future-past entangled states [15] in the exotic ghost-like Euclidean CFT dual (which is spatial with no time). This was based on various positivity properties that were explicitly observed in toy ghost-spin models [27]. (Relatedly it is worth noting that a single  $Z_{CFT}$  copy via replica facilitates evaluating boundary Renyi entropies: we expect this will dovetail with direct evaluation via  $Tr(\rho_A^n)$ .) It would be fascinating to analyse this carefully to see how bulk time emerges from this dual perspective, and we hope to report on this in the future.

## 8 $dS$ extremal surfaces: other aspects and speculations

### 8.1 $dS$ extremal surfaces, timelike components, maximal areas

In ordinary holographic entanglement in  $AdS$ -like spaces, we minimize over spatial directions and maximize in the time direction (over Cauchy slices), which then leads to expected RT/HRT extremal surfaces (and likewise for quantum extremal surfaces) [85]. In the no-boundary  $dS$  context, this requires some clarification since the space has a top Lorentzian component joined with a bottom Euclidean hemisphere. Surfaces anchored at the future boundary necessarily have timelike components in the Lorentzian region but are spacelike as expected in the Euclidean region: so we expect a maximization of the extremal surface area for the timelike component in the Lorentzian region but a minimization for the spatial component in the Euclidean region. This might look reasonable in pure  $dS$  naively, but disconcerting in the slow-roll inflation generalizations where the inflationary perturbation wiggles appear to not allow such clean segregations. We will examine this in a preliminary way and find things to be consistent at least in regions far from the complexification point where the Lorentzian component of the spacetime joins with the Euclidean one.

For simplicity let us consider a 3-dim metric of the schematic form in (A.12),

$$ds^2 = g_{rr} dr^2 + r^2(d\theta^2 + \sin^2 \theta d\phi^2). \quad (8.1)$$

We are considering a maximal subregion (half-circle) on the boundary Euclidean time slice given by the equatorial plane  $\theta = \frac{\pi}{2}$ . Now we see that the nature of the area functional

changes depending on whether we are in the Lorentzian or Euclidean region: we have

$$\begin{aligned} g_{rr} < 0 : \quad iA_L &= i \int \sqrt{|g_{rr}|} dr^2 - r^2 d\phi^2, \\ g_{rr} > 0 : \quad A_E &= \int \sqrt{g_{rr}} dr^2 + r^2 d\phi^2. \end{aligned} \quad (8.2)$$

In the Euclidean region, we obtain a minimal area surface stretching along the  $r$ -direction alone, with no excursions in the  $\phi$ -direction (for maximal subregions): this is as for  $AdS$  spacelike extremal surfaces. In the Lorentzian region  $g_{rr} < 0$  however, we see that minimization leads to null surfaces with vanishing area and no bearing on boundary entanglement entropy in the dual theory (which is admittedly exotic and ghost-like, but allows complex-valued entanglement generalizations at least in toy models [26, 27]). Interpreting this area integral with an appropriate time contour leads to a maximum total proper time instead. Thus we find

$$iA_L \rightarrow i \int \sqrt{|g_{rr}|} dr, \quad A_E \rightarrow \int \sqrt{g_{rr}} dr. \quad (8.3)$$

The proper time here being maximized is analogous to ordinary particle trajectories as timelike geodesics. This of course fits the structure of the  $dS$  area integrals (2.3). The  $dS_4$  and other higher dimensional cases are similar structurally.

Let us now examine this in the  $dS_3$  slow-roll case near the future boundary: then at large  $r$ , the area functional (8.2) contains inside the radical

$$\frac{1}{r}(1 + \epsilon \log r) dr^2 - r^2 d\phi^2 \quad (8.4)$$

where we have used (A.13) and expanded the slow-roll contribution  $\beta_>$  in (A.15). Had this  $O(\epsilon)$ -correction been negative, it could have competed with the  $(-r^2 d\phi^2)$ -term potentially spoiling the timelike nature of the surface and maximization. As it stands, the small slow-roll correction is positive consistent with the expectation that the timelike nature near the future boundary in pure  $dS$  does not change much due to the slow-roll perturbations in the Lorentzian region. We note however that numerically examining  $\beta_>(r)$  reveals non-positive behaviour in the vicinity of the complexification point  $r = 1^+$ : we expect that things are more murky here on the timelike/spacelike nature of the extremal surface.

For the Euclidean part, we need to continue  $\beta_>(r) \rightarrow \beta_<(r)$  valid in the  $r < 1$  region: then expanding near the nbp (*i.e.* far from the complexification point) gives inside the radical

$$\frac{1 + \epsilon r^2 \frac{1}{4}(-4 - 2i\pi + \log(16))}{1 - r^2} dr^2 + r^2 d\phi^2 \quad (8.5)$$

Thus the slow roll contribution has a negative real part near  $r = 0$ , and does not compete with the  $(r^2 d\phi^2)$ -term, thereby vindicating minimization in the Euclidean region alongwith

the slow-roll corrections. In the vicinity of the complexification point  $r \sim 1^-$ , the signs become murky as for  $r \sim 1^+$ .

Similar things happen for  $dS_4$  slow-roll: near the future boundary,  $\beta_>(r)$  in (A.14) gives a positive contribution preserving maximization, while  $\beta_<(r)$  near the no-boundary point gives a negative contribution preserving minimization.

It would be interesting to systematize the rules for extremal surfaces with timelike components.

## 8.2 The imaginary part in no-boundary $dS$ areas

We have recovered the no-boundary  $dS_3, dS_4$  extremal surface areas (4.14), (4.35), from the  $n \rightarrow 1$  limit of the boundary Renyi entropies via replica. The imaginary part in these contains  $+i$ , which can be obtained via the  $AdS$  analytic continuation  $L \rightarrow il$ . The Wavefunction in the boundary Renyi calculation (4.1) corresponds to the expanding branch of  $dS$  as we have seen. On the other hand, the areas (2.5), (2.4), with the imaginary part containing  $-i$  could be understood via the  $AdS$  analytic continuation  $L \rightarrow -il$ . As we saw in (3.7), (3.11), these arise if we instead used the Wavefunction with the leading divergent term of the opposite sign (which corresponds to the contracting  $dS$  branch). The technical point is that the areas correspond to codim-2 surfaces whose leading (imaginary) divergence is one  $l^2$ -factor less than the leading divergence in the Wavefunction, which leads to the single relative minus sign.

In the  $dS_3$  case we saw that the boundary-quotient variables (4.17) describe a Schwarzschild  $dS_3$  geometry and the cosmic brane (which becomes the  $dS$  extremal surface as  $n \rightarrow 1$ ) is the  $r = 0$  singularity. There is no obvious physical interpretation of this singularity as a “physical” cosmic brane, nor is one necessary.

However say we engage in the speculation of thinking of these (complex) areas as amplitudes for cosmic branes. Then the no-boundary extremal surface area (taken standalone) with the  $-i$  sign is akin to the amplitude for a cosmic brane created from “nothing”, *i.e.* with HH no-boundary initial conditions: but this arises from the contracting branch Wavefunction in the Renyi calculation as we have seen. Instead if we fix the Wavefunction to correspond to the expanding branch, then the codim-2 pure  $dS_4, dS_3$  surface areas (4.14), (4.35), contain  $+i$  and interpreting these as amplitudes for creation appears to require negative energy. To see this, let us express the areas as (with  $S_0$  half  $dS_{4,3}$  entropy respectively)

$$\psi_{cb}(R_c) = e^{S_0} e^{\pm i \frac{S_0}{l} R_c}, \quad S_0 = \frac{\pi l^2}{2G_4}; \quad \psi_{cb}(R_c) = e^{S_0} e^{\pm i \frac{2}{\pi} S_0 \log\left(\frac{2R_c}{l}\right)}, \quad S_0 = \frac{\pi l}{4G_3}, \quad (8.6)$$

writing both signs  $\pm i$  in the imaginary part. Defining  $R_c$  as the bulk time endpoint of the cosmic brane, the Lorentzian timelike part is a pure phase which resembles the phase from

time evolution starting at  $t = l$  and ending at  $t = R_c$ . The “energy” is  $\mp \frac{S_0}{l}$ : this is only defined upto numerical factors (*e.g.* by rescaling  $R_c \rightarrow kR_c$ ). Then the time derivative satisfies

$$i \frac{\partial}{\partial R_c} \psi_{cb}(R_c) = \mp \frac{S_0}{l} \psi_{cb}(R_c). \quad (8.7)$$

This reflects a Schrodinger-like time evolution for the amplitude  $\psi_{cb}(R_c)$ , evolving forward in time  $t_F \equiv R_c$  (of the future boundary) but with energy being negative if we take  $+i$  in the areas. Alternatively we view the cosmic brane as positive energy but as starting at the future boundary and evolving backward in time.

The cosmic brane evolving forward in time, from the no-boundary point (nbp)  $r = 0$  to the complexification point  $r = 1$  (beginning of the Lorentzian region) to the future boundary  $r = \frac{R_c}{l}$ , is encoded in the area integrals in (2.3) with the time contour  $\int_0^l(\dots) + \int_l^{R_c}(\dots)$  (Figure 10). The opposite sign reflects inverse time evolution.

Likewise consider the no-boundary extremal surface areas [23] for slow-roll inflation, with areas to  $O(\epsilon)$  given in (A.17). From the time contours used in defining the area integrals in the complex time-plane (Figure 10), we have the area integrals arising as in (A.16): so this again corresponds to the cosmic brane evolving forward in time, but with negative energy in the corresponding Schrodinger evolution equation. To see this for the  $dS_4$  case in (A.17), the time derivative gives

$$i \frac{\partial}{\partial R_c} \psi_{cb}^{sr4}(R_c) = \mp \frac{S_0}{l} \left( 1 - \frac{\epsilon}{6} + \epsilon \log \frac{R_c}{l} \right) \psi_{cb}^{sr4}(R_c). \quad (8.8)$$

For these slow-roll cases there is further  $R_c$ -dependence, akin to a driving potential. As  $R_c$  increases, the term inside the bracket increases, albeit suppressed by the slow-roll parameter  $\epsilon$ : so this suggests external “energy” is being pumped into the system, consistent with the inflaton rolling down the hill. This falls out of a perturbative correction when

$$\epsilon \log \frac{R_c}{l} \sim O(1) \quad i.e. \quad R_c \sim l e^{1/\epsilon}. \quad (8.9)$$

This means the future boundary cannot be taken “too far” in the future to preserve the validity of this  $O(\epsilon)$  expression. Roughly speaking, going too far into the future means inflation does not remain slow-roll.

For the  $dS_3$  slow-roll case in (A.17), the natural time parameter is perhaps  $\log R_c$ , giving

$$i \frac{\partial}{\partial \log R_c} \psi_{cb}^{sr3}(R_c) = \mp \frac{l}{2G_3} \left( \frac{1}{\pi} - \frac{\epsilon}{8} + \frac{\epsilon}{2} \log \frac{R_c}{l} \right) \psi_{cb}^{sr3}(R_c) \quad (8.10)$$

for evolution. Qualitatively this is similar to the  $dS_4$  slow-roll case, the increase with  $R_c$  suggesting “energy” being pumped in, but the detailed  $R_c$ /time dependence is different.

It is worth noting two points: (1) the finite real part, which is half  $dS$  entropy, decreases with the slow-roll correction (always negative; see (A.17)), which might suggest that the number of degrees of freedom has decreased, consistent with the thinking that the maximum amount of “stuff” in the space has decreased. This stems from  $l$ -dependence. (2) The imaginary part on the other hand evolves to increase with  $R_c$  as above, so “energy” is being pumped in, in some sense. This stems from  $R_c$ -dependence. In this light, it would be interesting to understand analogs of the entropic c-function, and reinterpret the (forward or inverse) time evolution in terms of boundary holographic RG flows. This point of view does not require a cosmic brane interpretation per se: we are simply trying to recast the evolution equation for the extremal surface area as an RG evolution equation for boundary entanglement entropy. This is reminiscent of [86] and inverse RG flows: it would be interesting to explore this further.

## 9 Discussion

We have developed further previous work on de Sitter extremal surfaces and time entanglement structures in quantum mechanics. In the first part, we first discussed explicit quotient geometries as tools to evaluate the extremal surface areas. Then we constructed smooth bulk geometries with replica boundary conditions at the future boundary and evaluated boundary Renyi entropies in  $dS/CFT$ . This puts on a firmer footing previous Lewkowycz-Maldacena replica arguments [22] based on analytic continuation for the extremal surface areas via appropriate cosmic branes.

We have seen various features in the de Sitter studies, which we now recap and summarize.

- (1) The quotient metrics (sec. 3) are adequate near  $n = 1$  for calculating boundary entanglement entropy via  $dS/CFT$  but are akin to the singular spaces in [67]. In accord however with  $AdS/CFT$  logic (*e.g.* for perturbations) [71], we require smooth bulk geometries at finite  $n$ . In sec. 4, we constructed smooth bulk geometries with replica boundary conditions which we used to evaluate boundary Renyi entropies in  $dS/CFT$ . The bulk calculation via  $Z_{CFT} = \Psi_{dS}$  pertains to the semiclassical de Sitter Wavefunction and thus evaluates pseudo-Renyi entropies as in eq.(4.1), which in general are complex-valued (technically the semiclassical analysis uses the bulk action alongwith the Gibbons-Hawking boundary term as well as appropriate counterterms).
- (2) The  $dS_3$  case (sec. 4.1) is most easily expressed in the static coordinatization which enables a simple visualization of the way the replica copies are glued together (Figure 3). There are close parallels with the  $AdS_3$  replica discussion in [59]. Evaluating (4.1) finally

results in the boundary Renyi entropies being pure imaginary, consistent with the imaginary central charge in  $dS_3/CFT_2$  [6]: the  $n = 1$  limit recovers the boundary entanglement entropy matching the extremal surface area. In terms of boundary quotiented variables, these are Schwarzschild  $dS_3$  geometries with mass related to  $n$ . The cosmic brane is then identified with the conical singularities at the North and South poles.

The Renyi entropies here appear relatively simple, structurally similar to entanglement entropies appended with simple multiplicative  $n$ -factors. These however pertain to simple (maximal) subregions: it is likely that generic subregions or multiple subregions lead to more complicated Renyi entropies. It might be interesting to study appropriate generalizations of the  $AdS_3$  case [74], [75], which might reveal nontrivial aspects in the present nonunitary  $dS_3/CFT_2$  context here.

(3) The 4-dim de Sitter geometry (sec. 4.2) involves hyperbolic foliations and is a complex geometry which satisfies a regularity criterion that amounts to requiring a smooth Euclidean continuation (which amounts to a  $-AdS$  space). This is based on a regularity criterion that was studied for certain complex  $dS_4$  branes in [76] (see also [77] for related discussions). The entry of complex metrics here is not new: this is known from various previous studies in cosmology including [87], as also discussed more recently in [88]. For instance, the regularity criteria above (as well as in no-boundary  $dS$ -like geometries) are analogous to positive frequency rather than reality. It would be interesting to understand how these interface with *e.g.* the KSW criterion [89, 90].

In this regard, it is worth noting that *e.g.* no-boundary pure  $dS_4$  is a semiclassical geometry with a semiclassical picture of time, defined by the time contour in (4.19), which goes from Lorentzian to Euclidean: in these variables, the geometry “ends” in the Euclidean part where  $f(r = il) = 0$ . The corresponding Renyi-replica geometries (4.22) also retain this semiclassical picture of the time contour, with the geometry “ending” at the complex horizon  $f(r_h) = 0$  as we have seen in (4.26). So while these are complex geometries, we are thinking of them with the crutch of the semiclassical time contour and the corresponding geometric picture of time. This is consistent and adequate as we have seen for the relatively simple subregions we have been discussing (as for the  $dS_3$  case also, above), with the expectation that the time contour dovetails with the geometric picture of time in the semiclassical regimes near pure de Sitter. However more generally when there exist competing extremal surfaces, one expects competing complex geometry saddles for the corresponding Renyi analysis. It would thus be interesting to understand how to systematize the rules for complex geometries and time contours in general. Of course these intertwine with various related issues in quantum cosmology beginning with [87].

The embedding of the hyperbolic foliations into global  $dS_4$  is nontrivial and illustrates how

the  $n = 1$  limit recovers the known complex-valued extremal surface area. Relatedly, it might be interesting to understand replicas in global  $dS_4$  directly. This analysis can be also understood via analytic continuation from a  $-AdS$  framework (with close parallels to the  $AdS$  hyperbolic black holes and Renyi analysis in [60]), and is valid for de Sitter in any dimension (sec. 4.3).

(4) In the end, our analyses of boundary (pseudo-)Renyi entropies via  $dS/CFT$  end up being analytic continuations of appropriate  $AdS$  studies. This might appear boring(!) but in fact this is required for consistency, given the fact that these are entanglement or Renyi entropies in the boundary  $Z_{CFT}$  evaluated via holography. Indeed we recall that the extremal surfaces were defined via subregions on boundary Euclidean time slices and were bulk simulations of boundary entanglement entropy [12, 15, 18, 19]). Thus the analytic continuation here is in accord with boundary correlation functions in  $dS/CFT$  obtainable via known analytic continuations from  $AdS$  [6].

(5) We have seen that the imaginary parts of the extremal surface areas differ depending on the  $AdS$  analytic continuation being either  $L_{AdS} \rightarrow \pm il_{dS}$ . From the point of view of the codim-2  $dS$  extremal surfaces regarded standalone, choosing  $L \rightarrow -il$  gives (2.3), which reflects the time contour Figure 10. However from the point of view of the Renyi calculations here, we have seen  $L \rightarrow il$  arising naturally: in this context we focus on the expanding branch of the Wavefunction with  $\log \Psi$  scaling as  $-i(..)$  in the leading divergence with the codim-2 area arising as the first subleading term with one  $l^2$ -factor less, which thus gives  $+i$  in  $\text{Im}(\text{area})$ . There does not appear to be any inconsistency however, since it is unclear if one should insist on the timelike+Euclidean cosmic brane in these  $dS$  cases here admitting a physical interpretation. For instance the cosmic brane in the  $dS_3$  case arises as the conical singularity (timelike in the Lorentzian region) in the Schwarzschild  $dS_3$  boundary-quotient description (4.17). See however the speculative remarks in sec. 8.2.

(6) The timelike components in the extremal surfaces might appear novel from the point of view of systematizing the rules for extremal surfaces. We have seen (sec. 8.1) that in particular they are maximal area, akin to the fact that timelike geodesics for ordinary massive particles correspond to maximum proper time. In the no-boundary context, this becomes more interesting since the Euclidean part continues to be minimal area while the Lorentzian/timelike part is maximal area. In the case of no-boundary slow-roll inflation, there are nontrivial corrections: as we saw, the maximal/minimal area properties for time-like/Euclidean components continue to hold away from the complexification point. Thinking of these areas in the complex-time-plane requires more care towards formulating the framework of extremal surfaces in such cases.

(7) Relatedly, it is worth noting that in the cases we have discussed pertaining to maximal

subregions, the codim-2 extremal surfaces are uniquely defined with no competing saddles (this is also vindicated by the analytic continuation from  $AdS$ ). Thus we expect that the replica geometries and the associated Renyi entropies are unambiguous as the relevant saddles. The geometries and the corresponding Renyi entropies we have described corroborate this expectation. However it is unclear how to rigorously establish this in these sorts of cosmological backgrounds. These questions, and those in (6) above, in some sense might interface with understanding covariant formulations of such extremal surfaces (perhaps generalizing [63]) and related issues such as analogs of entropy inequalities and subregion duality in de Sitter like spaces.

$dS/CFT$  suggests exotic nonunitary ghost-like CFT duals to de Sitter space. Evaluating boundary Renyi entropies in such CFTs directly is an interesting open question, perhaps developing aspects of [71], [74], [75], in the present context. It is also perhaps of interest to study these in the toy ghost-spin models [26, 27] where entanglement studies explicitly reveal complex-valued entropies arising naturally, the negative norm contributions here leading to imaginary components (we note that these are also pseudo-entropies strictly speaking since the adjoint of a state  $|\psi\rangle$  being nontrivial makes  $\rho_A = Tr_B(|\psi\rangle\langle\psi|)$  akin to a reduced transition matrix). In the present context, it is of interest to study (pseudo-)Renyi entropies directly from  $Tr(\rho_A^n)$  towards gaining insights into nonunitary theories. Related questions arise on analogs of (pseudo-)Renyi entropy inequalities in de Sitter and dual contexts. Certain observations on  $dS$  area/entropy inequalities (and simple qubit pseudo-entropies) were made in [22]: while these perhaps lead to more questions than answers(!) in de Sitter, they can be recognized via analytic continuation as encoding the well-known  $AdS$  entropy inequalities. It would be interesting to explore similar issues with the Renyi entropies here.

In the second part (independent of de Sitter), we studied various aspects of time entanglement in quantum mechanics, in particular the reduced time evolution operator, weak values, operators localized to subregions (sec. 6.1), and autocorrelation functions. The transition matrix operator  $\mathbb{T}$  in (6.17) containing time-evolved versions of two distinct states, and thus two copies of the time evolution operator, was useful in recasting correlation functions of operators localized to subregions, and relates to the spacetime density operator in [58]. Finally we discussed aspects of future-past entangled states towards exploring the way the timelike separations here intertwine with factorization aspects of autocorrelation functions over long timescales.

There are various questions that linger in obtaining a deeper understanding of time entanglement structures in quantum systems, and in particular of the emergence of time via entanglement-like structures with timelike separations. Part of our motivation here was to connect aspects of time entanglement and pseudo-entropy in [18], [19], [21], with some

aspects of the studies in [58]: we hope to explore and develop this further.

Finally, in sec. 7, we attempted a synthesis of the quantum mechanical time entanglement aspects with de Sitter space, and considered a “cosmological transition matrix”. This involves two copies of the de Sitter Wavefunction, at the past and the future boundary, and is reminiscent of the picture in [5] of de Sitter space as a collection of past-future amplitudes. We discussed how de Sitter entropy and the future-past surface area arise from special cases here. This suggests tantalizing related aspects in two copies of the dual ghost-like CFT and the emergence of bulk time: we are engaged in ongoing work in this regard, and hope to report on it in the future.

**Acknowledgements:** It is a pleasure to thank Cesar Agon, Alok Laddha, Alexey Milekhin, Onkar Parrikar, Sabrina Pasterski, Sunil Sake, Sandip Trivedi and especially Rob Myers and Ronak Soni for useful discussions and comments. KN thanks the hospitality of Perimeter Institute, Waterloo, CA, as this work was nearing completion. This work is partially supported by a grant to CMI from the Infosys Foundation.

## A More on $dS$ -like quotient geometries

### A.1 Future-past extremal surface area via quotient

Here we discuss quotient geometries for future-past timelike surfaces stretching between  $I^\pm$  [15, 17] in entirely Lorentzian de Sitter, reviewed in sec. 2. The (pure imaginary)  $dS_4$ ,  $dS_3$  areas are

$$(dS_4) \quad S_{fp} = -i \frac{\pi l^2 R_c}{G_4} \frac{R_c}{l}; \quad (dS_3) \quad S_{fp} = -i \frac{l}{G_3} \log \frac{R_c}{l}. \quad (\text{A.1})$$

Roughly two copies of the no-boundary surfaces (2.1) earlier glued with appropriate time-contours make up the future-past surfaces [19]: the areas of the IR extremal surfaces satisfy

$$S_{fp} = S_{nb} - S_{nb}^*, \quad \text{Re}(S_{nb}) = \frac{1}{2} \cdot dS \text{ entropy}, \quad (\text{A.2})$$

encapsulating the fact that the future-past surface area  $S_{fp}$  pertains to two copies of the Wavefunction, arising from  $I^+ \cup I^-$  glued appropriately at the midslice. These future-past surface areas can be obtained as follows. Consider (for concreteness) global  $n$ -quotient  $dS_4$

$$ds^2 = -l^2 d\eta^2 + l^2 \cosh^2 \eta \left( d\theta_1^2 + \frac{1}{n^2} \sin^2 \theta_1 d\theta_2^2 + \cos^2 \theta_1 d\theta_3^2 \right), \quad (\text{A.3})$$

where the time coordinate has the range  $\eta \in [-\eta_0, \eta_0]$  with  $\eta_0$  the future/past boundary cutoff. The  $\eta$ -coordinate being real essentially restricts the no-boundary  $dS_4$  metric (3.8) to the Lorentzian region automatically since  $r = l \cosh \eta > l$ . At the moment of time symmetry

$\eta = 0$  we have a 3-sphere of minimal size (for  $n = 1$ ). The global  $dS_4$  geometry (with  $n = 1$ ) can be thought of as gluing an expanding branch de Sitter with  $\eta > 0$  to the contracting branch de Sitter  $\eta < 0$  at the midslice  $\eta = 0$ . This is entirely Lorentzian: the Euclidean hemisphere is absent. The future-past extremal surface is encoded by a time contour [19] that goes from the past boundary  $I^-$  to the future boundary  $I^+$  running entirely along the Lorentzian timelike direction. This gives the pure imaginary area: the first relation in (A.2) implies that the Euclidean parts of the two no-boundary time contours cancel.

The quotient calculation is along the lines of sec. 3.1-3.2. The quotient space (A.3) contains conical singularities emanating from the subregion boundary as described after (3.8), running along the  $\eta$ -direction (time) wrapping the  $S^1$  parametrized by  $\theta_3$ . These are desingularized by the cosmic brane source term whose action/area is

$$iS_{\text{sing}} = -I_{\text{brane}} = -\frac{n-1}{n} \frac{A_{\text{brane}}}{4G}, \quad A_{\text{brane}} = -2\pi l^2 i \int_{-\eta_0}^{\eta_0} d\eta \cosh \eta = -4\pi l R_c, \quad (\text{A.4})$$

using  $\sinh \eta_0 \approx \cosh \eta_0 = \frac{R_c}{l}$  for large  $\eta_0$ . In terms of the  $r$ -coordinate in (3.8), we have  $A_{\text{brane}} = 2\pi l^2 \int r \sqrt{\frac{dr^2}{-(\frac{r^2}{l^2} - 1)}}$  which is the imaginary part in (3.9). Thus, as in (3.3), the total boundary entanglement entropy obtained is the  $dS_4$  area in (A.1).

We now give an alternate derivation using the on-shell action:

$$\begin{aligned} S &= \frac{1}{16\pi G_4} \int d^4x \sqrt{-g} \left( \mathbf{R} - \frac{6}{l^2} \right) - \frac{1}{8\pi G_4} \int d^3\sigma \sqrt{\gamma} K \\ &= \frac{6}{l^2} \frac{V_{S^3} l^4}{16\pi G_4} \int_0^{\eta_0} \cosh^3 \eta - \frac{6l^2 V_{S^3}}{16\pi G_4} \tanh \eta_0 \cosh^3(\eta_0) \\ &\quad + \frac{6}{l^2} \frac{V_{S^3} l^4}{16\pi G_4} \int_{-\eta_0}^0 \cosh^3 \eta - \frac{6l^2 V_{S^3}}{16\pi G_4} \tanh \eta_0 \cosh^3 \eta_0 \\ &= S_+ + S_- = -\frac{16\pi^2 l^2}{16\pi G_4} \sinh^3 \eta_0 = -\frac{\pi l^2}{G_4} \left( \frac{R_c^2}{l^2} - 1 \right)^{3/2}. \end{aligned} \quad (\text{A.5})$$

where  $S_+$  corresponds to the contribution coming from the expanding branch while  $S_-$  corresponds to the contribution coming from contracting branch. In the above we used  $K = \frac{3\tanh(\eta_0)}{l}$ . Also the fact that the normal at the lower boundary points in an opposite direction relative to the upper boundary leads to the Gibbons-Hawking-York contribution being the same at both ends. The final equality arises from  $\cosh \eta_0 = \frac{R_c}{l}$ .

It is instructive to recast the above noting that the no-boundary Wavefunction is

$$\log \Psi_{\text{nb}} = S_{hs} - iS_+, \quad \log \Psi_{\text{nb}}^* = S_{hs} + iS_-, \quad (\text{A.6})$$

where  $S_{hs}$  is the Euclidean hemisphere part and  $-iS_{\pm}$  are the Lorentzian parts. We use  $-iS_+$  here (as stated in the comments after (3.7), sec. C) correlating this sign with the analytic

continuation  $L \rightarrow -il$ . Thus we obtain

$$\log \Psi_{nb} - \log \Psi_{nb}^* = -i(S_+ + S_-) \equiv -iS. \quad (\text{A.7})$$

Finally using (3.11), we obtain the boundary entanglement entropy,

$$\mathcal{S}_{fp} = \left(1 - \frac{R_c}{3}\partial_{R_c}\right)(\log \Psi_{nb} - \log \Psi_{nb}^*) \equiv S_{nb} - S_{nb}^* = -i\frac{\pi l^2}{G_4} \frac{R_c}{l}. \quad (\text{A.8})$$

matching (A.1). In this form, using (A.7), we see that the future-past area pertains to the product amplitude  $\Psi_{nb} \Psi_{nb}^{*-1}$  which in a sense encodes evolving from  $I^-$  to the midslice  $\eta = 0$  and thereon to  $I^+$ .

## A.2 $dS \rightarrow$ Euclidean sphere: $dS$ entropy

In sec. A.1 we recovered the pure imaginary future-past areas via quotients. Here we compute the real part of the no-boundary extremal surface area (3.11), which satisfies (A.2), as the entropy from a quotient space corresponding to two copies of the Euclidean hemisphere joined to a full Euclidean sphere. Consider the  $n$ -quotient  $S^4$  metric

$$ds^2 = l^2 d\theta^2 + l^2 \cos^2 \theta \left( d\theta_1^2 + \frac{1}{n^2} \sin^2 \theta_1 d\theta_2^2 + \cos^2 \theta_1 d\theta_3^2 \right). \quad (\text{A.9})$$

This can be obtained by Euclideanizing the time  $\eta$ -direction in the entirely Lorentzian  $dS_4$  metric (A.3) as  $\eta \rightarrow -i\theta$ . However it is worth noting that the metric (A.3) is equivalent to the Lorentzian part of the no-boundary metric (3.8) using  $r = l \cosh \eta > l$ : the above Euclidean sphere metric then maps to the hemisphere part with  $r = l \cos \theta < l$ .

Thus the locus of the conical singularity here maps to that in the hemisphere part  $r < l$  of the no-boundary surface in (3.8). The cosmic brane action then becomes

$$I_{brane} = \frac{n-1}{n} \frac{l^2}{4G_4} (2\pi) \left( 2 \int_0^{\pi/2} d\theta \cos \theta \right) = \frac{n-1}{n} \frac{\pi l^2}{G_4} \rightarrow \mathcal{S} = \frac{\pi l^2}{G_4}. \quad (\text{A.10})$$

The  $2\pi$ -factor is from the  $\theta_3$ -circle while the factor of 2 inside the brackets is from the two hemispheres. The extremal surface area as  $n \rightarrow 1$  is obtained via (3.3), which is of course the total  $dS$  entropy arising from the two hemispheres. Note that  $I_{brane}$  above in terms of the  $r$ -coordinate is  $\frac{n-1}{n}$  times  $\frac{V_{S^1}}{4G_4} (2 \int_0^l \frac{r dr}{\sqrt{1-\frac{r^2}{l^2}}})$  which is twice the Euclidean part of the area integral (3.9). The no-boundary point  $r = 0$  here is  $\theta = \frac{\pi}{2}$ .

Likewise  $dS_3$  entropy can be obtained from the cosmic brane action in an  $n$ -quotient  $S^3$  metric  $ds^2 = l^2 d\theta^2 + l^2 \cos^2 \theta (d\theta_1^2 + \frac{1}{n^2} \sin^2 \theta_1 d\theta_2^2)$ , which is essentially two copies of the hemisphere part of the no-boundary  $dS_3$  metric (3.4) with  $n = 1$  after quotienting. Similar  $dS_{d+1}$  entropy can be recovered from the  $S^{d+1}$  quotient appropriately Euclideanizing (3.12).

Pictorially, the future-past surface sec. A.1 is a trumpet-like geometry obtained by removing the Euclidean hemisphere contribution in the no-boundary areas (A.1), (A.2): the time contour [19] encoding this is entirely Lorentzian going from  $I^-$  to  $I^+$ . The real extremal surface in the Euclidean sphere discussed here arises from a distinct time contour. With the no-boundary surface defined by the time contour  $[nbp \rightarrow 0 \rightarrow R_c]$  (Figure 10), the real sphere part here is the time contour  $[nbp \rightarrow 0 \rightarrow R_c] + [R_c \rightarrow 0 \rightarrow npb] \equiv [nbp \rightarrow 0 \rightarrow npb]$ .

### A.3 No-boundary slow-roll inflation, extremal surfaces, quotient

No-boundary extremal surfaces in slow-roll inflation models were studied in [23], with certain inflationary cosmological perturbations to no-boundary de Sitter space [87] which preserve the spatial spherical isometry of  $dS$  in global coordinates. These perturbations are described by scalar inflaton perturbations defined imposing regularity at the no-boundary point: this induces corresponding metric perturbations as well. The perturbations have explicit analytic (although still adequately complicated) expressions to  $O(\epsilon)$  in the slow-roll parameter  $\epsilon$ , as described in [88] and related previous work. The inflationary perturbations induce small wiggles around pure de Sitter, so the metric has various interesting real and imaginary pieces. Thus the no-boundary extremal surface areas now have nontrivial real and imaginary pieces which now arise from both the Euclidean hemisphere and the Lorentzian timelike regions. In general it turns out that the corresponding area integrals must be regarded carefully in the complex time-plane defining appropriate contours (Figure 10) that avoid extra poles at the complexification point that arise from the slow-roll perturbations (similar in spirit to calculations of the semiclassical Wavefunction of the Universe). Doing this carefully, we eventually find divergent pure imaginary pieces from near the future boundary as well as real and imaginary finite slow-roll corrections to the leading half de Sitter entropy  $\frac{\pi l^2}{2G_4}$  contribution from the hemisphere. These finite  $O(\epsilon)$  corrections precisely match the finite  $O(\epsilon)$  corrections in the expansion of the semiclassical Wavefunction of the Universe (equivalently the on-shell action) in slow-roll inflation described in [88]. This is consistent with the Lewkowycz-Maldacena interpretation in [22] of these no-boundary extremal surface areas giving the probability for cosmic brane creation but now in the slow-roll no-boundary geometry.

The slow-roll inflation background arises in the Einstein-scalar theory with action

$$I = \frac{1}{16\pi G_{d+1}} \int d^{d+1}x \sqrt{g} (R - (\partial\phi)^2 - 2V(\phi)) - \frac{1}{8\pi G_{d+1}} \int d^d x \sqrt{h} K. \quad (\text{A.11})$$

The Einstein-inflaton equations can be solved perturbatively in the slow-roll approximation: this has substantial literature reviewed in [88] which we refer to (see also [23] for various

details). We restrict to the minisuperspace approximation with inflationary perturbations preserving the  $S^d$  spherical symmetry: the spacetime metric near global  $dS_{d+1}$  is

$$ds^2 = -dt^2 + a(t)^2 d\Omega_d^2 \equiv g_{rr} dr^2 + r^2 d\Omega_d^2, \quad (\text{A.12})$$

For pure de Sitter in the above global coordinates, we have  $a(t) = l \cosh \tau \equiv l r$  with  $\tau = \frac{t}{l}$  and  $g_{aa} = \frac{1}{1-r^2} < 0$  in the Lorentzian region  $r > 1$ . The region  $r < 1$  gives  $g_{aa} > 0$  and describes the Euclidean hemisphere. The metric component  $g_{rr}$  to  $O(\epsilon)$  gives

$$g_{rr} = \frac{1}{1-r^2} (1 + 2\epsilon \beta_>(r)), \quad (\text{A.13})$$

where the slow roll correction  $\beta_>(r)$  is a function of the rolling inflaton profile  $\phi(r)$ , given below in (A.14), (A.15). The Hamiltonian constraint in an ADM formulation allows expressing the metric in terms of the inflaton scalar. Solving for and inputting the inflaton profile gives the metric (A.13) with  $\beta(r)$  in the  $r > 1$  Lorentzian region for  $dS_4$ :

$$\beta_>(r) = \frac{8 - 9r^4 + 4ir^2\sqrt{r^2 - 1} + 8i\sqrt{r^2 - 1} - 6ir^4\sqrt{r^2 - 1} + r^6(6\log(1 - i\sqrt{r^2 - 1}) - 1 + 3i\pi)}{6r^4(r^2 - 1)}. \quad (\text{A.14})$$

To continue this to the  $r < 1$  hemisphere region, we note that it is adequate to replace  $-i\sqrt{r^2 - 1}$  by  $\sqrt{1 - r^2}$  in  $\beta_>(r)$ : this defines  $\beta_<(r)$ . Likewise the  $dS_3$  slow-roll case gives

$$\begin{aligned} \beta_>(r) = & \frac{1}{32r^2(r^2 - 1)} \left[ -4r^4(1 + \log 16) + 4r^2 - 4\log^2(r + \sqrt{r^2 - 1}) \right. \\ & + 4(2r\sqrt{r^2 - 1}(2r^2 - 1) + i\pi) \log(r + \sqrt{r^2 - 1}) \\ & \left. - 4i\pi(-2r^4 - r\sqrt{r^2 - 1} + 2r^3\sqrt{r^2 - 1}) + \pi^2 \right]. \end{aligned} \quad (\text{A.15})$$

The IR no-boundary extremal surface area  $S_{sr_{d+1}} = S_{d+1}^{r<1} + S_{d+1}^{r>1}$  after expanding to  $O(\epsilon)$  gives for  $dS_4, dS_3$ ,

$$\begin{aligned} S_{sr_4} \simeq & \frac{\pi l^2}{2G_4} \left( -i \int_1^{R_c/l} \frac{1 + \epsilon \beta_>(r)}{\sqrt{r^2 - 1}} r dr + \int_0^1 \frac{1 + \epsilon \beta_<(r)}{\sqrt{1 - r^2}} r dr \right) \\ S_{sr_3} \simeq & \frac{l}{2G_3} \left( -i \int_1^{R_c/l} \frac{1 + \epsilon \beta_>(r)}{\sqrt{r^2 - 1}} dr + \int_0^1 \frac{1 + \epsilon \beta_<(r)}{\sqrt{1 - r^2}} dr \right). \end{aligned} \quad (\text{A.16})$$

with the leading  $dS_{d+1}$  piece and the  $O(\epsilon)$  slow roll correction, where  $\beta_<(r)$  is to be obtained by analytically continuing  $\beta_>(r)$  in the Lorentzian region  $r > 1$  to the hemisphere region where  $r < 1$ . The  $\beta$ -factors lead to extra poles at the complexification point so these areas must necessarily be defined as complex time-plane integrals with appropriate contours in the complex time  $r$ -plane (Figure 10), as discussed in detail in [23]. The time coordinate  $\tau$

defines the contour on the left, from the no-boundary point in the Euclidean region at  $\tau = i\frac{\pi}{2}$  going around the complexification point at  $\tau = 0$  and thereon to the Lorentzian region with real  $\tau$  going to the future boundary  $\tau \rightarrow \infty$ . With the coordinate  $r = \cosh \tau$  the nbp is  $r = 0$  and the complexification point at  $r = 1$ . Using the above expressions, we eventually

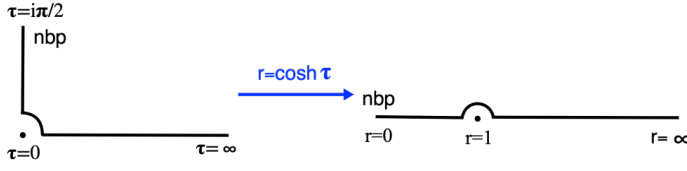


Figure 10: Time contour in the complex  $r$ -plane (right) and the  $\tau$ -plane (left).

obtain, to  $O(\epsilon)$ , the  $dS_4$ ,  $dS_3$  slow-roll areas [23] as

$$\begin{aligned} S_{sr_4} &= \frac{\pi l^2}{2G_4} \left( -i \frac{R_c}{l} + 1 \right) + \epsilon \frac{\pi l^2}{2G_4} \left( -i \frac{R_c}{l} \log \frac{R_c}{l} + i \frac{7}{6} \frac{R_c}{l} + \log 4 - \frac{7}{2} + i\pi \right), \quad (\text{A.17}) \\ S_{sr_3} &= \frac{l}{2G_3} \left( \frac{\pi}{2} - \frac{i}{\pi} \log \frac{R_c}{l} \right) \\ &+ \epsilon \frac{l}{2G_3} \left( -\frac{\pi}{16} (1 + \log 16) + \frac{i}{16} \left( 2 \log \frac{R_c}{l} - 4 \left( \log \frac{R_c}{l} \right)^2 + 3\pi^2 + 4(\log 2)^2 - 6 \log 2 \right) \right). \end{aligned}$$

Towards defining a replica formulation for these areas, it is instructive to note that the  $S^3$  symmetric form (A.12) of the metric here ensures that the  $n$ -quotient space is essentially similar structurally to (3.8): we obtain

$$ds^2 = g_{rr} dr^2 + r^2 \left( d\theta_1^2 + \frac{1}{n^2} \sin^2 \theta_1 d\theta_2^2 + \cos^2 \theta_1 d\theta_3^2 \right). \quad (\text{A.18})$$

We see that the singularity structure here is essentially identical to that in pure  $dS_4$  since the replica construction and subsequent quotienting only involves the  $S^3$  part of the space leaving  $g_{rr}$  unaffected. Likewise the inflaton is unaffected since it has no  $S^3$ -dependence. Thus the required cosmic brane source locus is structurally similar to that in  $dS_4$ : the resulting area of course has the same complications that the unreplicated metric exhibits, and is given by (A.16). The cosmic brane part of the action  $iS_{sing} = -I_{brane} = -\frac{n-1}{n} \frac{A_{brane}}{4G_4} = -\frac{n-1}{n} S_{sr_4}$  in the  $n \rightarrow 1$  limit then results in the entropy/area  $S_{sr_4}$  above.

## B $dS_{d+1} \rightarrow -AdS$ and boundary Renyi

In this section we will consider boundary Renyi entropies in higher dim- $dS_{d+1}$  (see sec. 4.3)

$$ds^2 = -\frac{dr^2}{f(r)} + l^2 f(r) d\phi^2 + r^2 dH_{d-1}^2, \quad f(r) = \frac{r^2}{l^2} + 1 + \frac{c_1}{r^{d-2}}, \quad (\text{B.1})$$

where

$$dH_{d-1}^2 = d\chi^2 + \sinh^2(\chi)d\Omega_{d-2}^2. \quad (\text{B.2})$$

As described for  $dS_4$  after (4.22), analytically continuing to  $-AdS$  space with  $r \rightarrow i\rho$  gives

$$-f(\rho) = \frac{\rho^2}{l^2} - 1 - \frac{\omega^d}{\rho^{d-2}}, \quad \omega^d = -i^{-d}c_1. \quad (\text{B.3})$$

Now at the horizon  $\rho_h$  the vanishing of the blackening factor leads to the condition

$$\omega^d = \frac{\rho_h^d}{l^2} - \rho_h^{d-2}. \quad (\text{B.4})$$

Demanding that there is no conical deficit at horizon leads to

$$-\frac{l}{2}f'(\rho_h)n = 1 \quad (\text{B.5})$$

which yields the solution

$$\rho_h = l \frac{1 + \sqrt{1 + d(d-2)n^2}}{nd}. \quad (\text{B.6})$$

When  $n = 1$  we get  $\rho_h = l$  and as a result  $\omega = 0$ .

The action is given by

$$\tilde{I}_n = \frac{1}{16\pi G} \int d^{d+1}x \sqrt{g}(R - 2\Lambda) - \frac{1}{8\pi G} \int d^d x \sqrt{\gamma} K \quad (\text{B.7})$$

Substituting  $R = \frac{d(d+1)}{l^2}$ ,  $\Lambda = \frac{d(d-1)}{2l^2}$ , and

$$\sqrt{\gamma} K = l \left( d \frac{\rho^d}{l^2} - (d-1)\rho^{d-2} - \omega^d \frac{d}{2} \right) \sinh^{d-2}(\chi), \quad (\text{B.8})$$

we get

$$\tilde{I}_n = \frac{4\pi n}{l} \frac{V_{d-1}}{16\pi G} \left( (1-d)\rho_c^d + (d-1)\rho_c^{d-2}l^2 - \rho_h^d + l^2\omega^d \frac{d}{2} \right). \quad (\text{B.9})$$

To remove the cutoff dependent terms we add the following counterterms

$$I_{ct} = \frac{1}{16\pi G} \int d^d x \sqrt{\gamma} (\alpha R_b + \beta) \quad (\text{B.10})$$

such that the regulated action is

$$I_n = \tilde{I}_n + I_{ct}. \quad (\text{B.11})$$

It is worth noting that the above counterterms remove all divergences upto  $d = 4$ , while for  $d = 5, 6$  they only remove the leading and subleading divergences leaving extra divergences to worry about. One then needs additional counterterms such as  $R_b^2$  to remove these sub-subleading divergences (as in the well-known formulations of holographic renormalization

procedures [78–81]). However the Renyi entropy involves the combination  $I_n - nI_1$ , and these divergences get subtracted out: as a result eq.(B.10) is enough for our purposes. Using

$$R_b = \frac{(d-1)(d-2)}{\rho_c^2}, \quad \alpha = -\frac{l}{d-2}, \quad \beta = 2\frac{d-1}{l}, \quad (\text{B.12})$$

we get

$$I_n - nI_1 = -\frac{2\pi n}{l} \frac{V_{d-1}}{16\pi G} (\rho_h^d + l^2 \rho_h^{d-2} - 2l^d). \quad (\text{B.13})$$

To calculate the boundary Renyi entropy (4.1), we note now that

$$\log(\Psi) = iI_{dS} = i^{d+1}I_{-AdS}. \quad (\text{B.14})$$

Substituting and simplifying we obtain

$$S_n = \frac{1}{1-n} i^{d-1} \frac{2\pi n}{l} \frac{V_{d-1}}{16\pi G} (\rho_h^d + l^2 \rho_h^{d-2} - 2l^d) \quad (\text{B.15})$$

In the limit  $n \rightarrow 1$  we obtain

$$S_{EE} = \frac{1}{1-n} i^{d-1} \frac{2\pi}{l} \frac{V_{d-1}}{16\pi G} 2l^d (1-n) = \frac{1}{4G} i^{d-1} V_{d-1} l^{d-1} \quad (\text{B.16})$$

which is eq.(4.56). As is clear, there are various parallels with the Renyi studies in [60].

## C The on-shell action for $dS_{d+1}$

The  $dS_{d+1}$  action is given by

$$I_g = \frac{1}{16\pi G} \int d^{d+1}x \sqrt{-g} (\mathbf{R} - 2\Lambda) - \frac{1}{8\pi G} \int d^d x \sqrt{\gamma} K, \quad (\text{C.1})$$

where  $\mathbf{R}$ ,  $l$ ,  $\gamma$ ,  $K$  are the Ricci scalar,  $dS_{d+1}$  scale, the induced metric on the boundary and the trace of the extrinsic curvature respectively.

We are evaluating the Wavefunction for no-boundary  $dS_{d+1}$  space with a Lorentzian part evolving from the Euclidean hemisphere. With the (future) boundary at  $r = R_c$ , the outward pointing normal and the extrinsic curvature are (and  $\mathbf{R} = \frac{d(d+1)}{l^2}$ ,  $\Lambda = \frac{d(d-1)}{2l^2}$ )

$$n^r = \sqrt{\frac{r^2}{l^2} - 1}, \quad K = \nabla_\mu n^\mu = \frac{1}{\sqrt{-g}} \partial_r (\sqrt{-g} n^r) = \frac{1}{r^d} \sqrt{\frac{r^2}{l^2} - 1} \partial_r (r^d) \sim \frac{d}{l} - \frac{dl}{2r^2}. \quad (\text{C.2})$$

Using these in (C.1), we obtain the on-shell action for the Lorentzian part as

$$16\pi G I_g^L = \Omega_d \int_l^{R_c} dr r^d \frac{1}{\sqrt{\frac{r^2}{l^2} - 1}} - 2\Omega_d \left( \frac{d}{l} - \frac{dl}{2R_c^2} \right) R_c^d \quad (\text{C.3})$$

Depending on whether  $d$  is odd or even the integrand above will give different results. For example if  $d$  is even there will be a log divergence which will be absent when  $d$  is odd.

Let us mention then the answers for some specific values of  $d$  that were used in the text. For  $d = 2$

$$iI_g^L = \frac{i}{16\pi G} \left( -8\pi \frac{R_c^2}{l} + 4\pi l + 8\pi l \log\left(\frac{2R_c}{l}\right) \right), \quad (\text{C.4})$$

while for  $d = 3$  one gets

$$iI_g^L = \frac{i}{16\pi G} 2\pi^2 R_c^3 \left( -\frac{4}{l} + \frac{6l}{R_c^2} \right). \quad (\text{C.5})$$

The Euclidean part for any  $d$  is half the volume of the  $d + 1$ -dim sphere

$$-I_g^E = \frac{1}{2} \frac{l^{d-1}}{16\pi G} \Omega_{d+1}. \quad (\text{C.6})$$

The total Wavefunction above then pertains to the expanding branch with  $R_c$  the future boundary cutoff and is given by

$$\log \Psi = iI_g^L - I_g^E, \quad (\text{C.7})$$

with the specific  $I_g^{L,E}$  for  $dS_3, dS_4$  as above.

The arguments above are intrinsic to de Sitter but they can be obtained via analytic continuation from  $AdS$ . Consider the Euclidean  $AdS_3$  action with the Einstein-Hilbert and Gibbons-Hawking terms:

$$16\pi G_3 S = - \int d^3x \sqrt{g} \left( \mathbf{R} + \frac{2}{L^2} \right) - 2 \int d^2\sigma \sqrt{\gamma} K, \quad (\text{C.8})$$

The Ricci scalar here in  $AdS_3$  is  $\mathbf{R} = -\frac{6}{L^2}$ . The global  $EAdS_3$  metric is given by

$$ds^2 = L^2 d\tau^2 + L^2 \sinh^2 \tau (d\theta^2 + \sin^2 \theta d\phi^2), \quad (\text{C.9})$$

where the range is  $\tau = (0, \tau_0)$  with boundary at  $\tau = \tau_0$ . The trace of the extrinsic curvature is  $K = \frac{2\coth(\tau_0)}{L}$ . The on-shell action for the  $EAdS_3$  metric (C.9), along the same lines as for  $dS_3$  earlier, is obtained as

$$-S = \frac{4\pi L}{16\pi G_3} (2\tau_0 + \sinh(2\tau_0)), \quad (\text{C.10})$$

Using the analytic continuation from  $AdS_3 \rightarrow dS_3$  as

$$\tau_0 = \eta_0 + \frac{i\pi}{2}, \quad L = -il, \quad (\text{C.11})$$

and  $l \cosh(\eta_0) = R_c$ , we obtain for large  $R_c$  the semiclassical Wavefunction  $\Psi_1 \sim e^{-S}$  as (3.6), which then gives (3.7). On the other hand, the analytic continuation  $L \rightarrow il$  gives the

Wavefunction (C.7) for the expanding branch and is apt for evaluating correlation functions (see *e.g.* [91])).

Likewise  $EAdS_4$  with  $ds^2 = L^2(d\tau^2 + \sinh^2(\tau)d\Omega_3^2)$  and boundary  $\tau_0$  has action

$$-S = \log Z = \int d^4x \left( \mathbf{R} + \frac{6}{L^2} \right) + 2 \int d\sigma \sqrt{\gamma} K = L^2 V_{S^3} (\cosh(3\tau_0) + 3 \cosh(\tau_0) - 4). \quad (\text{C.12})$$

## D Autocorrelation functions, T operator: examples

In the following, we illustrate the explicit construction of the T operator through a series of concrete examples. We consider a two-state system with the Hamiltonian<sup>1</sup>

$$H = -J S_z^1 \otimes S_z^2, \quad (\text{D.1})$$

where  $J$  is a coupling constant and  $S_z$  is the spin operator. In the  $S_z$  eigenbasis ( $|0\rangle$ ,  $|1\rangle$ ), the Hamiltonian (D.1) takes the following form

$$H = -J (|00\rangle\langle 00| - |01\rangle\langle 01| - |10\rangle\langle 10| + |11\rangle\langle 11|).$$

Since correlation functions involving only  $S_z$  are time-independent, we focus only on those, where either of  $S_x$  or  $S_y$  is time-evolved. To compute the autocorrelation functions, we need the time-evolved operators defined as below

$$S_x^2(t) \equiv e^{iHt} (\mathbb{I}^1 \otimes S_x^2(0)) e^{-iHt}; \quad S_y^2(t) \equiv e^{iHt} (\mathbb{I}^1 \otimes S_y^2(0)) e^{-iHt}. \quad (\text{D.2})$$

In the  $S_z$  eigenbasis, the operators  $S_x$  and  $S_y$  are given by

$$\begin{aligned} \mathbb{I}^1 \otimes S_x^2 &= |00\rangle\langle 01| + |01\rangle\langle 00| + |10\rangle\langle 11| + |11\rangle\langle 10|, \\ \mathbb{I}^1 \otimes S_y^2 &= -i|00\rangle\langle 01| + i|01\rangle\langle 00| - i|10\rangle\langle 11| + i|11\rangle\langle 10|. \end{aligned} \quad (\text{D.3})$$

Using standard Pauli matrix identities, we can express the time evolution operator as

$$e^{iHt} = (\mathbb{I}^1 \otimes \mathbb{I}^2) \cos(Jt) - i(S_z^1 \otimes S_z^2) \sin(Jt). \quad (\text{D.4})$$

Using (D.2), (D.3), and (D.4), we compute various autocorrelation functions for a generic state  $|\psi\rangle = \sum_{ij} C_{ij} |ij\rangle$ , and extract the corresponding components of the T operator. Some examples are given here

---

<sup>1</sup>We define  $S_{(x, y, z)} = \frac{\hbar}{2} \sigma_{(x, y, z)}$ . For calculation simplicity, we set  $\hbar = 2$  in the rest of this section. Further, superscripts “1” and “2” correspond to subregions one and two everywhere appearing in this section.

### Case 1:

$$\langle S_x^1(0)S_x^2(t) \rangle = \langle \psi | S_x^1(0) S_x^2(t) | \psi \rangle = (C_{00}^* C_{11} + C_{11}^* C_{00}) e^{2iJt} + (C_{01}^* C_{10} + C_{10}^* C_{01}) e^{-2iJt}. \quad (\text{D.5})$$

This yields the non-zero  $\mathbb{T}$  components:

$$T_{0101} = C_{00}^* C_{11} e^{2iJt}, \quad T_{1010} = C_{11}^* C_{00} e^{2iJt}, \quad T_{0110} = C_{01}^* C_{10} e^{-2iJt}, \quad T_{1001} = C_{10}^* C_{01} e^{-2iJt}.$$

### Case 2:

$$\langle S_z^1(0)S_x^2(t) \rangle = \langle \psi | S_z^1(0) S_x^2(t) | \psi \rangle = (C_{01}^* C_{00} - C_{10}^* C_{11}) e^{2iJt} + (C_{00}^* C_{01} - C_{11}^* C_{10}) e^{-2iJt}. \quad (\text{D.6})$$

Resulting non-zero  $\mathbb{T}$  components:

$$T_{0010} = C_{01}^* C_{00} e^{2iJt}, \quad T_{1011} = -C_{10}^* C_{11} e^{2iJt}, \quad T_{0001} = C_{00}^* C_{01} e^{-2iJt}, \quad T_{1110} = -C_{11}^* C_{10} e^{-2iJt}.$$

### Case 3:

$$\langle S_z^1(0)S_y^2(t) \rangle = \langle \psi | S_z^1(0) S_y^2(t) | \psi \rangle = i(C_{01}^* C_{00} + C_{10}^* C_{11}) e^{2iJt} - i(C_{00}^* C_{01} + C_{11}^* C_{10}) e^{-2iJt}. \quad (\text{D.7})$$

Corresponding non-zero  $\mathbb{T}$  components:

$$T_{0010} = C_{01}^* C_{00} e^{2iJt}, \quad T_{1011} = C_{10}^* C_{11} e^{2iJt}, \quad T_{0001} = -C_{00}^* C_{01} e^{-2iJt}, \quad T_{1110} = -C_{11}^* C_{10} e^{-2iJt}.$$

### Case 4:

$$\langle S_x^1(0)S_y^2(t) \rangle = \langle \psi | S_x^1(0) S_y^2(t) | \psi \rangle = (-iC_{00}^* C_{11} + iC_{11}^* C_{00}) e^{-2iJt} + (iC_{01}^* C_{10} - iC_{10}^* C_{01}) e^{2iJt}. \quad (\text{D.8})$$

The corresponding non-zero entries of the  $\mathbb{T}$  operator take the form:

$$T_{0101} = -C_{00}^* C_{11} e^{-2iJt}, \quad T_{1010} = C_{11}^* C_{00} e^{-2iJt}, \quad T_{0110} = C_{01}^* C_{10} e^{2iJt}, \quad T_{1001} = -C_{10}^* C_{01} e^{2iJt}.$$

## References

- [1] J. M. Maldacena, *The Large  $N$  limit of superconformal field theories and supergravity*, *Adv. Theor. Math. Phys.* **2** (1998) 231 [[hep-th/9711200](#)].
- [2] S. S. Gubser, I. R. Klebanov and A. M. Polyakov, *Gauge theory correlators from noncritical string theory*, *Phys. Lett. B* **428** (1998) 105 [[hep-th/9802109](#)].
- [3] E. Witten, *Anti de Sitter space and holography*, *Adv. Theor. Math. Phys.* **2** (1998) 253 [[hep-th/9802150](#)].

- [4] A. Strominger, *The dS / CFT correspondence*, *JHEP* **10** (2001) 034 [[hep-th/0106113](#)].
- [5] E. Witten, *Quantum gravity in de Sitter space*, in *Strings 2001: International Conference*, 6, 2001, [hep-th/0106109](#).
- [6] J. M. Maldacena, *Non-Gaussian features of primordial fluctuations in single field inflationary models*, *JHEP* **05** (2003) 013 [[astro-ph/0210603](#)].
- [7] D. Anninos, T. Hartman and A. Strominger, *Higher Spin Realization of the dS/CFT Correspondence*, *Class. Quant. Grav.* **34** (2017) 015009 [[1108.5735](#)].
- [8] S. Ryu and T. Takayanagi, *Holographic derivation of entanglement entropy from AdS/CFT*, *Phys. Rev. Lett.* **96** (2006) 181602 [[hep-th/0603001](#)].
- [9] S. Ryu and T. Takayanagi, *Aspects of Holographic Entanglement Entropy*, *JHEP* **08** (2006) 045 [[hep-th/0605073](#)].
- [10] V. E. Hubeny, M. Rangamani and T. Takayanagi, *A Covariant holographic entanglement entropy proposal*, *JHEP* **07** (2007) 062 [[0705.0016](#)].
- [11] M. Rangamani and T. Takayanagi, *Holographic Entanglement Entropy*, vol. 931. Springer, 2017, [10.1007/978-3-319-52573-0](#), [[1609.01287](#)].
- [12] K. Narayan, *Extremal surfaces in de Sitter spacetime*, *Phys. Rev. D* **91** (2015) 126011 [[1501.03019](#)].
- [13] Y. Sato, *Comments on Entanglement Entropy in the dS/CFT Correspondence*, *Phys. Rev. D* **91** (2015) 086009 [[1501.04903](#)].
- [14] K. Narayan, *de Sitter space and extremal surfaces for spheres*, *Phys. Lett. B* **753** (2016) 308 [[1504.07430](#)].
- [15] K. Narayan, *On extremal surfaces and de Sitter entropy*, *Phys. Lett. B* **779** (2018) 214 [[1711.01107](#)].
- [16] K. Narayan, *de Sitter entropy as entanglement*, *Int. J. Mod. Phys. D* **28** (2019) 1944019 [[1904.01223](#)].
- [17] K. Narayan, *de Sitter future-past extremal surfaces and the entanglement wedge*, *Phys. Rev. D* **101** (2020) 086014 [[2002.11950](#)].
- [18] K. Doi, J. Harper, A. Mollabashi, T. Takayanagi and Y. Taki, *Pseudoentropy in dS/CFT and Timelike Entanglement Entropy*, *Phys. Rev. Lett.* **130** (2023) 031601 [[2210.09457](#)].
- [19] K. Narayan, *de Sitter space, extremal surfaces, and time entanglement*, *Phys. Rev. D* **107** (2023) 126004 [[2210.12963](#)].
- [20] K. Doi, J. Harper, A. Mollabashi, T. Takayanagi and Y. Taki, *Timelike entanglement entropy*, *JHEP* **05** (2023) 052 [[2302.11695](#)].

[21] K. Narayan and H. K. Saini, *Notes on time entanglement and pseudo-entropy*, *Eur. Phys. J. C* **84** (2024) 499 [[2303.01307](#)].

[22] K. Narayan, *Further remarks on de Sitter space, extremal surfaces, and time entanglement*, *Phys. Rev. D* **109** (2024) 086009 [[2310.00320](#)].

[23] K. Goswami, K. Narayan and G. Yadav, *No-boundary extremal surfaces in slow-roll inflation and other cosmologies*, *JHEP* **03** (2025) 193 [[2409.14208](#)].

[24] G. W. Gibbons and S. W. Hawking, *Cosmological Event Horizons, Thermodynamics, and Particle Creation*, *Phys. Rev. D* **15** (1977) 2738.

[25] M. Spradlin, A. Strominger and A. Volovich, *Les Houches lectures on de Sitter space*, in *Les Houches Summer School: Session 76: Euro Summer School on Unity of Fundamental Physics: Gravity, Gauge Theory and Strings*, pp. 423–453, 10, 2001, [hep-th/0110007](#).

[26] K. Narayan, *On  $dS_4$  extremal surfaces and entanglement entropy in some ghost CFTs*, *Phys. Rev. D* **94** (2016) 046001 [[1602.06505](#)].

[27] D. P. Jatkar and K. Narayan, *Ghost-spin chains, entanglement and bc-ghost CFTs*, *Phys. Rev. D* **96** (2017) 106015 [[1706.06828](#)].

[28] Y. Nakata, T. Takayanagi, Y. Taki, K. Tamaoka and Z. Wei, *New holographic generalization of entanglement entropy*, *Phys. Rev. D* **103** (2021) 026005 [[2005.13801](#)].

[29] A. Mollabashi, N. Shiba, T. Takayanagi, K. Tamaoka and Z. Wei, *Pseudo Entropy in Free Quantum Field Theories*, *Phys. Rev. Lett.* **126** (2021) 081601 [[2011.09648](#)].

[30] A. Mollabashi, N. Shiba, T. Takayanagi, K. Tamaoka and Z. Wei, *Aspects of pseudoentropy in field theories*, *Phys. Rev. Res.* **3** (2021) 033254 [[2106.03118](#)].

[31] Y. Hikida, T. Nishioka, T. Takayanagi and Y. Taki, *CFT duals of three-dimensional de Sitter gravity*, *JHEP* **05** (2022) 129 [[2203.02852](#)].

[32] Y. Hikida, T. Nishioka, T. Takayanagi and Y. Taki, *Holography in de Sitter Space via Chern-Simons Gauge Theory*, *Phys. Rev. Lett.* **129** (2022) 041601 [[2110.03197](#)].

[33] W.-z. Guo, S. He and Y.-X. Zhang, *Constructible reality condition of pseudo entropy via pseudo-Hermiticity*, *JHEP* **05** (2023) 021 [[2209.07308](#)].

[34] B. Liu, H. Chen and B. Lian, *Entanglement entropy of free fermions in timelike slices*, *Phys. Rev. B* **110** (2024) 144306 [[2210.03134](#)].

[35] Z. Li, Z.-Q. Xiao and R.-Q. Yang, *On holographic time-like entanglement entropy*, *JHEP* **04** (2023) 004 [[2211.14883](#)].

[36] J. Cotler and A. Strominger, *Cosmic ER=EPR in  $dS/CFT$* , [2302.00632](#).

[37] X. Jiang, P. Wang, H. Wu and H. Yang, *Timelike entanglement entropy and  $TT^-$  deformation*, *Phys. Rev. D* **108** (2023) 046004 [[2302.13872](#)].

[38] Z. Chen, *Complex-valued Holographic Pseudo Entropy via Real-time AdS/CFT Correspondence*, [2302.14303](#).

[39] X. Jiang, P. Wang, H. Wu and H. Yang, *Timelike entanglement entropy in  $dS_3/CFT_2$* , *JHEP* **08** (2023) 216 [[2304.10376](#)].

[40] C.-S. Chu and H. Parihar, *Time-like entanglement entropy in  $AdS/BCFT$* , *JHEP* **06** (2023) 173 [[2304.10907](#)].

[41] H.-Y. Chen, Y. Hikida, Y. Taki and T. Uetoko, *Complex saddles of Chern-Simons gravity and  $dS_3/CFT_2$  correspondence*, *Phys. Rev. D* **108** (2023) 066005 [[2306.03330](#)].

[42] D. Chen, X. Jiang and H. Yang, *Holographic  $TT^-$  deformed entanglement entropy in  $dS_3/CFT_2$* , *Phys. Rev. D* **109** (2024) 026011 [[2307.04673](#)].

[43] P.-Z. He and H.-Q. Zhang, *Holographic timelike entanglement entropy from Rindler method\**, *Chin. Phys. C* **48** (2024) 115113 [[2307.09803](#)].

[44] F. Omidi, *Pseudo Rényi Entanglement Entropies For an Excited State and Its Time Evolution in a 2D CFT*, [2309.04112](#).

[45] N. L. Diaz, J. M. Matera and R. Rossignoli, *Spacetime quantum and classical mechanics with dynamical foliation*, *Phys. Rev. D* **109** (2024) 105008 [[2311.06486](#)].

[46] S. He, Y.-X. Zhang, L. Zhao and Z.-X. Zhao, *Entanglement and pseudo entanglement dynamics versus fusion in CFT*, *JHEP* **06** (2024) 177 [[2312.02679](#)].

[47] S. Grieninger, K. Ikeda and D. E. Kharzeev, *Temporal entanglement entropy as a probe of renormalization group flow*, *JHEP* **05** (2024) 030 [[2312.08534](#)].

[48] A. Das, S. Sachdeva and D. Sarkar, *Bulk reconstruction using timelike entanglement in  $(A)dS$* , *Phys. Rev. D* **109** (2024) 066007 [[2312.16056](#)].

[49] W.-z. Guo, S. He and Y.-X. Zhang, *Relation between timelike and spacelike entanglement entropy*, [2402.00268](#).

[50] D. Basu and V. Raj, *Reflected entropy and timelike entanglement in  $TT^-$ -deformed CFT2s*, *Phys. Rev. D* **110** (2024) 046009 [[2402.07253](#)].

[51] S. Carignano and L. Tagliacozzo, *Loschmidt echo, emerging dual unitarity and scaling of generalized temporal entropies after quenches to the critical point*, [2405.14706](#).

[52] R. Fareghbal, *Flat-space limit of holographic pseudoentropy in  $(A)dS$  spacetimes*, *Phys. Rev. D* **110** (2024) 066019 [[2408.03061](#)].

[53] M. P. Heller, F. Ori and A. Serantes, *Geometric Interpretation of Timelike Entanglement Entropy*, *Phys. Rev. Lett.* **134** (2025) 131601 [[2408.15752](#)].

[54] A. Bou-Comas, C. R. Marimón, J. T. Schneider, S. Carignano and L. Tagliacozzo, *Measuring temporal entanglement in experiments as a hallmark for integrability*, [2409.05517](#).

[55] J. Xu and W.-z. Guo, *Imaginary part of timelike entanglement entropy*, *JHEP* **02** (2025) 094 [[2410.22684](#)].

[56] P. Caputa, B. Chen, T. Takayanagi and T. Tsuda, *Thermal pseudo-entropy*, *JHEP* **01** (2025) 003 [[2411.08948](#)].

[57] M. Afrasiar, J. K. Basak and D. Giataganas, *Holographic timelike entanglement entropy in non-relativistic theories*, *JHEP* **05** (2025) 205 [[2411.18514](#)].

[58] A. Milekhin, Z. Adamska and J. Preskill, *Observable and computable entanglement in time*, [2502.12240](#).

[59] A. Lewkowycz and J. Maldacena, *Generalized gravitational entropy*, *JHEP* **08** (2013) 090 [[1304.4926](#)].

[60] L.-Y. Hung, R. C. Myers, M. Smolkin and A. Yale, *Holographic Calculations of Renyi Entropy*, *JHEP* **12** (2011) 047 [[1110.1084](#)].

[61] T. Hartman and J. Maldacena, *Time Evolution of Entanglement Entropy from Black Hole Interiors*, *JHEP* **05** (2013) 014 [[1303.1080](#)].

[62] J. M. Maldacena, *Eternal black holes in anti-de Sitter*, *JHEP* **04** (2003) 021 [[hep-th/0106112](#)].

[63] X. Dong, A. Lewkowycz and M. Rangamani, *Deriving covariant holographic entanglement*, *JHEP* **11** (2016) 028 [[1607.07506](#)].

[64] X. Dong, *The Gravity Dual of Renyi Entropy*, *Nature Commun.* **7** (2016) 12472 [[1601.06788](#)].

[65] X. Dong, *Holographic Entanglement Entropy for General Higher Derivative Gravity*, *JHEP* **01** (2014) 044 [[1310.5713](#)].

[66] H. Casini, M. Huerta and R. C. Myers, *Towards a derivation of holographic entanglement entropy*, *JHEP* **05** (2011) 036 [[1102.0440](#)].

[67] D. V. Fursaev, *Proof of the holographic formula for entanglement entropy*, *JHEP* **09** (2006) 018 [[hep-th/0606184](#)].

[68] W. Donnelly and V. Shyam, *Entanglement entropy and  $T\bar{T}$  deformation*, *Phys. Rev. Lett.* **121** (2018) 131602 [[1806.07444](#)].

[69] D. V. Fursaev and S. N. Solodukhin, *On the description of the Riemannian geometry in the presence of conical defects*, *Phys. Rev. D* **52** (1995) 2133 [[hep-th/9501127](#)].

[70] C. Arias, F. Diaz and P. Sundell, *De Sitter Space and Entanglement*, *Class. Quant. Grav.* **37** (2020) 015009 [[1901.04554](#)].

[71] M. Headrick, *Entanglement Renyi entropies in holographic theories*, *Phys. Rev. D* **82** (2010) 126010 [[1006.0047](#)].

[72] J. Camps, *Gravity duals of boundary cones*, *JHEP* **09** (2016) 139 [[1605.08588](#)].

[73] G. T. Horowitz and E. Shaghoulian, *Detachable circles and temperature-inversion dualities for  $CFT_d$* , *JHEP* **01** (2018) 135 [[1709.06084](#)].

[74] T. Hartman, *Entanglement Entropy at Large Central Charge*, [1303.6955](#).

[75] T. Faulkner, *The Entanglement Renyi Entropies of Disjoint Intervals in  $AdS/CFT$* , [1303.7221](#).

[76] D. Das, S. R. Das and K. Narayan,  *$dS/CFT$  at uniform energy density and a de Sitter 'bluewall'*, *JHEP* **04** (2014) 116 [[1312.1625](#)].

[77] J. Maldacena, G. J. Turiaci and Z. Yang, *Two dimensional Nearly de Sitter gravity*, *JHEP* **01** (2021) 139 [[1904.01911](#)].

[78] V. Balasubramanian and P. Kraus, *A Stress tensor for Anti-de Sitter gravity*, *Commun. Math. Phys.* **208** (1999) 413 [[hep-th/9902121](#)].

[79] R. C. Myers, *Stress tensors and Casimir energies in the  $AdS / CFT$  correspondence*, *Phys. Rev. D* **60** (1999) 046002 [[hep-th/9903203](#)].

[80] S. de Haro, S. N. Solodukhin and K. Skenderis, *Holographic reconstruction of space-time and renormalization in the  $AdS / CFT$  correspondence*, *Commun. Math. Phys.* **217** (2001) 595 [[hep-th/0002230](#)].

[81] K. Skenderis, *Lecture notes on holographic renormalization*, *Class. Quant. Grav.* **19** (2002) 5849 [[hep-th/0209067](#)].

[82] M. Van Raamsdonk, *Building up spacetime with quantum entanglement*, *Gen. Rel. Grav.* **42** (2010) 2323 [[1005.3035](#)].

[83] M. Van Raamsdonk, *Comments on quantum gravity and entanglement*, [0907.2939](#).

[84] J. Maldacena and L. Susskind, *Cool horizons for entangled black holes*, *Fortsch. Phys.* **61** (2013) 781 [[1306.0533](#)].

[85] A. C. Wall, *Maximin Surfaces, and the Strong Subadditivity of the Covariant Holographic Entanglement Entropy*, *Class. Quant. Grav.* **31** (2014) 225007 [[1211.3494](#)].

[86] A. Strominger, *Inflation and the  $dS / CFT$  correspondence*, *JHEP* **11** (2001) 049 [[hep-th/0110087](#)].

[87] J. B. Hartle and S. W. Hawking, *Wave Function of the Universe*, *Phys. Rev. D* **28** (1983) 2960.

[88] J. Maldacena, *Comments on the no boundary wavefunction and slow roll inflation*, [2403.10510](#).

[89] M. Kontsevich and G. Segal, *Wick Rotation and the Positivity of Energy in Quantum Field Theory*, *Quart. J. Math. Oxford Ser.* **72** (2021) 673 [[2105.10161](#)].

- [90] E. Witten, *A Note On Complex Spacetime Metrics*, [2111.06514](https://arxiv.org/abs/2111.06514).
- [91] I. Dey, K. K. Nanda, A. Roy and S. P. Trivedi, *Aspects of  $dS/CFT$  holography*, *JHEP* **05** (2025) 168 [[2407.02417](https://arxiv.org/abs/2407.02417)].